CVD-Grown Graphene : Domain Structure Control and Characterizations

小川, 友以

https://doi.org/10.15017/1441277

出版情報：九州大学, 2013, 博士（工学）, 課程博士
バージョン：
権利関係：全文ファイル公表済

CVD-Grown Graphene:

Domain Structure Control and Characterizations

A Dissertation Presented to

the Graduate School of Engineering Sciences

of Kyushu University

Yui OGAWA

2014

Abstract

Graphene is a promising candidate for future nanoelectronics due to its unique and extraordinary physical properties. In order to prepare high quality graphene, controllable synthesis and subsequent characterizations are required. In this thesis, I have focused on the domain structure of chemical vapor deposition (CVD)-grown graphene and related physical properties. CVD growth is known as a powerful method to produce large area graphene with low cost. The quality of CVD-grown graphene, however, should be much improved for realization of various applications, especially for graphene-based electronics applications. An effective approach to control the structure of graphene is tuning the orientation of graphene domains. I have compared the domain structure and quality of graphene grown on heteroepitaxial Cu(111) and Cu(100) by low energy electron diffraction and microscopy (LEED and LEEM). Subsequently, the interfaces of adjacent graphene domains are investigated based on Raman spectroscopy and charge transport measurements, and the charge scattering sites in CVD-grown graphene are discussed. In addition, fictionalization of CVD-grown graphene by molecular self-assembly has been performed. Considering assembled structure of molecules, domain structure of CVD-grown graphene can be easily observed by low-temperature scanning tunneling microscopy (LT-STM). These results contribute to the development of CVD synthesis of high quality graphene and observation of graphene's domain structures, which are expected to assist the future development of graphene-based electronics.

要旨

グラフェンはその特異な物理的特性から次世代エレクトロニクス材料として期待されている。高品質のグラフェンを合成するために、その構造制御と評価が求められている。本論文では、CVD（chemical vapor deposition）合成法におけるグラフェンのドメイン構造制御とその物理的特性の評価を行った。CVD 法は大面積化かつ低コスト化という観点から注目されているグラフェンの合成方法である。しかしながら、グラフェンのエレクトロニクス材料の応用に向けて、より高品質なグラフェン、理想的には単結晶グラフェンの合成法開発が望まれる。CVD グラフェンのドメイン構造制御の有効な手法として、ドメインの方位を揃えた成長が挙げられる。異なる結晶面を持つMgO基板上に堆積させたヘテロエピタキシャルCu(111) 面とCu(100)面上に成長したグラフェンのドメイン構造について低エネルギー電子線回折および顕微鏡(LEED, LEEM)を用いて検討した。続いて、２つの隣接する CVD グラフェンのドメイン境界について、Raman 分光とキャリア輸送特性の測定によって検討し、電荷散乱サイトについて議論した。さらに、有機分子を用いたグラフェンの機能化へ向けた、π共役系分子の自己組織化膜についても研究を行った。走査トンネル顕微鏡（STM）による分子の自己組織化構造の観察により、CVD グラフェンのドメイン構造が可視化できるということを見出した。これらの結果は高品質グラフェンの CVD 合成とその構造評価の可能性を拡げ、グラフェンのエレクトロニクス分野における応用の発展に寄与するものと期待される。

Table of contents

Abstract

Table of Contents

Chapter 1. Introduction

1-1 Graphene and its research fields ---------- 01
1-1.1 Nanocarbon materials ---------- 02
1-1.2 Graphene ---------- 04
1-1.3 Applications ---------- 05
1-2 Motivation and purpose ---------- 06
1-3 Outline ---------- 06
References

Chapter 2. Graphene

2-1 Fundamental structure and physical properties of graphene ---------- 12
2-2 Preparation methods of graphene films ---------- 15
2-3 Growth mechanism of CVD-grown graphene on metal catalysts ---------- 16
2-4 Domain structure of CVD-grown graphene ---------- 18
2-4.1 Morphology and observation of domain structure ---------- 18
2-4.2 Electrical transport property rerated to domain boundaries in CVD-grown graphene ---------- 20
2-5 Recent research trends of CVD-grown graphene ---------- 20
2-5.1 Synthesis of single-crystal graphene ---------- 21
2-5.2 Functionalization of CVD-grown graphene ---------- 22
2-6 Wet transfer process ---------- 22
References

Chapter 3. Domain structure in single-layer graphene grown on Cu (111) and Cu (100) films

Abstract ---------- 28
3-1 Introduction ---------- 30
3-2 Experiment ---------- 31
3-3 Results and discussion ---------- 32
3-4 Summary ---------- 47
References

Chapter 4. Transport properties and structure of the interface between CVD-grown graphene domains

Abstract ---------- 50
4-1 Introduction ---------- 51
4-2 Experiment ---------- 52
4-3 Results and discussion ---------- 53
4-4 Summary ---------- 66
References

Chapter 5. Self-assembly of polar phthalocyanine molecules on CVD-grown graphene

Abstract ---------- 69
5-1 Introduction ---------- 70
5-2 Experiment ---------- 71
5-3 Results and discussion ---------- 72
5-4 Summary ---------- 81
References

Chapter 6. Conclusions and outlook

6.1 Conclusions ---------- 85
6.2 Future outlook ---------- 86
References

Acknowledgements

List of publications

Chapter 1:

Introduction

1-4 Graphene and its research fields

Although the current electronics industry has developed based on the semiconductor material, silicon, the technical advantages from improving such performances are diminishing especially in terms of integration and miniaturization issues.[1] From the viewpoint of new flexible devices, new materials are desired for breakthrough. Carbon electronics has captured the attention of many researchers due to their potential in electronics applications as well as environmental impact and harmlessness to human bodies.[2-4] The use of nanocarbon materials for electronics can realize extremely small and novel electronic devices for future technologies.[5]

Carbon has the atomic number 6 and electrons occupy the $1s^2$, $2s^2$, $2p_x^1$, and $2p_y^1$ atomic orbitals in the ground state. Pure carbon material exists in several different allotropes, thanks to the formation of sp-, sp^2-, and sp^3- hybridized orbitals, with carbon atoms. The most well known allotropes are diamond (sp^3) which is an electrical insulator and graphite (sp^2) which is electrically conductive material. These materials have different atomic structures reflecting different bonding orbitals. Figure 1.1 describes the formation of sp^2 hybrid orbitals, which is the bonding in a graphene sheet (as well as graphite). Carbon atoms have four valence electrons, two in the 2s subshell and two in the 2p subshell, and electrons in 1s

which are not available for bonding. When three carbon atoms make use of sp^2 hybrid orbitals for σ bonding, the three bonds lie on the same plane, where the bond angle between the hybridized orbitals is 120°. Then, one set of π bond electrons are left and free electrons contributing to conduction exist above and below the plane of carbon atoms in graphene.

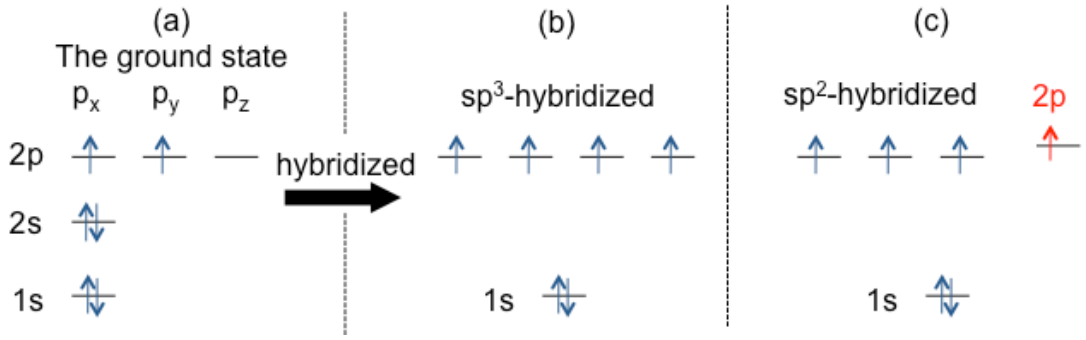

Figure 1.1 Atomic orbital diagram of a carbon atom. The four electrons in the doubly occupied spherical and the half occupied dumbbell-shaped 2p-orbitals participate in the chemical bonding of carbon. (a) Ground states, (b) sp^3-hybridised as in a diamond, and (c) sp^2-hybridised as in graphite and graphene.

In the following three sections, nanocarbon materials, especially "graphene", as well as their possible applications are briefly introduced. I then discuss our challenges of this thesis in detail, including motivation for the control and characterization of the domain structure of chemical vapor deposition (CVD)-grown graphene.

1-4.1 Nanocarbon materials

Nanocarbon materials, such as fullerenes, carbon nanotubes (CNTs), and graphene, have attracted great interest of researchers due to their novel properties. A basic building of allotropes of carbon materials with sp^2-hybridized orbitals is depicted in Figure 1.2. The graphene sheet is tightly packed into a two-dimensional (2D) honeycomb lattice and other carbon allotropes can be geometrically constructed as variations on the lattice structure of graphene; wrapped up into 0D fullerenes, rolled into 1D CNTs or

stacked into 3D graphite.[6]

Figure 1.2 Illustration of nanocarbon materials with different dimensionalities ((b) fullerene, (c) CNT, and

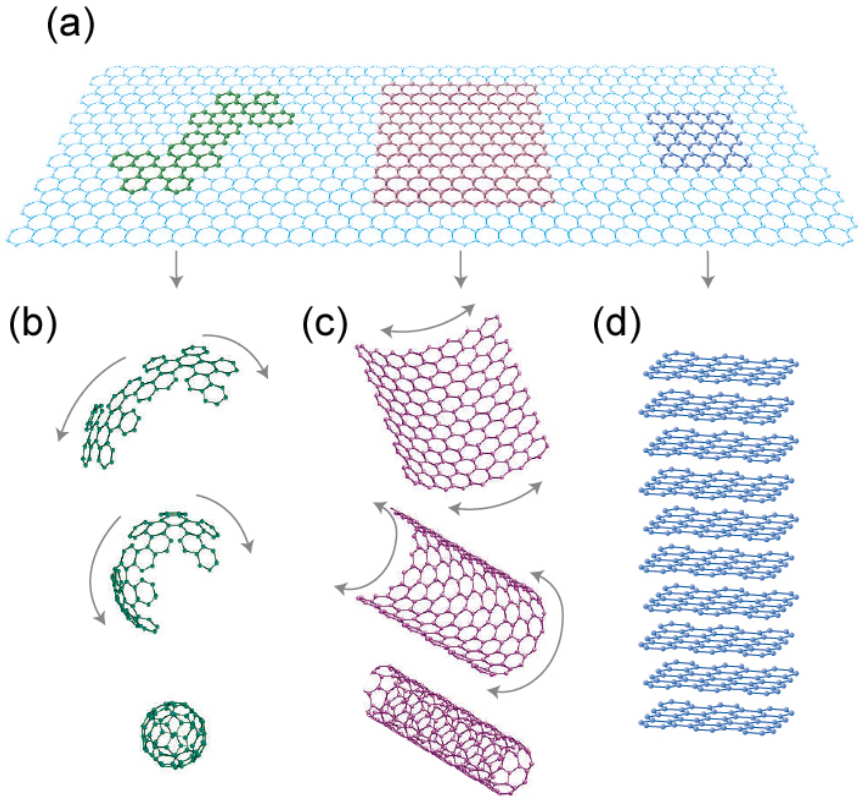

(d) graphite) building from 2D graphene film (a) (adapted from [6]).

CNTs have a cylindrical structure rolled up of graphene sheet (Figure 1.2(c)). Prof. Sumio Ijima discovered them in 1991 while working in NEC by using transmission electron microscopy (TEM).[7,8] Depending on how single-walled CNTs (SWCNTs) are rolled, their diameter, precise atomic structure, and electrical structure (metallic- or semiconducting-) vary. SWCNTs have a diameter around 1 nm as well as aspect ratios significantly exceeding that of any other known material, effectively making them one-dimensional objects. Similar to graphene, CNTs show very high carrier mobility and mechanical strength.[9,10] Also, graphene can be wrapped up into a spherical shape, forming a zero-dimensional structure, so called "fullerene" (also known as buckyball) (Figure 1.2 (b)). They were discovered in 1985 and the 60-carbon (C_{60}) buckyball was the first carbon nanomaterial to gain widespread attention.[11]

Even though they are not the focus of this thesis, they have great potentials in various fields, especially in electronics and related fields.

1-4.2 Graphene

Graphene is a single atomic layered sheet of sp^2-hybridized carbon atoms with a hexagonal lattice, as shown in Figure 1.2a, and shows unique physical properties, such as extremely high carrier mobility, high optical transparency, and superior mechanical flexibility.[12-16] However, graphene has no band gap so that it cannot completely turn off a current flow even when tuned by electric gating. This has prevented graphene from being used as the active material in logic transistors so far. The electronic structure of graphene will be explained in more detail in Chapter 2-1. Nevertheless, possibilities for the use of graphene in electronics applications either as a metal or semiconductor still exist because of its excellent unique physical properties.

Here, graphene history is briefly introduced (Figure 1.3).[17] The earliest reports related to graphene oxide (or graphite oxide) (GO) and graphite intercalation compounds (GICs) can be traced back to the 1840s and they were popular research topics for more than 100 years.[18-22] Also, some theoretical works on graphite had been done during the 1970s and the fact that effectively massless charge carriers in graphene would carry electric current was predicted theoretically in 1984.[23] The growth of graphene on metal surfaces have been reported since the 1970s, but strong interactions with the metal surface always prevented the true properties of graphene being measured experimentally.[24-26] Around the same time, graphene produced from silicon carbide had been demonstrated.[27] Regarding the name of atomic layered sheet of carbons, “graphene” was defined in 1986 since Boehm et al. recommended standardizing the term as “the ending -ene is used for fused polycyclic aromatic hydrocarbons”.[28,29]

In 2004, two researchers Andre Geim and Konstantin Novoselov at Manchester University, United

Kingdom (UK), discovered a new approach to produce graphene through mechanical exfoliation by using the scotch tape.[30] In the first publication, the ambipolar electric field effect on graphene which is a semimetal with a tiny overlap between valence and conductance bands was discussed.[30] Subsequently, the quantum Hall effect even at room temperature was reported.[12,31,32] This simple and useful exfoliation method made huge and widespread impact on graphene research in many areas of physics and materials science, and Geim and Novoselov won the Nobel Prize in Physics in 2010; *"for groundbreaking experiments regarding the two-dimensional material graphene"*.[33,34]

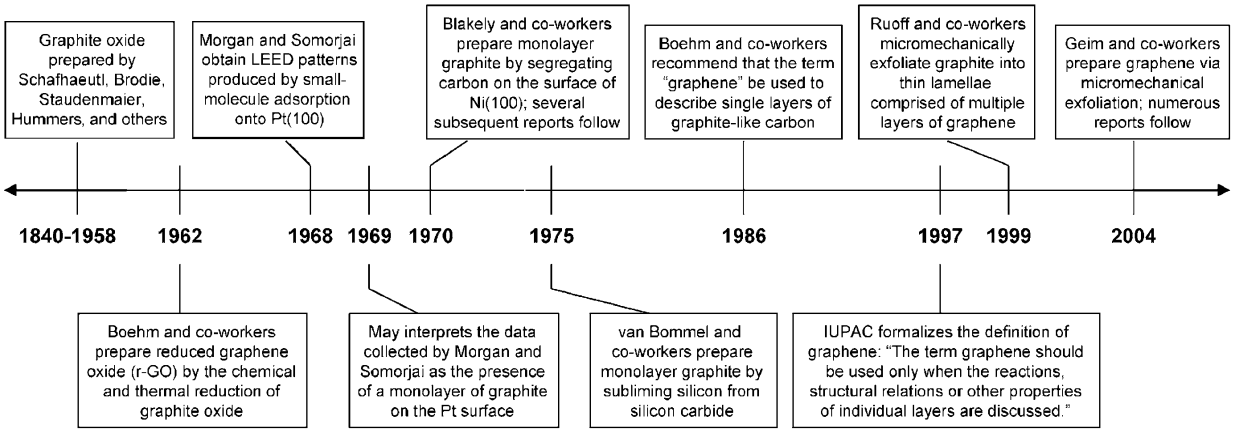

Figure 1.3 Timeline of graphene history selected events in the preparation, isolation, and characterization. (adapted from [17])

1-4.3 Applications

Graphene's unique physical properties can bring about various applications, e.g. transparent electrodes for touch panels,[35] solar cells,[36] integrated circuits,[37] high-frequency transistors,[38] capacitors,[39] sensors,[40] photonics, plasmonics, and broadband optoelectronic devices,[41] and energy storage devices.[42,43] In particular, many researchers in the world have been interested in developing electronics applications of graphene. These electronic devices inevitably require large-area graphene with high

crystallinity.

1-5 Motivation and purpose

For realization of graphene applications, a scalable process is required. CVD growth over the surface of transition metal films is one promising method to offer large-area graphene with low cost.[35,44,45] The CVD growth on a Cu catalyst is most widely studied due to the preferential growth of single-layer grpahene thanks to the low carbon solubility. However, recent works demonstrate that the single-layer graphene films are polycrystalline, consisting of a number of small graphene domains whose orientations are randomly distributed due to nature of Cu catalysts.[46,47] The domain boundaries are believed to significantly influence the electrical, mechanical, thermal, and magnetic properties of graphene.[48-53] Thus, tailoring the domain structure of CVD-grown graphene and investigation of physical properties at domain boundaries are essential challenges. Moreover, developing observation methods of the domain structure is also an important issue.

In this thesis, therefore, controlling the domain structure and characterization of domain boundaries in single-layer graphene grown by CVD method have been studied. To observe and discuss domain structure in CVD-grown graphene grown on Cu catalyst, new observation methods are also explored.

1-6 Outline of this thesis

Chapter 1 is the introduction part of this thesis where graphene, its research fields, and motivation and purpose are explained. In Chapter 2, the overviews of the fundamental structure and physical properties and preparation methods of graphene are described. In particular, graphene synthesized by the CVD method is discussed in more detail. Chapter 3 presents crystalline plane-dependent graphene orientation using heteroepitaxial Cu(111) and Cu(100) films. Subsequently in Chapter 4, the domain boundaries

between two large hexagonal graphene domains are characterized in terms of electrical transport properties and structural defects. These studies relate to the growth mechanism and domain structure of CVD-grown graphene, which is very important for the future development of graphene-based electronics. In Chapter 5, the self-assembled structure of dipole phthalocyanine molecules, chloro-aluminum phthalocyanine (ClAlPc), on graphene grown on a Cu film is discussed. Finally, in Chapter 6, the results are concluded and future outlook for graphene and 2D nanosheets (beyond graphene materials) is presented.

References:

[1] A. Aizcorbe, Moore's Law and the Semiconductor Industry: A Vintage Model. *Scand. J. of Economics* **107**, 603 (2005).

[2] P. Avouris, Z. Chen, V. Perebeinos, Carbon-based electronics. *Nat. Nanotechnol.* **2**, 605 (2007).

[3] T. W. Kelley, T. W. Kelley, P. F. Baude, C. Gerlach, D. E. Ender, D. Muyres, M. A. Haase, D. E. Vogel, S. D. Theiss, Recent Progress in Organic Electronics: Materials, Devices, and Processes. *Chem. Mater*. **16**, 4413 (2004).

[4] J. R. Heath, Molecular Electronics. *Annual Rev. Mater. Res.* **39**, 1 (2009).

[5] W. Lu, C. M. Lieber, Nanoelectronics from the Bottom Up. *Nat. Mater.* **6**, 841 (2007).

[6] A. K. Geim, K. S. Novoselov, The Rise of Graphene. *Nat. Mater.* **6**, 183 (2007).

[7] S. Iijima, Helical Microtubules of Graphitic Carbon *Nature* **354**, 56 (1991).

[8] S. Iijima, T. Ichihashi, Single-Shell Carbon Nanotubes of 1-nm diameter. *Nature*, **363**, 603 (1993).

[9] R. Saito, G. Dresselhaus, M. S. Dresselhaus, Physical Properties of Carbon Nanotubes, Imperial College Press, London (1998).

[10] G. Dresselhaus, M. S. Dresselhaus, P. C. Eklund, Science of Fullerene and Carbon Nanotubes, Academic Press, New York, NY, San Diego, CA (1996).

[11] H. W. Kroto, J. R. Heath, S. C. O'brine, R. F. Curl, R. E. Smallley, C_{60}: Buckminsterfullerene *Nature* **318**, 162 (1985).

[12] K. S. Novoselov, Z. Jiang, Y. Zhang, S. V. Morozov, H. L. Stormer, U. Zeitler, J. C. Maan, G. S. Boebinger, P. Kim, A. K. Geim, Room-Temperature Quantum Hall Effect in Graphene. *Science* **315**, 1379 (2007).

[13] F. Schwierz, Graphene transistors. *Nat. Nanotech.* **5**, 487 (2010).

[14] M. H. Rümmeli, C.G. Rocha, F. Ortmann, I. Ibrahim, H. Sevincli, F. Börrnert, J. Kunstmann, A. Bachmatiuk, M. Pötschke, M. Shiraishi, et al. Graphene: Piecing It Together. *Adv. Mater.* **23**, 447 (2011).

[15] Z. Sun, D. K. James, J. M. Tour, Graphene Chemistry: Synthesis and Manipulation. *J. Phys. Chem. Lett.* **2**, 2425 (2011).

[16] X. Huang,Z. Yin, S. Wu, X. Qi, Q. He, Q. Zhang, Q. Yan, F. Boey, H. Zhang, Graphene-Based Materials: Synthesis, Characterization, Properties, and Applications. *Small* **7**, 1876 (2011).

[17] D. R. Dreyer, R. S. Ruoff, C. W. Bielawski, From Conception to Realization: An Historial Account of Graphene and Some Perspectives for Its Future. *Angew. Chem. Int. Ed.* **49**, 9336 (2010).

[18] C. Schafhaeutl, Ueber die Verbindungen des Kohlenstoffes mit Silicium, Eisen und anderen Metallen, welche die verschiedenen Gallungen von Roheisen, Stahl und Schmiedeeisen bilden. *J. Prakt. Chem.* **21**, 129 (1840).

[19] C. Schafhaeutl, On the Combinations of Carbon with Silicon and Iron, and Other Metals, Forming the Different Species of Cast Iron, Steel, and Malleable Iron. *Phil. Mag.* **16**, 570 (1840).

[20] H.-P. Boehm, E. Stumpp, Citation Errors Concerning the First Report on Exfoliated Graphite. *Carbon* **45**, 1381 (2007).

[21] D. R. Dreyer, S. Park, C. W. Bielawski, R. S. Ruoff, The Chemistry of Graphene Oxide. *Chem. Soc. Rev.* **39**, 228 (2010).

[22] W. Gao, L. B. Alemany, L. Ci, P. M. Ajayan, New Insights into the Structure and Reduction of Graphite Oxide. *Nat. Chem.* **1**, 403 (2009).

[23] G. W. Semenoff, Condensed-Matter Simulation of a Three-Dimensional Anomaly. *Phys. Rev. Lett.* **53**, 2449 (1984).

[24] A. E. Morgan, G. A. Somorjai, Low Energy Electron Diffraction Studies of Gas Adsorption on the Platinum (100) Single Crystal Surface. *Surf. Sci.* **12**, 405 (1968).

[25] J. M. Blakely, J. S. Kim, H. C. Potter, Segregation of Carbon to the (100) Surface of Nickel. *J. Appl. Phys.* **41**, 2693 (1970).

[26] T. A. Land, T. Michely, R. J. Behm, J. C. Hemminger, G. Comsa, STM Investigation of Single Layer Graphite Structures Produced on Pt(111) by Hydrocarbon Decomposition. *Surf. Sci.* **264**, 261 (1992).

[27] A. J. van Bommel, J. E. Crombeen, A. van Tooren, LEED and Auger Electron Observations of the SiC(0001) Surface. *Surf. Sci*. **48**, 463 (1975).

[28] H. P. Boehm, R. Setton, E. Stumpp, Nomenclature and Terminology of Graphite Intercalation Compounds. *Carbon* **24**, 241 (1986).

[29] E. Fitzer, K.-H. Köchling, H. P. Boehm, H. Marsh, Recommended Terminology for the Description of Carbon as a Solid. *Pure Appl. Chem.* **67**, 473 (1995).

[30] K. S. Novoselov, A. K. Geim, S. V. Morozov, D. Jiang, Y. Zhang, S. V. Dubonos, I. V. Grigorieva, A. A. Firsov, Electric Field Effect in Atomically Thin Carbon Films. *Science* **306**, 666 (2004).

[31] K. S. Novoselov, A. K. Geim, S. V. Morozov, D. Jiang, M. I. Katsnelson, I. V. Grigorieva, S. V. Dubonos, A. A. Firsov, Two-dimensional Gas of Massless Dirac Fermions in Graphene. *Nature* **438**, 197 (2005).

[32] Y. Zhang, Y.-W. Tan, H. L. Stormer, P. Kim, Experimental Observation of the Quantum Hall Effect and Berry's Phase in Graphene, *Nature* **438**, 201 (2005).

[33] A. K. Gime, Nobel Lecture: Random Walk to Graphene. *Rev. Mod. Phys*. **83**, 851 (2011).

[34] K. S. Novoselov, Nobel Lecture: Graphene: Materials in the Flatland. *Rev. Mod. Phys.* **83**, 837 (2011).

[35] S. Bae, H. Kim, Y. Lee, X. Xu, J. S. Park, Y. Zheng, J. Balakrishnan, T. Lei, H. R. Kim, Y. I. Song, Y.-J. Kim, K. S. Kim, B. Özyilmaz, J.-H. Ahn, B. H. Hong, S. Iijima, Roll-to-Roll Production of 30-in. Graphene Films for Transparent Electrodes. *Nat. Nanotechnol.* **5**, 574 (2010).

[36] H. Park, P. R. Brown, V. Bulovic, J. Kong, Graphene As Transparent Conducting Electrodes in Organic Photovoltaics: Studies in Graphene Morphology, Hole Transporting Layers, and Counter Electrodes. *Nano Lett.* **12**, 133 (2012).

[37] Y. M. Lin, A. V. Garcia, S. J. Han, D. B. Farmer, I. Meric, Y. Sun, Y. Wu, C. Dimitrakopoulos, A. Grill, P. Avouris, K. A. Jenkins, Wafer-Scale Graphene Integrated Circuit. *Science* **332**, 1294 (2011).

[38] T. M. Lin, C. Dimitrakopoulos, K. A. Jenkins, D. B. Farmer, H. Y. Chiu, A. Grill, P. Avouris, 100-GHz Transistors from Wafer- Scale Epitaxial Graphene. *Science*, **327**, 662 (2011).

[39] J. Chen , C. Li , G. Shi, Graphene Materials for Electrochemical Capacitors. *J. Phys. Chem. Lett.* **4**, 1244 (2013).

[40] Y. Ohno, K. Maehashi, Y. Yamashiro, K. Matsumoto, Electrolyte-Gated Graphene Field-Effect Transistors for Detecting pH and Protein Adsorption. *Nano Lett.* **9**, 3318 (2009).

[41] Q. Bao, K. P. Loh, Graphene Photonics, Plasmonics, and Broadband Optoelectronic Devices. *ACS Nano*, **6**, 3677 (2012).

[42] S.-K. Lee, K. Rana, J.-H. Ahn, Graphene Films for Flexible Organic and Energy Storage Devices. *J. Phys. Chem. Lett*. **4**, 831 (2013).

[43] L. Dai, D. W. Chang, J.-B. Baek, W. Lu. Carbon Nanomaterials for Advanced Energy Conversion and Storage. *Small* **8**, 1130, (2012).

[44] A. Reina, X. Jia, J. Ho, D. Nezich, H. Son, V. Bulovic, M. S. Dresselhaus, J. Kong, Large Area, Few-Layer Graphene Films on Arbitrary Substrates by Chemical Vapor Deposition. *Nano Lett*. **9**, 30 (2009).

[45] X. Li, W. Cai, J. An, S. Kim, J. Nah, D. Yang, R. Piner, A. Velamakanni, I. Jung, E. Tutuc, S. K. Banerjee, L. Colombo, R. S. Ruoff, Large-Area Synthesis of High-Quality and Uniform Graphene Films on Copper Foils. *Science*, **324**, 1312 (2009).

[46] P. Y. Huang, C. S. Ruiz-Vargas, A. M. van der Zande, W. S. Whitney, M. P. Levendorf, J. W. Kevek, S. Garg, J. S. Alden, C. J. Hustedt, Y. Zhu, Grains and Grain Boundaries in Single-Layer Graphene Atomic Patchwork Quilts. *Nature* **469**, 389 (2011).

[47] K. Kim, Z. Lee, W. Regan, C. Kisielowski, M. F. Crommie, A. Zettl, Grain Boundary Mapping in Polycrystalline Graphene. *ACS Nano* **5**, 2142 (2012).

[48] O. V. Yazyev, S. G. Louie, Electronic Transport in Polycrystalline gGaphene. *Nat. Mater.* **9**, 806 (2010).

[49] S. Malola, H. Häkkinen, P. Koskinen, Structural, Chemical, and Dynamical Trends in Graphene Grain Boundaries. *Phys. Rev. B* **81**, 165447 (2010).

[50] R. Grantab, V. B. Shenoy, R. S. Ruoff, Anomalous Strength Characteristics of Tilt Grain Boundaries in Graphene. *Science* **330**, 946 (2010).

[51] M. A. Bissett, W. Izumida, R. Saito, H. Ago, Effect of Domain Boundaries on the Raman Spectra of Mechanically Strained Graphene. *ACS Nano* **6**, 10229 (2012).

[52] J. Cervenka, M. I. Katsnelson, C.F.J. Flipse, Room-Temperature Ferromagnetism in Graphite Driven by Two-Dimensional Networks of Point Defects. *Nat. Phys*. **5**, 840 (2009).

[53] A. Mesaros, S. Papanikolaou, C. F. J. Flipse, D. Sadri, J. Zaanen, Electronic States of Graphene Grain Boundaries. *Phys. Rev. B* **82**, 205119 (2010).

Chapter 2:

Graphene

2-1 Fundamental structure and physical properties of graphene[1-5]

Fundamental structure of graphene

In graphene (a single layer of graphite), sp^2-carbon atoms form in-plane covalent bonds affecting the planar hexagonal "honeycomb structure". Graphene has a lattice constant $a=\sqrt{3}a_0$ where $a_0 \approx 0.142$ nm is the carbon-carbon bond distance. The unit cell of graphene can be taken as the area enclosed by the rhombus with a basis of two atoms (A and B) in Figure 2.1a. The blue and yellow circles represent sites of the corresponding A and B triangular sublattices. The real space basis vectors of unit cell $\boldsymbol{a}_1$ and $_2$ are written as

$$\boldsymbol{a}_1=\begin{pmatrix}\sqrt{3}a/2\\ a/2\end{pmatrix}, \boldsymbol{a}_2=\begin{pmatrix}\sqrt{3}a/2\\ -a/2\end{pmatrix} \quad (2.1)$$

When the first Brillouin zone is selected as shown in Figure 2.1b, we obtain three high symmetry points; Γ, K, and M as indicated. The reciprocal basis vectors $\boldsymbol{b}_1$ and $\boldsymbol{b}_2$ can be represented as

$$\boldsymbol{b}_1=\begin{pmatrix}2\pi/\sqrt{3}a\\ 2\pi/a\end{pmatrix}, \boldsymbol{b}_2=\begin{pmatrix}2\pi/\sqrt{3}a\\ -2\pi/a\end{pmatrix} \quad (2.2)$$

Thus, the reciprocal lattice constant is $4\pi/\sqrt{3}$.

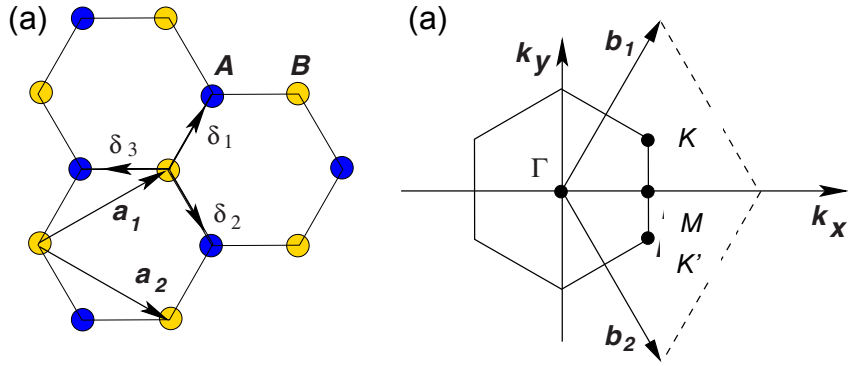

Figure 2.1 Crystal structure and Brillouin zone of graphene. (A) Real space lattice of graphene made out of two interpenetrating triangular lattices. $\boldsymbol{a}_1$ and $\boldsymbol{a}_2$ are real space basis vectors of the unit cell. (B) The first Brillouin zone in reciprocal lattice. $\boldsymbol{b}_1$ and $\boldsymbol{b}_2$ are reciprocal basis vectors. Three high symmetry points *Γ*, *K*, and *M* are labeled (adapted from [2]).

The term "graphene" is used often for ultrathin graphite layers. However, the electronic properties of graphene depend strongly on the number of graphene layers. The interplane distance between two adjacent graphene layers in AB stacked graphite is 0.335 nm. Only single-layer graphene (SLG) and double-layer graphene (DLG) are zero-gap semiconductors with a single type of electrons and holes. In the case of the so-called few layer graphene (FLG, 3 to 10 ~ layers), the valence and conduction bands overlap, and several charge carriers (electrons or holes) appear.

Electronic structure of graphene

The atomic orbitals of the carbon atoms hybridize in the sp^2 configuration in graphene, leaving one set of p_z orbitals perpendicular to the graphene plane to form delocalized π (occupied or valence band) and π^* bonds (unoccupied or conduction band). A tight binding calculation is applied to describe the band structure of single-layer graphene by considering only nearest neighbor interactions. In this simplest approximation, the dispersion relation in graphene can be written as:[4]

$$E^{\pm}(k_x, k_y) = \pm\gamma_0\sqrt{1 + 4\cos\frac{\sqrt{3}k_x a}{2}\cos\frac{k_y a}{2} + 4\cos^2\frac{k_y a}{2}} \qquad (2.3)$$

where a is $\sqrt{3}a_0$, γ_0 is the nearest neighbor overlap integral, and $\mathbf{k} = (k_x, k_y)$is the electron wave vector. The resulting band structure is shown in Figure 2.2. The occupied valence and empty conduction bands meet at the highly symmetric K and K' points. In intrinsic (non-doped) graphene, the Fermi level E_F is situated at the point known as the Dirac or charge neutrality points. Since it is further indicated that the electronic density of states (DOS) precisely vanishes at these points, graphene is classified into a zero band gap material.

The electrical properties of graphene reflect the energy band structure at the Dirac points as shown in Figure 2.2 (right). The linear dispersion relationship between energy $E(\boldsymbol{k})$ and momentum k can be approximated to first order as

$$E(\boldsymbol{k}) = \pm v_F k \qquad (2.4)$$

where $\underset{k}{\rightarrow}$ is the wave vector measured relative to the Dirac points, and $v_F \approx 10^6$ m/s is the Fermi velocity. Therefore, charge carriers in graphene close to the Dirac points thus behave as massless Dirac Fermions.

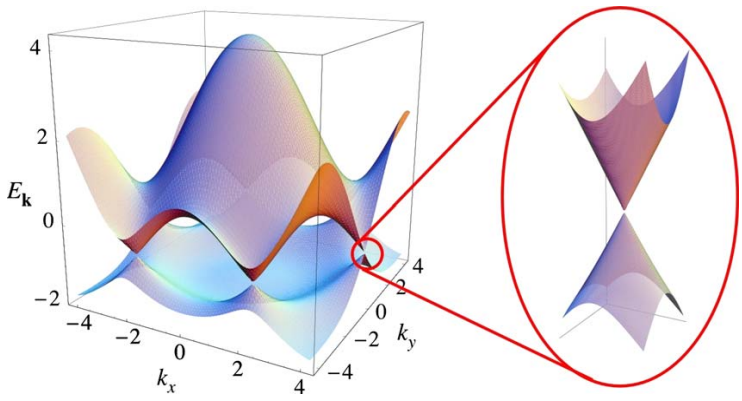

Figure 2.2 Three-dimensional band structure of graphene. The valence and conduction bands meet at the Dirac points. The right figure is zoomed the one of Dirac points showing the linear dispersion relation at small k values. (adapted from [2])

2-2 Preparation methods of graphene films

There are several preparation methods of graphene: mechanical exfoliation, chemical reduction of graphene oxide (GO), epitaxial growth on a silicon carbide (SiC) substrate by thermal decomposition, and chemical vapor deposition (CVD).[5-22]

- *Mechanical exfoliation*

Due to the layered structure of graphite with weak π–π stacking, a simple approach to obtain a 2D sheet by the exfoliation technique is to peel off carbon layer-by-layer from graphite mechanically and/or chemically. Mechanical exfoliation involves attaching an adhesive tape to the surface of graphite, such as Kish graphite (single crystal graphite flakes) and highly ordered pyrolytic graphite (HOPG), to obtain a flake, applying a force, and rubbing it against another substrate to reduce the thickness. Exfoliated graphene has originally been used to investigate physical properties of graphene because it could give highly crystalline graphene flakes. However, the flake size is limited up to several micrometers, and it lacks uniformity in the number of layers.[5]

- *Reduced-GO (r-GO)*

Chemical reduction of GO is a possible route for the large-scale production and manipulation of graphene.[6-8] The most common method to produce GO is the Hummers method, which is one example of the chemical exfoliation of graphite.[9] GO is strongly hydrophilic due to the attachment of epoxide and hydroxyl groups to the basal planes and carbonyl and carboxyl groups at the edges. In the following steps, partial reduction of GO can be achieved by treating with hydrazine hydrate, hydrogen plasma, or a strong pulse of light. Some defects and the attached functional groups still remain in r-GO. Thus, the quality of r-GO is limited by the precursor quality and the efficiency of the reducing agent (or process).

- *Epitaxial Growth on SiC Substrate*

Epitaxial growth of graphene is achievable on insulating (or semiconducting) SiC substrates. By annealing at high temperature, sublimation of silicon atoms on the surface of SiC substrate occurs, reconstructing graphene on the top of the substrate. This technique is very clean because no metal or hydrocarbons are needed during the growth. Moreover, the grown graphene can be patterned using standard lithography. Although the technique is suitable for radio and THz frequency electronics where excellent performance is required, the price of the initial SiC wafer is relatively expensive compared to that of silicon wafers.[10,11] In addition, graphene transfer is difficult due to the formation of buffer layer.

- *CVD growth*

As mentioned in Chapter 1, the CVD method can produce large-area graphene, and is scalable for industrial production because the sizes of graphene are limited only by the metal film and furnace size.[12,13] CVD graphene on a metal film is easy to transfer to a target substrate, e.g. a SiO_2/Si substrate and plastic materials. In addition, it is possible to control the number of layers and the shape of the graphene film by optimization of the growth conditions. A carbon source, such as hydrocarbon gases, is introduced into a reactor and decomposed at high temperature. Subsequently, a graphene film grows on the surface of a metal film catalyst. Indeed, graphene growth has been demonstrated on a variety of transition metals; Ni,[14,15] Co,[16,17] Ru,[18,19] Ir,[20] Pd[21], and Cu.[22] In particular, CVD growth on a Cu catalyst is one of the most promising and widely employed methods to produce large-area single-layer graphene due to the low carbon solubility and low cost of Cu.

2-3 Growth mechanism of CVD-grown graphene on metal catalysts[23-27]

During the CVD growth, hydrocarbon gases are fed into the reactor, such as a quartz tube covered with an electrical furnace, and pass over the surface of metal catalyst at elevated temperature. The catalyst decomposes the hydrocarbon gases to provide a supply of carbon atoms, and a graphene film is formed on

the catalyst surface. There are multiple nucleation sites of graphene domains across the surface. In general, each domain has one or more crystal orientations distinct from neighboring domains, and as a result their interfaces form domain boundaries.[28,29] The grain boundaries and the surface roughness of Cu are known to stimulate the graphene nucleation.[30,31] Because various parameters of CVD growth, e.g. temperature, pressure, a balance of gases (CH_4, H_2, and Ar), crystallininity of the metal catalyst, and impurities, should be considered to control the domain structure of graphene, optimization of the CVD condition is for the most part an experimental study.

CVD growth using Cu catalysts can provide large-area and single-layer graphene, and Cu foil is most widely used as a catalyst metal. This is because Cu metal has a relatively low C solubility (0.001−0.008 wt % at 1083 °C) compared with that of like Ni (or Co) (≈0.6 wt % at 1326 °C).[22,23,32,33] Figure 2.3 shows the phase diagram of Ni-C and Cu-C. The low C solubility can limit the C atom diffusion into the Cu catalyst, leading to graphene growth only on the surface.[23] Furthermore, it is able to stabilize graphene π electrons with only weak bonds on the Cu surface because of Cu's electron configuration (3d orbitals are fully occupied).

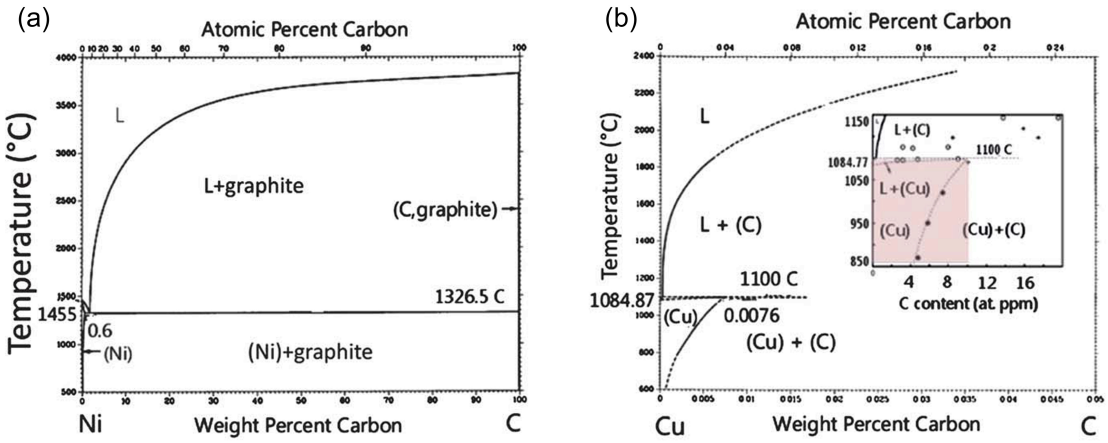

Figure 2.3 Phase diagrams of nickel and carbon (Ni-C) (a) and copper and carbon (Cu-C) (b).[32,33] (adapted from [23])

2-4 Domain structure of CVD-grown graphene

2-4.1 Morphology and observation of domain structure

Recently, it is found that CVD-grown graphene grown on Cu foil is polycrystalline consisting of a number of small domains that are separated by domain boundaries. The presence of domian boundaries in polycrystalline graphene films are theoretically predicted to alter its electronic,[34,35] mechanical,[36,37] and chemical properties,[38] from those of the pristine perfect graphene lattice.

Various techniques have been reported to observe spatially resolved information about the domain structure in graphene. High-resolution transmission electron microscopy (HR-TEM)[29,39] and scanning tunneling microscopy (STM)[40,41] can provide atomic scale images of the graphene lattice, although the observation areas are limited. The imaging process based on electron diffractions enables an observation of configuration (size and orientations) of the domain structure of graphene over large areas, because the angle distribution of graphene domains is given by selecting the diffraction conditions. Both dark-field TEM (DF-TEM) and DF low energy electron microscopy (DE-LEEM) have been successfully applied to analyze domain structures. Figure 2.4a,b shows the DF-TEM image and corresponding diffraction patterns.[29] A single crystal of graphene should give one set of diffraction, but many sets of 6-fold-symmetric spots were observed from CVD-grown graphene grown on Cu foil. In DF-TEM, by placing a small aperture at one set of diffraction allows us to selectively convert to the real space image of the graphene domains in the limited range of angles. Each color is assigned to the orientation of graphene domain in Figure 2.4a,b. Although TEM analysis can realize the visualization of domain structures as well as the atomic observation, it sometimes suffers from contamination and damage during the graphene transfer to a TEM grid. In contrast, DF-LEEM does not require a transfer process and has the advantage of obtaining information regarding graphene's orientation relative to the substrate, as shown in Figure 2.4c-f.[42] The numbers, which are 1, 2, and 3, in Figure 2.4c-f show different Cu grains.

CVD-grown graphene has many domains with different orientations even in one Cu grain. It is also able to determine the number of graphene layers from the electron reflectivity as a function of accelerating voltage in the bright field (BF)-LEEM.[43]

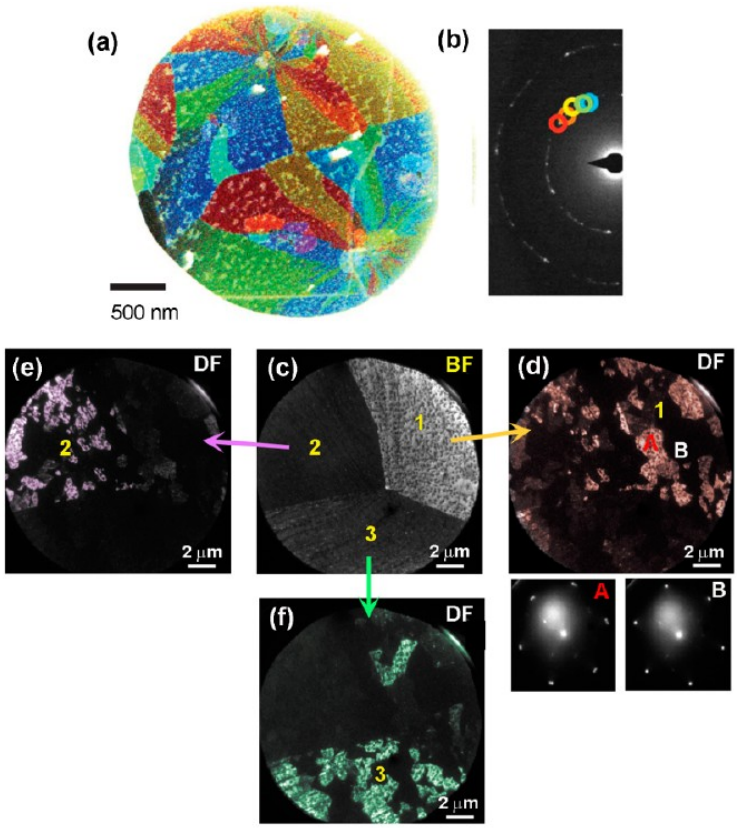

Figure 2.4 The electron micrograph of domain structures of single-layer graphene grown on Cu foil. DF-TEM image of the transferred graphene (a) and corresponding electron diffraction patterns (b).[29] Different colors are used for graphene domains with different hexagon orientations. BF-LEEM image of the as-grown graphene on Cu foil with numbers indicating different Cu grains (c) and DF-LEEM images showing the distribution of graphene domains (d-f).[42] (adapted from 24)

There are other methods to observe the graphene domains indirectly. Self-assembly of liquid crystal molecules on graphene has been utilized to visualize the domain structure using a polarized optical microscope (POM), because the orientation of adsorbed molecules can reflect the orientation of a graphene domain.[44] The spatially resolved mapping of Raman spectroscopy enables us to represent the

presence of defects in graphene[45] and the domain structure of ^{13}C- and ^{12}C-labeled graphene.[461 The CVD growth using $^{13}C/^{12}C$ isotope-labeled CH_4 also indicates that the graphene domains develop laterally with increasing growth time.

2-4.2 Electrical transport property rerated to domain boundaries in CVD-grown graphene

The grain boundaries in polycrystalline graphene are expected to induce different electronic behaviors, which reflect their atomic arrangements. The electrical transport across grain boundaries with perfectly periodic structures may be either highly transmissive or reflective over a wide range of energies, depending on the relative orientations of adjacent domains.[34] An example of such an extended defect has been experimentally identified using STM for graphene grown on nickel, as its electronic density of states exhibited metallic character, in contrast to the semimetallic properties of the perfect graphene lattice.[41] As shown in the previous section, however, grain boundaries in CVD-grown graphene form not only periodic defect structures but also imperfect atomic connections or overlap one another even on the nanometer scale.[29,39,47,48] It is important to understand the electrical impact of realistic graphene grain boundaries and its influence on transport properties of large-scale graphene device.

2-5 Recent research trends of CVD-grown graphene

Considering influences of graphene's domain structure and boundaries (Figure 2.5b) on physical and chemical properties, tailoring the domain structure, especially synthesis of single-crystalline graphene without domain boundaries (Figure 2.5a), and improving observation techniques of domain structure is required. The following section, then, explains previous researches and essential challenges. In addition, recent research to tune graphene's properties are also introduced.

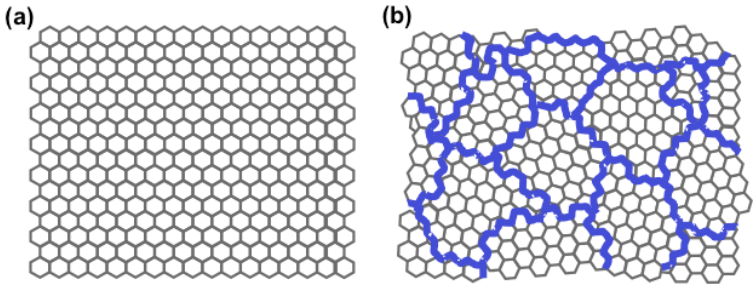

Figure 2.5 Illustration of atomic structure of graphene films; an ideal single crystal (a) and the polycrystalline CVD-grown graphene (b).

2-5.1 Synthesis of single-crystal graphene

Two approaches are proposed to realize synthesis of single-crystalline graphene. One is to obtain hexagonal single-crystal graphene domains as large as possible. In this approach, reducing the number of nucleation sites and increasing the domain size is required. Recently, large graphene domains are synthesized even on Cu foil which is polycrystalline by optimizing the CVD conditions, especially by tuning the balance of CH_4 and H_2 gases (Figure 2.6 a).[49-51]

Figure 2.6b depicts another approach which is orientation-controlled growth achieved by epitaxial CVD growth using single crystal or hetero-epitaxial metal films deposited on single-crystal sapphire (α-Al_2O_3(0001)) and/or MgO(111) substrates.[16,19,42,52] Due to the high crystallinity of the metal catalyst, graphene can epitaxially grow with respect to the crystal orientation of the catalyst.

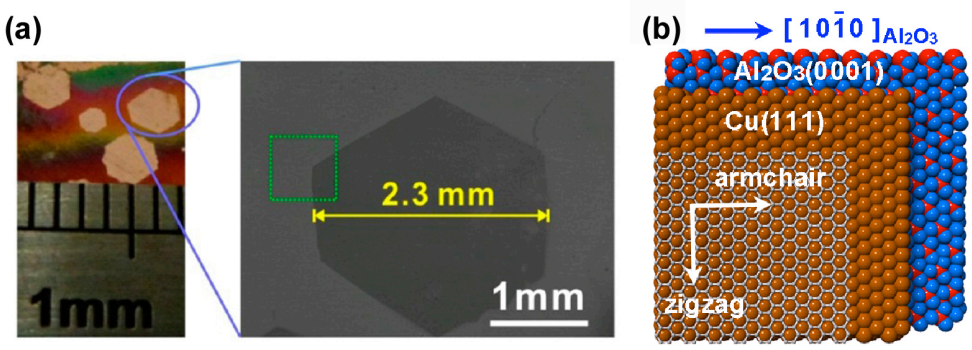

Figure 2.6 The recent achievements of synthesis of single-crystal graphene; (a) large hexagonal graphene domains (adapted from 50), and (b) illustration describing crystallographic relationship between graphene and the Cu film deposited on c-plane sapphire (adapted from 42).

2-5.2 Functionalization of graphene

Functionalized graphene is one of the key topics in graphene research for the realization of graphene-based flexible electronics. The functionalization is achieved through the formation of new covalent bonds or interaction between the functional groups and graphene, inducing some property changes for graphene.[35] Several approaches for graphene's functionalization, especially to improve tuning and modifying graphene's electronic structure, have been proposed by introducing different atoms/organic groups into graphene, such as heterogeneous atoms doping,[54-47] and diazonium coupling. [58-60] Furthermore, self-assembly of functional molecules on graphene is another promising method, because π-π interaction is a non-covalent interaction between the π orbitals of the graphene and the adsorbed molecules, thus maintaining the original sp^2-network of the graphene. [61-64]

2-6 Wet transfer process

For both fundamental and application based research, the transfer of graphene to arbitrary target substrates is required. CVD growth can provide transferrable high-quality and large-area graphene on a metal catalyst surface. However, it is a developing issue to achieve defect- and contamination-free transfer of clean graphene even now. The commonly used approach is a wet transfer assisted by a polymer (e.g. polymethyl methacrylate (PMMA), polydimethylsiloxane (PDMS), and polycarbonate (PC)) and a metal-etching, as shown Figure 2.7. [22,65] The polymer spin-coated and cured on the graphene surface serves as a supporting material. The metal catalyst film is then removed by etching solutions, leaving only the PMMA/graphene film. Aqueous iron nitrate ($Fe(NO_3)_3$) and iron chloride ($FeCl_3$) have been reported as possible etchants. The remnant etching solutions on the film is rinsed off using de-ionized (DI) water and aqueous hydrochloric acid (HCl), and then transferred onto a substrate.

Residual PMMA is removed by acetone, and a graphene film is placed on the top of the target substrate. However, this graphene transfer process is reported to sometimes cause cracks in the graphene due to gaps between the polymer/graphene films and the target substrate induced by large roughness of graphene on the metal catalyst. To this end, heating of the polymer up to its glass temperature (*Tg*) is effective way to introduce better contact between the polymer/graphene films and the substrate, avoiding cracks.[66]

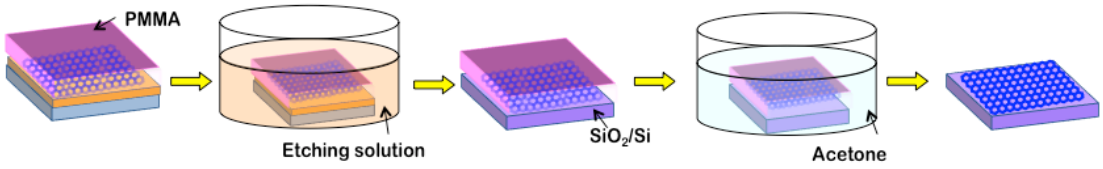

Figure 2.7 Schematic of transfer process of CVD-grown graphene using a polymer support and metal etching.

References:

[1] R. Saito, G. Dresselhaus, M. S. Dresselhaus, Physical Properties of Carbon nanotubes. Imperial College Press, London (1998).

[2] A. H. Castro Neto, F. Guinea, N. M. R. Peres, K. S. Novoselov, A. K. Geim, The Electronic Properties of Graphene. *Rev. Mod. Phys.* **81**, 109 (2009).

[3] S. D. Sarma, S. Adam, E. H. Hwang, E. Rossi, Electronic Transport in Two-Dimensional Graphene. *Rev. Mod. Phys.* **83**, 407 (2011).

[4] J. H. Warner, F. Schäffel, A. Bachmatiuk, M. H. Rümmeli, Graphene: Fundamental and Emergent applications. *Elsevier*, USA (2013).

[5] Y. H. Wu, T. Yu, Z. X. Shen, Two-Dimensional Carbon Nanostructures: Fundamental Properties, Synthesis, Characterization, and Potential Applications. *J. Appl. Phys.* **108**, 071301 (2010).

[6] S. J. Park and R. S. Ruoff, Chemical Methods for the Production of Graphenes. *Nat. Nanotech.* **4**, 217 (2009).

[7] S. Gilje, S. Han, M. Wang, K. L. Wang, R. B. Kaner, A Chemical Route to Graphene for Device Applications. *Nano Lett.* **7**, 3394 (2007).

[8] G. Eda, G. Fanchini, M. Chhowalla, Large-Area Ultrathin Films of Reduced Graphene Oxide as a Transparent and Flexible Electronic Material, *Nat. Nanotechnol.* **3**, 270 (2008).

[9] W. S. Hummers Jr., R. E. Offeman, Preparation of Graphitic Oxide. *J. Am. Chem. Soc*. **80**, 1339 (1958).

[10] C. Berger, Z. Song, X. Li, X. Wu, N. Brown, C. Naud, D. Mayou, T. Li, J. Hass, A. N. Marchenkov, E. H. Conrad, P. N. First, W. A. de Heer, Electronic Confinement and Coherence in Patterned Epitaxial Graphene. *Science* **312**, 1191 (2006).

[11] Y.-M. Lin, C. Dimitrakopoulos, K. A. Jenkins, D. B. Farmer, H.-Y. Chiu, A. Grill, 100-GHz Transistors from Wafer-Scale Epitaxial Graphene, *Science*, **327**, 662 (2010).

[12] S. Bae, H. Kim, Y. Lee, X. Xu, J. S. Park, Y. Zheng, J. Balakrishnan, T. Lei, H. R. Kim, Y. I. Song, Y.-J. Kim, K. S. Kim, B. Özyilmaz, J.-H. Ahn, B. H. Hong, S. Iijima, Roll-to-Roll Production of 30-in. Graphene Films for Transparent Electrodes. *Nat. Nanotechnol.* **5**, 574 (2010).

[13] T. Yamada, M. Ishihara, J. Kim, M. Hasegawa, S. Iijima, A Roll-to-Roll Microwave Plasma Chemical Vapor Deposition Process for the Production of 294 mm width Graphene Films at Low Temperature. *Carbon* **50**, 2615 (2012).

[14] Q. Yu, J. Lian, S. Siriponglert, H. Li, Y. P. Chen, S. S. Pei, Graphene Segregated on Ni Surfaces and Transferred to Insulators. *Appl. Phys. Lett*. **93**, 113103 (2008).

[15] A. Reina, X. Jia, J. Ho, D. Nezich, H. Son, V. Bulovic, M. S. Dresselhaus, J. Kong, Large Area, Few-Layer Graphene Films on Arbitrary Substrates by Chemical Vapor Deposition. *Nano Lett*. **9**, 30 (2009).

[16] H. Ago, Y. Ito, N. Mizuta, K. Yoshida, B. Hu, C. M. Orofeo, M. Tsuji, K. Ikeda, S. Mizuno, Epitaxial Chemical Vapor Deposition Growth of Single-Layer Graphene over Cobalt Film Crystallized on Sapphire. *ACS Nano* **4**, 740 (2010).

[17] A. Varykhalov, O. Rader, Graphene Grown on Co(0001) Films and Islands: Electronic Structure and its Precise Magnetization Dependence. *Phys. Rev. B* **80**, 35437 (2009).

[18] P. W. Sutter, J. I. Flege, E. A. Sutter, Epitaxial Graphene on Ruthenium. *Nat. Mater.* **7**, 406 (2008).

[19] S. Yoshii, K. Nozawa, K. Toyoda, N. Matsukawa, A. Odagawa, A. Tsujimura, Suppression of Inhomogeneous Segregation in Graphene Growth on Epitaxial Metal Films. *Nano Lett*. **11**, 2628 (2011).

[20] J. Coraux, A. T. N'Diaye, C. Busse, T. Michely, Structural Coherency of Graphene on Ir(111). *Nano Lett.* **8**, 565 (2008).

[21] Y. Murata, E. Starodub, B. B. Kappes, C. V. Ciobanu, N. C. Bartelt, K. F. McCarty, S. Kodambaka, Orientation-Dependent Work Function of Graphene on Pd(111). *Appl. Phys. Lett*. **97**, 143114 (2010).

[22] X. Li, W. Cai, J. An, S. Kim, J. Nah, D. Yang, R. Piner, A. Velamakanni, I. Jung, E. Tutuc, S. K. Banerjee, L. Colombo, R. S. Ruoff, Large-Area Synthesis of High-Quality and Uniform Graphene Films on Copper Foils. *Science*, **324**, 1312 (2009).

[23] C. Mattevi, H. Kima, M. Chhowalla, A review of Chemical Vapor Deposition of Graphene on copper. *J. Mater. Chem.* **21**, 3324 (2011).

[24] H. Ago, Y. Ogawa, M. Tsuji, S. Mizuno, H. Hibino, Catalytic Growth of Graphene: toward large-area single-crystalline. *J. Phys. Chem. Lett.*, **3**, 2228 (2012).

[25] Y. Zhang, L. Zhang, C. Zhou, Review of Chemical Vapor Deposition of graphene and related applications. *Acc. Chem. Res.* **46**, 2329 (2012).

[26] A. W. Tsen, L. Brown, R. W. Havaerner, J. Park, Polycrystallinity and Stacking in CVD graphene. *Acc. Chem. Res.* **46**, 2286 (2012).

[27] L. P. Bir1ó, P. Lambin, Grain Boundaries in Graphene Grown by chemical Vapor Deposition *New J. Phys.* **15**, 035024 (2013).

[28] J. M. Woffoed, S. Nie, K. F. McCarty, N. C. Bartelt, O. D. Dubon, Graphene Islands on Cu Foils: The Interplay between Shape, Orientation, and Defects. *Nano Lett.* **10**, 4890 (2010).

[29] P. Y. Huang, C. S.Ruiz-Vargas, A. M.van der Zande, W. S. Whitney, M. P. Levendorf, J. W. Kevek, S. Garg, J. S. Alden, C. J. Hustedt, Y. Zhu, Grains and Grain Boundaries in Single-Layer Graphene Atomic Patchwork Quilts. *Nature*, **469**, 389 (2011).

[30] J. D. Wood, S. W. Schmucker, A. S. Lyons, E. Pop, J. W. Lyding, Effects of Polycrystalline Cu Substrate on Graphene Growth by Chemical Vapor Deposition. *Nano Lett.* **11**, 4547 (2011).

[31] Z. Luo, Y. Lu, D. W.Singer, M. E.Berck, L. A.Somers, B. R.Goldsmith, A. T. C.Johnson, Effect of Substrate Roughness and Feedstock Concentration on Growth of Wafer-Scale Graphene at Atmospheric Pressure. *Chem. Mater.* **23**, 1441 (2011).

[32] ASM Handbook Vol. 3: Alloy Phase Diagrams. *ASM International*, USA (1992).

[33] G. A. Lopez, E. J. Mittemeijer, The solubility of C in solid Cu. *Scr. Mater.* **51**, 1 (2004).

[34] O. V. Yazyev, S. G. Louie, Electronic transport in polycrystalline graphene. *Nat. Mater.* **9**, 806 (2010).

[35] A. Mesaros, S. Papanikolaou, C. F. J. Flipse, D. Sadri, J. Zaanen, Electronic states of graphene grain boundaries. *Phys. Rev. B* **82**, 205119 (2010).

[36] R. Grantab, V. B. Shenoy, R. S. Ruoff, Anomalous Strength Characteristics of Tilt Grain Boundaries in Graphene. *Science* **330**, 946 (2010).

[37] J. Kotakoski, J. Meyer, J. Mechanical properties of polycrystalline graphene based on a realistic atomistic model. *Phys. Rev. B* **85**, 195447 (2012).

[38] S. Malola, H. Häkkinen, P. Koskinen, Structural, chemical, and dynamical trends in graphene grain boundaries. *Phys. Rev. B* **81**, 165447 (2010).

[39] K. Kim, Z. Lee, W. Regan, C. Kisielowski, M. F. Crommie, A. Zettl, Grain boundary mapping in polycrystalline graphene. *ACS Nano* **5**, 2142 (2011).

[40] G. Li, A. Luican, J.M.B. Lopes dos Santos, A. H. CastroNeto, A. Reina, J. Kong, E. Y. Andrei, Observation of Van Hove singularities in twisted graphene layers. *Nat. Phys.* **6**, 109 (2009) .

[41] J. Lahiri, Y. Lin, P. Bozkurt, I. I. Oleynik, M. Batzill, M. An extended defect in graphene as a metallic wire. *Nat. Nanotechnol*. **5**, 326 (2010).

[42] C. M. Orofeo, H. Hibino, K. Kawahara, Y. Ogawa, M. Tsuji, K. Ikeda, S. Mizuno, H. Ago, Influence of Cu Metal on the Domain Structure and Carrier Mobility in Single-Layer Graphene. *Carbon* **50**, 2189 (2012).

[43] H. Hibino, K. Kageshima, F. Maeda, M. Nagase, Y. Kobayashi, H. Yamaguchi, Microscopic Thickness Determination of Thin Graphite Films Formed on SiC from Quantized Oscillation in Reflectivity of Low-Energy Electrons. *Phys. Rev. B* **77**, 75413 (2008).

[44] D. W. Kim, Y. H. Kim, H. S. Jeong, H. T. Jung, Direct Visualization of Large-Area Graphene Domains and Boundaries by Optical Birefringency. *Nat. Nanotechnol*. **7**, 29 (2012).

[45] L.M. Malard, M.A.Pimenta, G. Dresselhaus, M. S. Dresselhaus, Ramanspectroscopyin graphene. *Phys. Rep*. **473**, 51 (2009).

[46] X. Li, W. Cai, L. Colombo, R. S. Ruoff, Evolution of Graphene Growth on Ni and Cu by Carbon Isotope Labeling. *Nano Lett*. **9**, 4268 (2009).

[47] J. C. Koepke, J. D. Wood, D. Estrada, Z. Y. Ong, K. T. He, E. Pop, J. W. Lyding, Atomic-scale evidence for potential barriers and strong carrier scattering at graohene domain boundaries: a scanning tunneling microscopy study. *ACS Nano*, **2013**, *7*, 75.

[48] A. W. Robertson, J. H. Warner, Hexagonal Single Crystal Domains of Few-Layer Graphene on Copper Foils. *Nano Lett*. **11**, 1182 (2011).

[49] Q. Yu, L. A. J auregui, W. Wu, R. Colby, J. Tian, Z. Su, H. Cao, Z. Liu, D. Pandey, D. Wei, T. F. Chung, P. Peng, N. P. Guisinger, E. A. Stach, J. Bao, S. S. Pei, Y. P. Chen, Control and Characterization of Individual Grains and Grain Boundaries in Graphene Grown by Chemical Vapor Deposition. *Nat. Mater.* **10**, 443 (2011).

[50] A.W. Robertson, A. Bachmatiuk, Y. A. Wu, F. Schäffel, B. Rellinghaus, B. Büchner, M. H. Rümmeli, J. H. Warner Atomic Structure of Interconnected Few-Layer Graphene Domains. *ACS Nano* **5**, 6610 (2011).

[51] H. Zhou, W. Jong, L. Liu, R. Cheng, Y. Chen, X. Huang, Y. Liu, Y. Wang, Y. Huang, X. Duan, Chemical Vapor Deposition Growth of Large Single Crystals of Monolayer and Bilayer Graphene. *Nat. Commun.* **4**, 2096 (2013).

[52] C. V. Van, A. Kimouche, A. R. Plantey, O. Fruchart, P. B. Guillemaud, N. Bendiab, J. Coraux, Epitaxial Graphene Prepared by Chemical Vapor Deposition on Single Crystal Thin Iridium Films on Sapphire. *Appl. Phys. Lett.* **98**, 181903 (2011).

[53] M. Aliofkhazraei, Advances in Graphene Science, *InTech Europe*, Croatia (2013).

[54] D. Wei, Y. Liu, Y. Wang, Synthesis of N-doped Graphene by Chemical Vapor Deposition and its Electrical Properties. *Nano Lett*. **9**, 1752.

[55] X. Wang, X. Li, L. Zhang, N-doping of Graphene through Electrothermal Reactions with Ammonia. *Science* **324**, 768 (2009).

[56] L. Zhao, R. He, K. T. Rim, T. Schiros, K. S. Kim, H. Zhou, C. Gutiérrez, S. P. Chockalingam, C. J. Arguello, L. Pálová, D. Nordlund, M. S. Hybertsen, D. R. Reichman, T. F. Heinz, P. Kim, A. Pinczuk, G. W. Flynn, A. N. Pasupathy, Visualizing Individual Nitrogen Dopants in Monolayer Graphene. *Science* **333**, 999 (2009).

[57] L. Zhao, M. Levendorf, S. Goncher, T. Schiros, L. Pálová, A. Zabet-Khosousi, K. T. Rim, C. Gutiérrez, D. Nordlund, C. Jaye, M. Hybertsen, D. Reichman, G. W. Flynn, J. Park, A. N. Pasupathy, Local Atomic and Electronic Structure of Boron Chemical Doping in Monolayer Graphene. *Nano Lett.* **13**, 4659 (2013).

[58] S. Niyogi, E. Bekyarova, M. E. Itkis, H. Zhang, K. Shepperd, J. Hicks, M. Sprinkle, C. Berger, C. N. Lau, W. A. deHeer, E. H. Conrad, R. C. Haddon, Spectroscopy of Covalently Functionalized Graphene. *Nano Lett*. **10**, 4061 (2010).

[59] C.-J. Shih, Q. H. Wang, Z. Jin, G. L. C. Paulus, D. Blankschtein, P. Jarillo-Herrero, M. S. Strano, Disorder Imposed Limits of Mono- and Bilayer Graphene Electronic Modification Using Covalent Chemistry. *Nano Lett.* **13**, 809 (2013).

[60] M. A. Bissett, S. Konabe, S. Okada, M. Tsuji, H. Ago, Enhanced Chemical of Graphene Induced by Mechanical Strain. *ACS Nano* **7**, 10335 (2013).

[61] Z. Zhang, H. Huang, X. Yang, L. Zang, Tailoring Electronic Properties of Graphene by π–π Stacking with Aromatic Molecules. *J. Phys. Chem. Lett.* **2**, 2897 (2011).

[62] Q. H. Wang, M. C. Hersam, Room-Temperature Molecular-Resolution Characterization of Self-Assembled Organic Monolayers on Epitaxial Graphene. *Nat. Chem.* **1**, 206 (2009).

[63] J. Cho, J. Smerdon, L. Gao, Ö. Süzer, J. R. Guest, N. P. Guisinger, Structural and Electronic Decoupling of C60 from Epitaxial Graphene on SiC. *Nano Lett.* **12**, 3018 (2012).

[64] M. Garnica, D. Stradi, S. Barja, F. Calleja, C. Díaz, M. Alcamí, N. Martín, A. L. Vázquez de Parga, F. Martín, R. Miranda, Long-Range Magnetic Order in a Purely Organic 2D Layer Adsorbed on Epitaxial Graphene. *Nat. Phys*. **9**, 368 (2009).

[65] A. Reina, H. Son, L. Jiao, B. Fan, M. S. Dresselhouse, Z. F. Liu, J. Kong, Transferring and Identification of Single- and Few-Layer Graphene on Arbitrary Substrate. *J. Phys. Chem. C* **112**, 17741 (2008).

[66] J. W. Suk, A. Kitt, C. W. Magnuson, Y. Hao, S. Ahmed, J. An, A. K. Swan, B. B. Goldberg, R. S. Ruoff, Transfer of CVD-Grown Monolayer Graphene onto Arbitrary Substrates. *ACS Nano* **5**, 6916 (2011).

Chapter 3:

Domain structure in single-layer graphene grown on Cu (111) and Cu (100) films

Abstract:

Size, orientation, and boundaries of graphene domains were the current focus of chemical vapor deposition (CVD) growth, because they were closely related to graphene's physical properties. Here, I studied the domain structure of single-layer graphene grown by ambient pressure CVD over heteroepitaxial Cu(111) and Cu(100) films. Low energy electron microscope measurements revealed that the Cu(111) film gave uniform single-layer graphene whose orientation was consistent with the underlying Cu lattice for areas over 1 mm^2. On the other hand, single-layer graphene grown on Cu(100) film exhibited clear multi-domain structure with two main orientations rotated by 30º. Moreover, a weak intensity Raman D-band was observed along the domain boundaries for the graphene grown on the Cu(100). Our results gave new insights on the growth mechanism of CVD-grown graphene over Cu metals and offer a new direction for the realization of single-crystalline graphene.

3-5 Introduction

Recent works demonstrate that CVD graphene has a polycrystalline structure consisting of a number of small graphene domains with random orientations, reflecting the polycrystalline nature of the Cu foil. The Cu foil is consisting of a face-centered cubic (fcc) (100) plane that has a square lattice is not suitable for orientation control of graphene domains in terms of mismatch of the lattice symmetry. Even though some groups synthesized large graphene domains on Cu foil through the optimization of the growth condition, it is still challenging to connect the domains atomically at the boundaries since the neighboring graphene domains have different orientations.

On the other hand, epitaxial CVD growth is a promising approach to control the orientations of graphene domains. The low energy electron diffraction (LEED) measurement with ~1 mm spot size has proven previously that the average orientation of hexagons is controlled by using heteroepitaxial metal films,[1,2] but the microscopic domain structure has not been well understood. These previous studies only investigated the metal films with hexagonal closed packed structure (hcp) (0001) or face-centered cubic (fcc) (111) planes whose symmetry match with the graphene structure, but commonly used Cu foil has four-fold symmetry fcc(100) plane.[3,4] Microscopic analysis, mainly scanning tunneling microscope (STM) observation, has been frequently used to determine the epitaxial relationship between CVD-grown graphene and underlying single crystal Cu(111) or Cu(100) films. These works present periodic moiré structures which can be explained by an epitaxial relationship and lattice mismatch between graphene and the Cu metal.[5-10] However, such a method is not applicable to wide area inspection, and a more systematic understanding is required. In addition, clarifying the influence of the Cu crystalline plane on graphene's domain structure is important for the understanding of the growth mechanism as well as maximizing graphene's physical properties for future electronic applications.

Here, I study domain structures of large-area, single-layer graphene films grown on heteroepitaxial

Cu(111) and (100) films which are deposited on single-crystal MgO(111) and (100) substrates, respectively. Low energy electron microscope (LEEM) is used to observe the domain structure for the as-grown graphene without a transfer process. By combination with Raman analysis, I investigate the strong influence of the Cu crystalline plane on domain structure, domain size and orientation of CVD-grown graphene.

3-6 Experiment

- *Preparation of Heteroepitaxial Cu Films for the Catalyst*

Single-crystalline MgO(111) and (100) substrates were cleaned by sonicating in acetone and isopropyl alcohol. A 500 nm thick Cu film was deposited on these substrates with a power of 300 W in Ar atmosphere (0.6 Pa) by radio frequency (RF) magnetron sputtering (Shibaura Mechatoronics Corp., CFS-4ES). During sputtering, the substrate temperature was kept at 300 ºC to promote epitaxial growth of the Cu film.

- *Synthesis of GrapheneFfilms*

For the ambient pressure CVD growth of graphene, the Cu film was annealed in a mixed Ar (800 sccm) and H_2 (14.2 sccm) flow for 30 minutes at 1000 ºC, followed by switching the gas to a mixture of CH_4 (0.5 sccm), H_2 (14.2 sccm), and Ar (800 sccm) for 10 minutes. After CVD, the sample was rapidly cooled down to room temperature by taking out the sample from the furnace in the flow of Ar and H_2 gases.

- *Transfer of Graphene to SiO_2/Si Substrate*

A wet transfer process was applied. After CVD, the surface of graphene film was covered with diluted PMMA by spin-coating, and the thin PMMA was mechanically supported with thermal tape (Revalpha, Nitto-Denko).[11] Then, the Cu film was dissolved with aqueous solution containing $FeCl_3$ and HCl to

release the graphene supported with PMMA and thermal tape. The thermal tape/PMMA/graphene stack was washed with deionized water and placed on the SiO_2/Si substrate. Finally, the thermal tape was removed by heating at 120 °C, followed by PMMA removal with acetone.

- *Characterizations*

Crystallinity of the heteroepitaxial Cu films was measured by x-ray diffraction (XRD) (Riguku, RINT 2500) and scanning electron microscopy (SEM) (Zeiss, Ultra55) equipped with electron backscattered diffraction (EBSD) (TSL Solutions, OIM). LEED and LEEM analyses were performed to characterize crystal orientations of the as-grown graphene films. LEED patterns of as-grown graphene were recorded in a ultra-high vacuum (UHV) chamber of 8×10^{-9} Pa with a Spectaleed (Omicron, Germany) instrument. LEEM images and spectra were measured with Elmitec LEEM III. To remove impurity from the surface, we applied thermal annealing in vacuum before the measurement. Transferred graphene films were analyzed by optical microscope, AFM (Bruker, Nanoscope IIIa), and Raman spectroscope (Tokyo Instruments, Nanofinder30). Excitation wavelength was 532 nm.

3-7 Results and discussion

Heteroepitaxial Cu films were prepared on MgO(111) and (100) substrates at 500 ºC by radio RF magnetron sputtering. After thermal annealing in H_2/Ar flow at 1000 ºC to improve the metal crystallinity, the sample was reacted with a mixed gas of CH_4/H_2/Ar flow at the same temperature to grow graphene on the Cu surface. From XRD, the Cu film deposited on MgO(111) showed a sharp diffraction peak at ~ 42° assigned to Cu(111) diffraction (Figure 3.1a). The EBSD image clearly shows that the Cu film has (111) plane normal to the substrate and it is free from the metal grain boundary (Figure 3.1b). In particular, twin structures observed for the Cu film sputtered on sapphire at room temperature[12] are completely suppressed, resulting in high quality single-crystalline Cu(111) film due to high temperature

sputtering and MgO crystal structure. The combined analyses of XRD and EBSD prove that the whole Cu film has a Cu(111) single crystal structure. Similarly, grain boundary-free single-crystalline Cu(100) film was successfully obtained on MgO(100) substrate, as seen in Figure 3.2. LEED patterns measured at 400 eV showed three and four sharp diffraction spots from the Cu(111) and Cu(100), respectively (Figure 3.1c and 3.2c). These results also prove the high crystallinity of the Cu film.

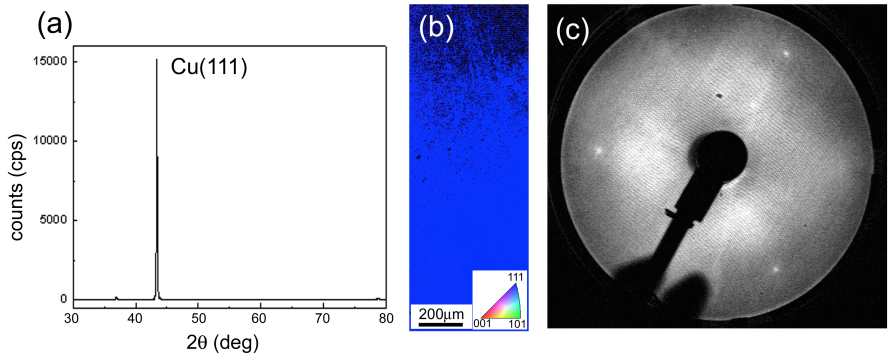

Figure 3.1 Heteroepitaxial Cu(111) film deposited on MgO(111). XRD profile (a) and EBSD data (b) of Cu films measured after CVD. (c) LEED patterns measured at high electron energy (400 eV).

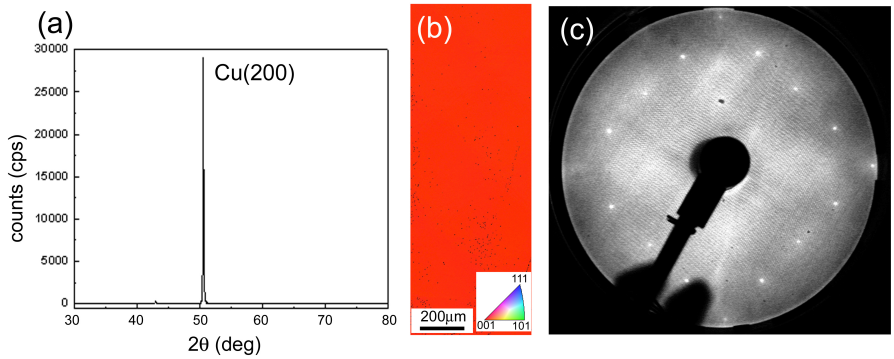

Figure 3.2 Heteroepitaxial Cu(100) film deposited on MgO(100). XRD profile (a) and EBSD data (b) of Cu films measured after CVD. (c) LEED patterns measured at high electron energy (400 eV).

After transferring both graphene films from Cu(111) and Cu(100) films onto target SiO_2/Si substrates, graphene films showed characteristic Raman spectra of single-layer graphene (Figure 3.3a and 3.4a); stronger 2D-band intensity than G-band (I_{2D}/I_G ~1.5) and narrow 2D-band with 30-40 cm^{-1} width. Negligible defect-related D-band intensity also indicates that the graphene is of high quality.[13,14] In

addition, analysis of optical contrast also supports the single-layer graphene and uniformity of the film (insets of Figure 3.3a and 3.4a).[15]

We investigated orientation of as-grown graphene on the Cu films by LEED. Shown in Figure 3.3b is LEED pattern measured with a 100 eV electron beam whose spot size is around 1 mm. The graphene formed on Cu/MgO(111) showed six sharp diffraction spots (Figure 3.3b). The analysis of the energy dependence signified that these six peaks are originated from both the graphene lattice (green circle) and Cu(111) lattice (red circle). This result proves that graphene is epitaxially formed on the Cu(111)/MgO(111). Note that Cu(111) lattice has three-fold symmetry while the graphene hexagonal lattice has six-fold symmetry. Thus, at high electron energy (400 eV), three diffraction spots coming solely from the Cu(111) lattice became prominent (Figure 3.1c). For comparison, we also performed LEED measurement for single crystalline Cu(111) substrate after surface cleaning process inside LEED chamber (not shown here). The LEED pattern of the pure Cu(111) surface is almost identical to that of graphene/Cu(111). In addition, their *I-V* curves of LEED patterns are essentially the same for the Cu(111) and graphene/Cu(111) except for the clear diffraction from graphene only at low incident electron energies. These results indicate the absence of reconstruction of Cu(111) surface due to graphene growth.

On the other hand, graphene/Cu(100)/MgO(100) showed a more complex LEED pattern (Figure 3.4b). There are two sets of diffraction patterns. We interpret that outer twelve broad streaks (green circle) are originated from graphene and inner four peaks (red) are from Cu(100) lattice, because the latter Cu(100) diffraction peaks are very sharp and become stronger with increasing the electron energy (Figure 3.2c). From the LEED pattern, it is concluded that the graphene covers the Cu surface with two preferential [10] orientations with angles of 0 ± 2º and 30 ± 2º with respect to the underlying Cu[011] lattice. Wofford et al. reported the evolution of four-lobed graphene domains in associated with square

Cu(100) lattice,[3] and our result is consistent with their observations. Note that there also exists weak and broad diffraction streak between 0º and 30º position corresponding to the mis-aligned graphene domains.

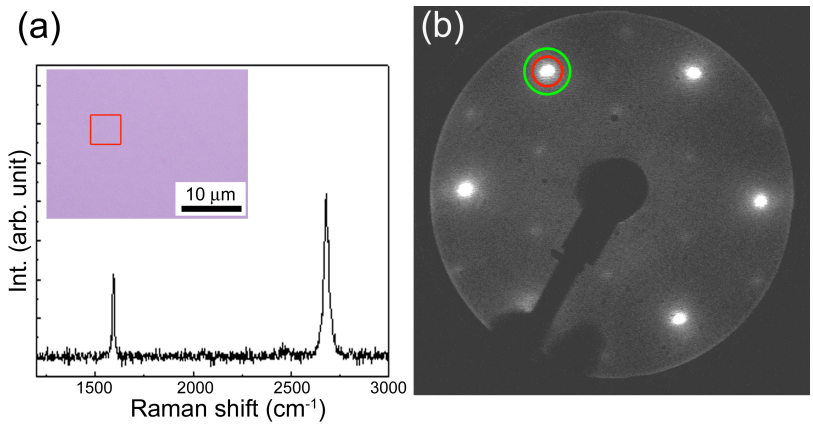

Figure 3.3 CVD graphene grown Cu(111). (a) Raman spectra and optical microscope images (inset) of graphene transferred on the SiO_2/Si substrate. (b) LEED images of as-grown graphene on Cu measured with 100 eV. Red square in (a) inset shows the area where Raman spectrum was obtained. Green and red circles in (b) show the diffraction spots originating in graphene and the underlying Cu lattice, respectively.

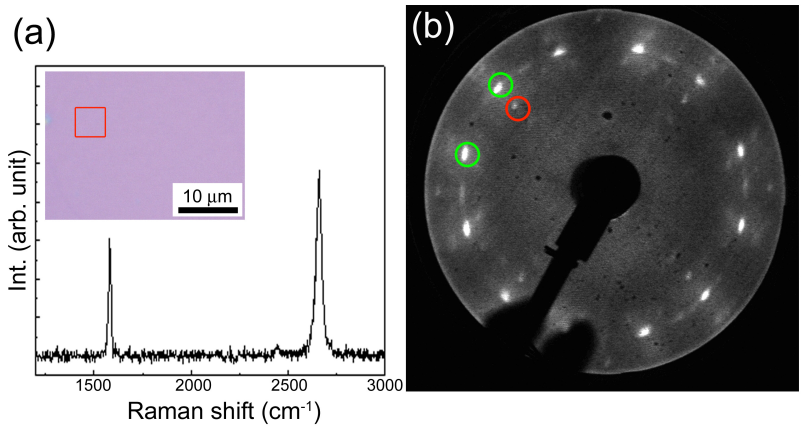

Figure 3.4 CVD graphene grown Cu(100). (a) Raman spectra and optical microscope images (inset) of graphene transferred on the SiO_2/Si substrate. (b) LEED images of as-grown graphene on Cu measured with 100 eV. Red square in (a) inset shows the area where Raman spectrum was obtained. Green and red circles in (b) show the diffraction spots originating in graphene and the underlying Cu lattice, respectively.

The above mentioned crystalline-plane dependent orientation of graphene hexagons is qualitatively consistent with the previous report.[1,3] However, the LEED analysis gives the average orientation of

graphene domains existing in a large beam spot size (~1 mm), thus it lacks information on the microscopic domain structure. Recently, spatial domain distribution was visualized by using dark-field TEM for single-layer graphene transferred from a Cu foil (Chapter 2). Relatively small graphene domains up to several μm are observed for the large-area graphene sheet. TEM observation requires a transfer process by dissolving the metal catalyst so that it is difficult to analyze the relative orientation of graphene domain against the metal lattice. In addition, TEM is not suitable for large-area inspection, partly because the graphene surface can be contaminated with PMMA residue. Another tool is STM which gives atomic resolution image of graphene on the metal. STM was used for atomic scale characterizations of single-layer graphene grown on Cu foil and single-crystalline Cu(111) and (100) films.[5-10] However, the scan area is typically very small, and it is not suitable for large-area statistical analysis.

To investigate the domain structure of the CVD-grown graphene, we measured LEEM for the graphene on the heteroepitaxial Cu films. Although LEEM is used to analyze graphene formed on metal catalyst and SiC substrates, the growth is usually done in an ultra-high vacuum chamber.[4,16] We measured the *ex-situ* LEEM for the graphene grown by the ambient pressure CVD. This ambient pressure CVD is advantageous because it is applicable to large-scale graphene growth with low cost and suppresses thermal evaporation of Cu which is problematic in vacuum CVD. In addition, the LEEM does not require a graphene transfer process and can scan large area by simply moving the sample stage. Moreover, the electron reflectivity enables determination of the graphene thickness.[16]

After introducing as-grown sample into the LEEM chamber, the sample was annealed to remove the surface adsorbents in vacuum because of inevitable exposure to air during the transfer. We measured bright-field (BF) and dark-field (DF) images that are formed from the reflection and diffraction of electron beams, respectively. From BF LEEM measurement, the spatial distribution of the number of graphene layers is obtained from the electron reflectivity as a function of accelerating voltage. Shown in Figure

3.5a-c is BF LEEM images of as-grown graphene on heteroepitaxial Cu(111) measured at different electron energies. The BF image showed the uniform white contrast except for some dark spots and linear lines. The reflectivity data measured at three points of Figure 3.5b is displayed in Figure 3.5d. The white area (marked with red square) shows a feature of single-layer graphene, indicating the formation of uniform single-layer graphene. The thick dark line observed at the center of Figure 3.5b (blue and green squares) is likely 2-3 layers of graphene. We interpret that this line represents a wrinkle of the graphene film that can be formed by different thermal expansion coefficients of graphene and Cu metal. The narrow lines running from upper left to lower right are probably originated from the surface morphology of the Cu film. The dark spots correspond to either metal nanoparticles or surface adsorbates that remain on the graphene surface.

The DF LEEM was measured for the same area, as shown in Figure 3.5e. The image was taken under the diffraction condition shown in the inset. The contrast of the DF image is quite uniform in the entire view, representing the single orientation of graphene in the measured area. Further measurement revealed that the diffraction pattern is unchanged after scanning ~1 mm (Figure 3.6a). In addition, large area (0.2 mm) DF LEEM images also indicate the uniform growth of orientation-controlled graphene without any clear boundary (Figure 3.6b). In the previous STM studies, it is proposed that there are two preferential graphene orientations on single-crystalline Cu (111) film; the angle between [10] direction of graphene and [101] direction of Cu(111) is 0º and 7º.[5,10] Gao et al suggested that graphene domains with 0º orientation occupy 30% in the measured area.[5] Whereas, in our case, the rotation-free (i.e. 0º orientation) graphene extends for very large area, occupying nearly 100%. Our optimized growth conditions are thus verified to produce highly-oriented single-layer graphene on heteroepitaxial Cu(111).

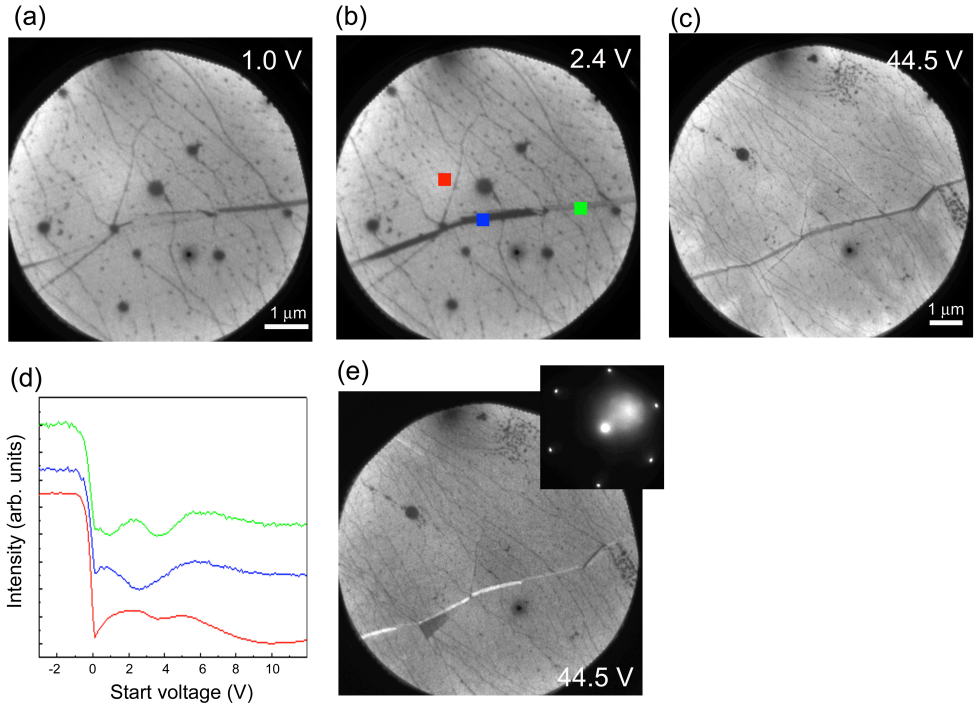

Figure 3.5 (a−c) BF LEEM images of as-grown graphene on heteroepitaxial Cu(111) measured with different electron energies. (d) Electron reflectivity data measured at points highlighted in (b). (e) DF LEEM image measured for the same area as (a−c) with the diffraction condition shown in the inset.

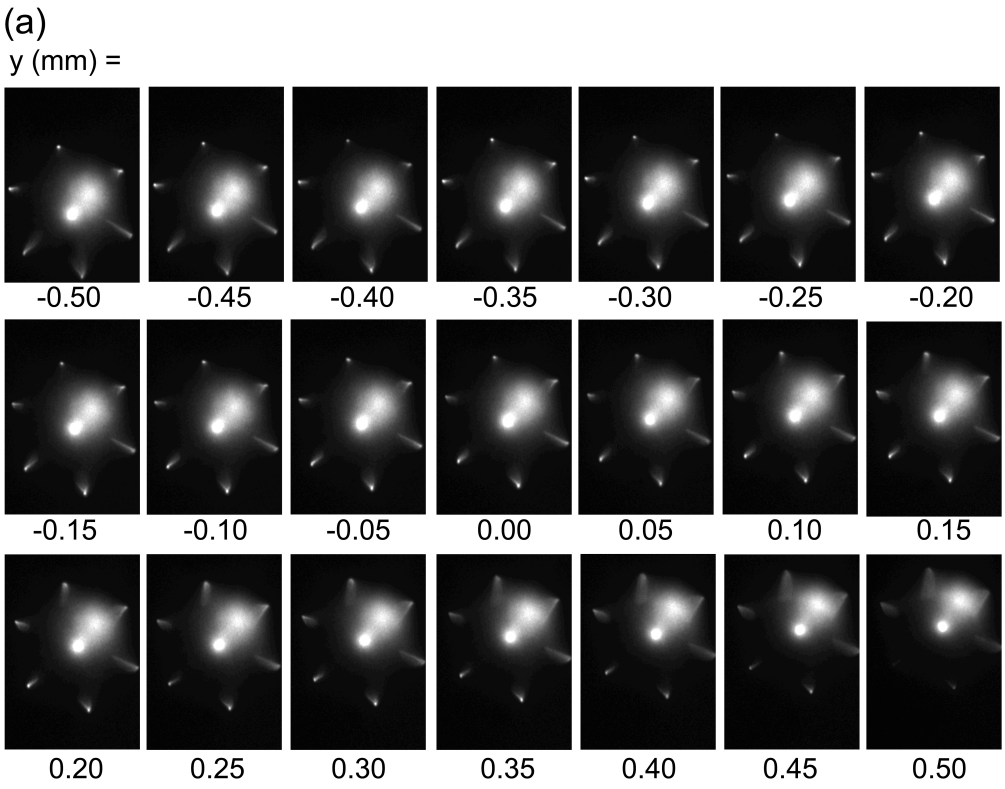

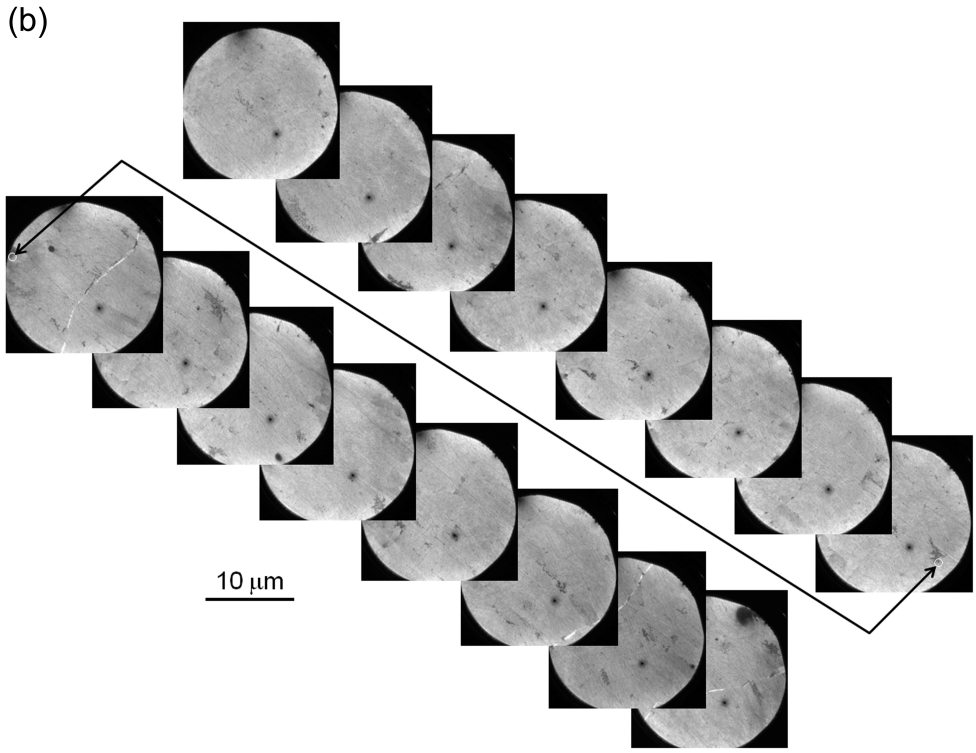

Figure 3.6 (a) LEED patterns of graphene/Cu(111) scanned for ~1 mm areas. The diffraction patterns are acquired along y direction of a substrate. (b) DF LEEM images scanned for ~200 μm areas. Dark spot indicated by the white circle is the defect in the microchannel plate.

I further studied the transferred graphene by atomic force microscope (AFM) and Raman mapping measurements. From the AFM image shown in Figure 3.7a, the graphene was found to have very smooth surface except for the linear wrinkles. The Raman mapping images of I_{2D}/I_G and I_D/I_G ratios are displayed in Figure 3.7c and 3.7d, respectively. Here, 532 nm excitation laser line with spot size of around 600 nm was used. Although there are some fluctuations in the I_{2D}/I_G ratio, all the measured areas displayed ratios higher than 1.5, indicating uniform single-layer graphene. As seen in the Raman spectra (Figure 3.7e) the D-band intensity was negligible. The I_D/I_G mapping also supports that the D-band is weak in the whole 5 μm × 5 μm measured area except for wrinkles (see Figure 3.8). Since the Raman D-band is associated with defects and domain boundary of a graphene film,[17] our epitaxial graphene film grown on Cu(111) might be free from domain boundary based on the absence of D-band and the DF LEEM images.

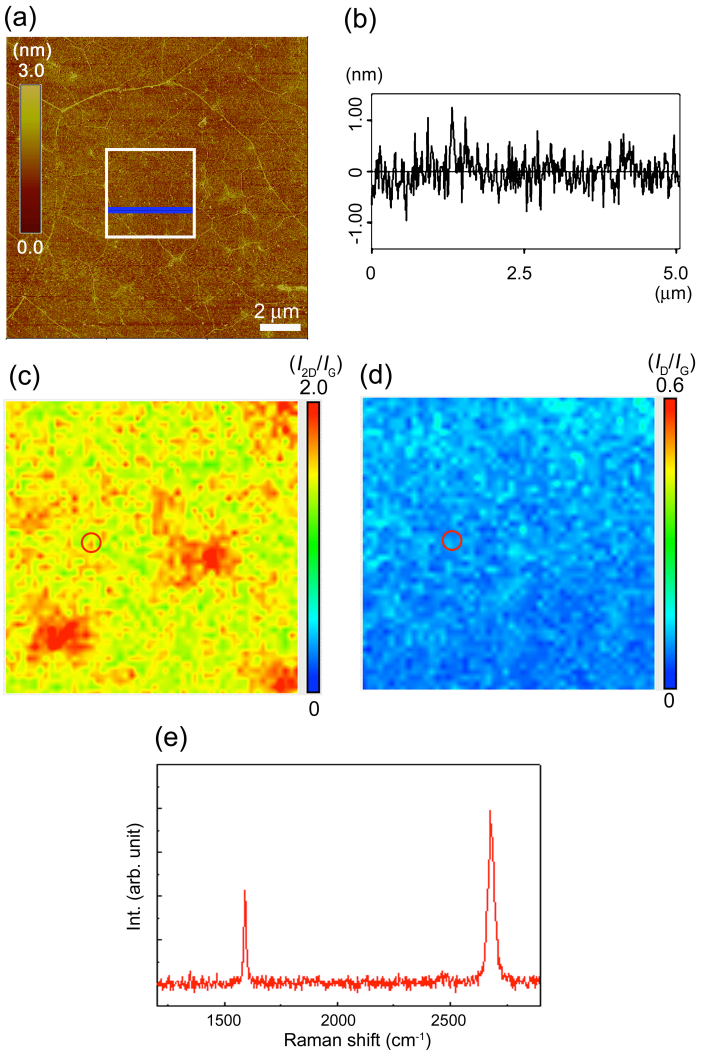

Figure 3.7 (a) AFM image of a graphene film transferred from Cu(111) onto the SiO_2/Si substrate. (b) Height profile measured by AFM along the blue line indicated in (a). Raman mapping images of the relative I_{2D}/I_G ratio (c) and I_D/I_G ratio (d). The measured 5 × 5 μm area is indicated by the white square shown in (a). (e) Raman spectrum measured at the point marked in (c,d).

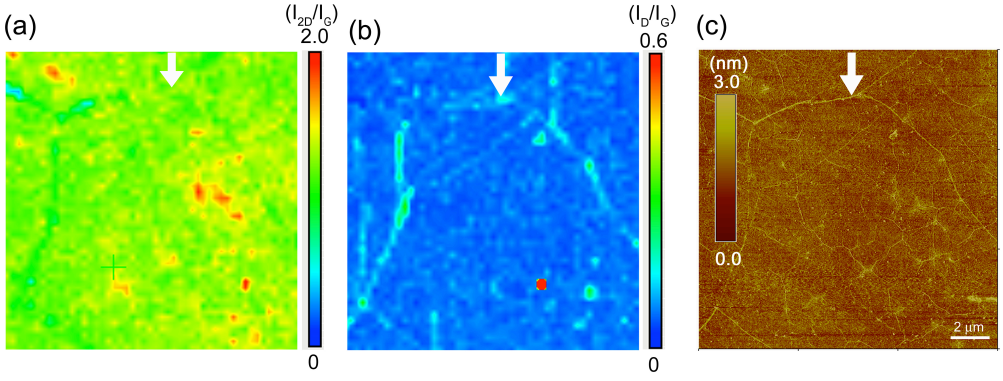

Figure 3.8 Raman mapping (a,b) and AFM (c) images of transferred graphene from Cu (111) onto SiO_2/Si substrate. White arrows show the identical graphene wrinkle.

We also performed LEEM measurements for the as-grown single-layer graphene on Cu(100), which can be regarded as a model system of widely studied Cu foil. Figure 3.9a,b shows BF LEEM images of the graphene on Cu(100) measured with different electron energies. The images show some dark contrasts with 1-2 μm size, and they became stronger with the increase of the energy. However, the electron reflectivity profiles (Figure 3.9c) indicate that the four points marked in Figure 3.8b are essentially the same, supporting the single-layer graphene for all the positions. This is consistent with the optical contrast shown in Figure 3.4a inset that proves uniform single-layer graphene formation even on Cu(100) surface. There are two possible reasons for the observed dark contrast in the BF LEEM images. One reason is slight surface oxidation of the Cu surface; the surface oxidation slightly increases the work function of Cu metal that can give dark contrast in the BF image. This is plausible, since we exposed our sample to air during transferring into the LEEM chamber. Another possibility is adsorption of impurities on the graphene surface; although we applied heat treatment prior to the LEEM measurement, the surface adsorbents are difficult to be removed completely from the graphene surface.

Interestingly, the DF LEEM images of graphene/Cu(100) (Figure 3.9d,e) showed a marked contrast to that of graphene on Cu(111) (see Figure 3.5e). We discovered that the as-grown graphene possesses a clear multi-domain structure with patches of small domains. Under one selected diffraction condition, a mosaic structure appeared (Figure 3.9d), while the diffraction condition rotated by 30 º gave a different mosaic pattern (Figure 3.9e). This can be attributed to the multiple graphene domain structure, similar to that reported by the dark field TEM analysis. The size of our graphene domains is below several μm, and domains form irregular boundaries. The domain structure was analyzed in terms of the domain orientation, as depicted in Figure 4f. The image analysis indicates that the graphene domains with 0º and 30º rotational angles occupy 46 % and 34%, respectively. Note that these two orientations, 0º and 30º rotation, are crystallographically equivalent. When the mis-orientation of ± 2º is allowed, the domains

occupy 55% (for 0± 2º) and 41% (for 30± 2º), as shown in Figure 4.10. We should note that most of the graphene domains prepared in our work have only two rotational directions, which are different from the previous graphene grown on Cu foil, in which a wide variation of rotational angles are observed. Being consistent with our epitaxial growth of graphene on the heteroepitaxial Cu(111), epitaxial graphene growth also occurs on heteroepitaxial Cu(100) surface. Previous STM studies suggested graphene growth with specific orientations, 0º, 30º, and 6º, against Cu (100) lattice,[7-10] but here we demonstrate the distribution of the two major graphene domains quantitatively.

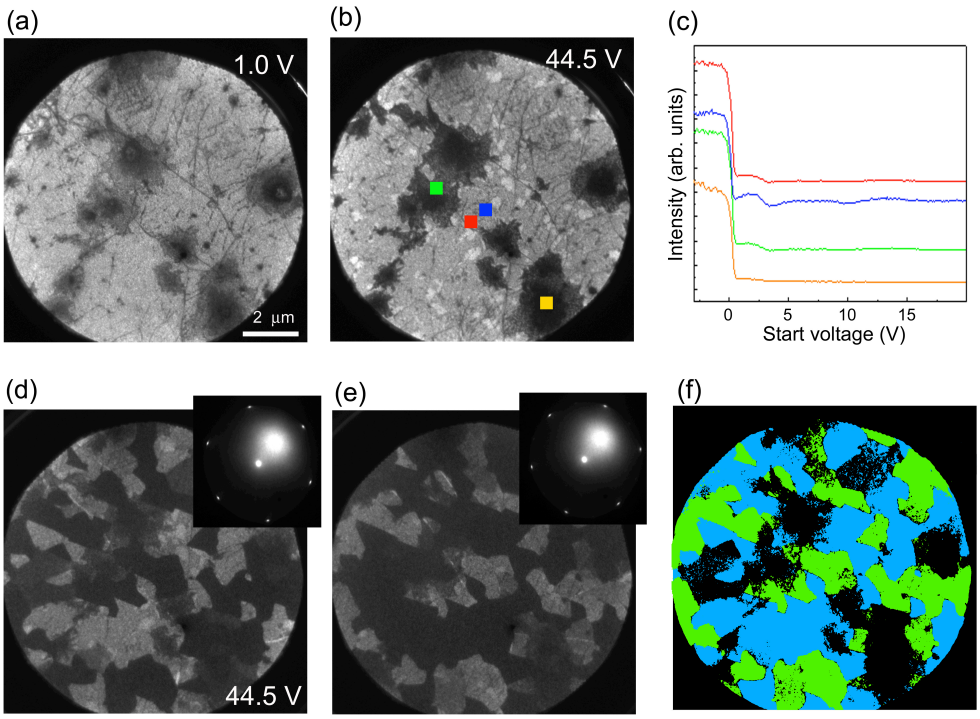

Figure 3.9 (a,b) BF LEEM images of graphene films grown on Cu(100) with 1.0 and 44.5 eV electron energies. (c) Electron reflectivity data measured at four different points marked in (b). (d,e) DF LEEM images of graphene measured under different diffraction conditions shown in the insets. (f) Spatial distribution of graphene domains determined from the DF LEEM images. The blue and green areas show the graphene domains rotated by 0° and 30° with respect to the underlying Cu lattice, respectively.

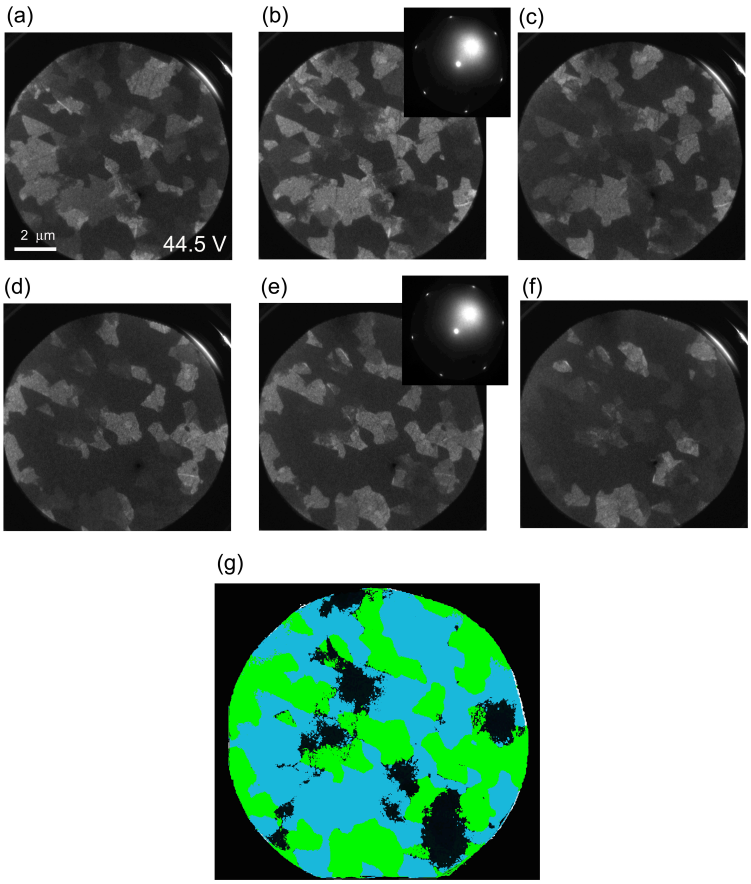

Figure 3.10 DF LEEM images of graphene films grown on Cu(100). The LEEM images were measured with different diffraction conditions: (a) -2°, (b) 0°, (c) +2°, (d) 28°, (e) 30°, and (f) 32°. (g) Result of image analysis of these LEEM images. Blue and green areas show graphene domains rotated by 0 ± 2° and 30 ± 2°, respectively.

The wrinkle structure was also observed for the transferred graphene from Cu(100) using AFM and Raman D-band intensity (Figure 3.12). Except for this wrinkle structure, the growth of uniform single-layer graphene was confirmed by optical microscope (see Figure 3.4a inset) and Raman mapping of I_{2D}/I_G ratio (Figure 3.11c). However, the I_D/I_G mapping shown in Figure 3.11d indicates curved line features in the D-band intensity. As seen in Figure 3.11d, the D-band weakly appeared along the line. Note that no wrinkle structure was observed by AFM for the mapped area. From the characteristic structure of curved D-band image and the scale that are comparable to the DF LEEM images (see Figure

3.9d-f), we infer that the observed D-band reflects the domain boundary of graphene. When two adjacent graphene domains with 30º rotation meet at the boundary, the boundary cannot be atomically connected, since the orientations of hexagons are different.

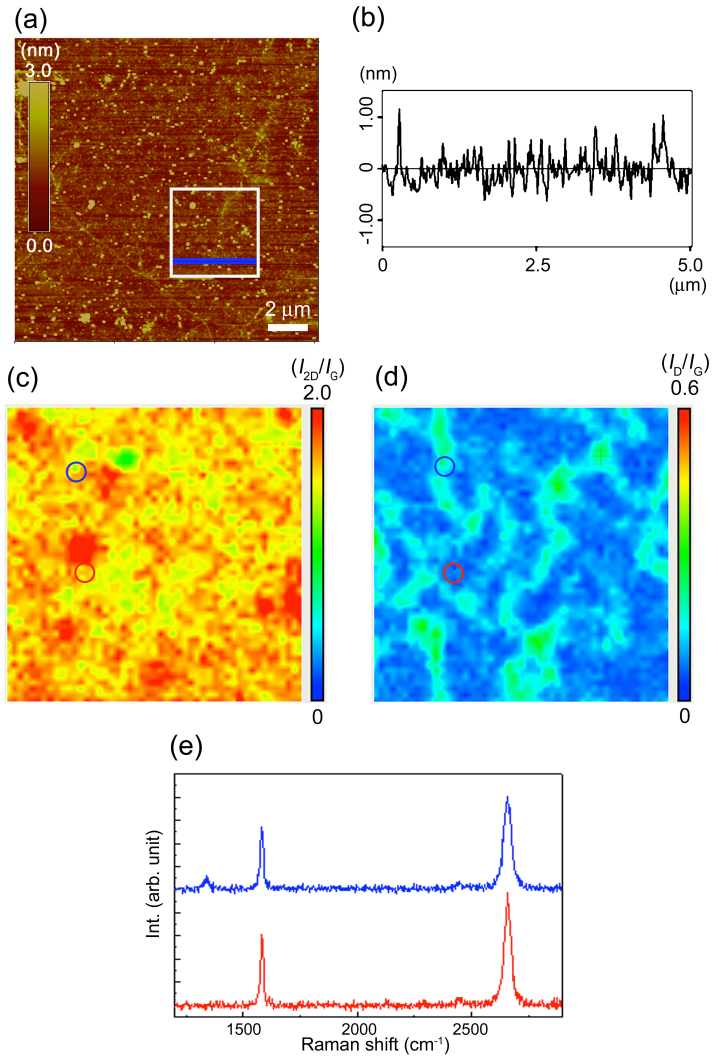

Figure 3.11 (a) AFM image of a graphene film transferred from Cu(100) onto the SiO_2/Si substrate. (b) Height profile measured along the blue line indicated in (a). Raman mapping images of I_{2D}/I_G (c) and I_D/I_G (d) ratios. The measured 5 × 5 μm area is indicated by a white square shown in (a). (e) Raman spectra measured at the points marked in (c,d).

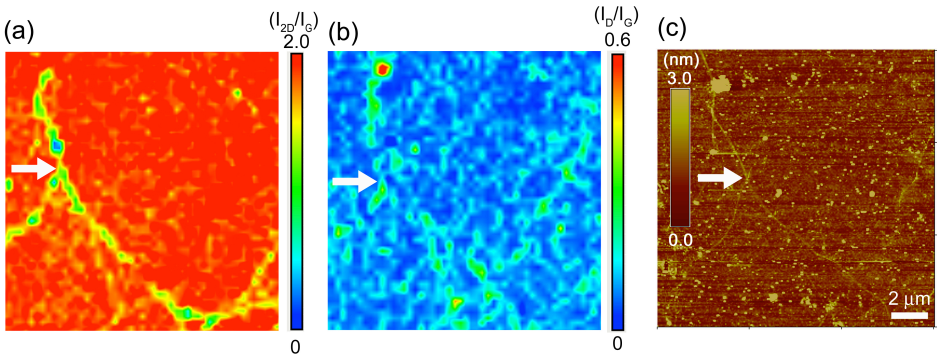

Figure 3.12 Raman mapping (a,b) and AFM (c) images of transferred graphene from Cu (100) onto SiO_2/Si substrate. White arrows show the identical graphene wrinkle

Here, atomic models of graphene grown on Cu(111) and Cu(100) metals are discussed. Figure 3.13 represents the graphene epitaxially grown on Cu(111), as revealed by LEED and LEEM. The relative orientation is described as $[10]_{graphene}//[101]_{Cu(111)}$. A periodic moiré pattern is seen in Figure 3.13, which is consistent with the previous STM images.[5] On the other hand, on Cu(100), there are two major orientations, $[10]_{graphene}//[011]_{Cu(100)}$ and $[01]_{graphene}//[011]_{Cu(100)}$. In both cases, C-C bond of graphene hexagons are aligned parallel to the Cu-Cu bond of the top most Cu surface. Stripe-like moiré pattern should appear as illustrated in Figure 3.13b, because Cu(100) has four-fold symmetry while graphene has six-fold symmetry. This is experimentally verified by STM for the graphene on Cu foil.[9] When graphene is grown on Cu(100) surface, grain boundary should remain due to the mis-oriented interface as illustrated in Figure 3.13b. The DF LEEM images (Figure 3.9d-f,3.10) clearly indicate the presence of domain boundaries. It is considered that this is the reason why the D-band was observed at the boundary (see Figure 3.11d) when the orientations of two adjacent graphene domains are not identical. In the case of single-layer graphene grown on Cu(111), all the graphene domain nuclei have the same hexagon orientation. Our LEEM and Raman results suggest that the boundary of the neighboring graphene domains grown on Cu(111) may be seamlessly connected during growth, in contrast to the graphene grown on Cu(100).

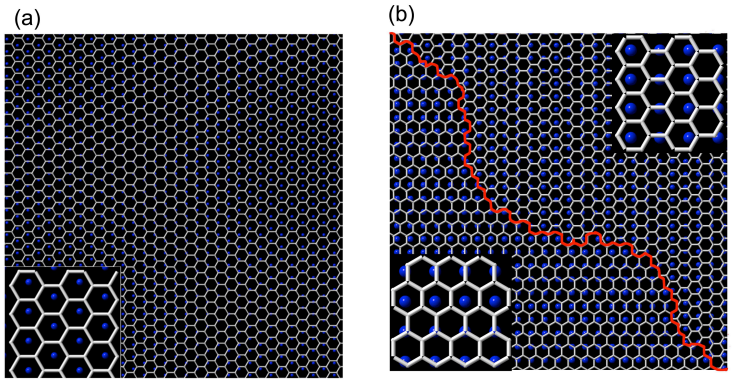

Figure 3.13 Atomic models of graphene grown on Cu(111) (a) and Cu(100) (b) surfaces. The graphene grown on Cu(111) is experimentally verified to have single orientation, while that on Cu(100) is found to have two orientations rotated by 30°. The red line in (b) represents a schematic of the domain boundary that is formed between two adjacent rotational domains.

Recently, graphene domain boundaries were studied by Raman mapping and scanning electron microscope (SEM) for the initial growth stage on Cu foil.[17] It was demonstrated that the graphene domain boundary gives increased D-band intensity, when the hexagonal graphene nuclei meets at the boundary. Therefore, the absence of D-band in the graphene on Cu(111) may indicate the boundary-free graphene growth. Based on STM observation, Lahiri et al. proposed the formation of one-dimensional defect lines for the graphene grown on Ni(111).[18] They suggested that carbon octagon-pentagon pair is formed at the boundary even for the orientation-controlled graphene film. However, their growth temperature is much lower than the typical CVD temperature (~1000 ºC) and they used Ni metal as a catalyst; they synthesized graphene by annealing the ethylene-adsorbed Ni(111) substrate at 620 ºC for 30 min. We reported that the graphene grown on Cu at 900 ºC gives higher D-band intensity than that at 1000 ºC, implying significant defect or boundary formation at low growth temperature.[2] Moreover, the domain structure can depend on metal employed for the graphene growth.[1] Therefore, the one-dimensional defect model proposed in the previous literature[18] cannot be simply applied to our system. However, since the lateral resolution of LEEM is not sufficient for the direct observation of atomic defects and/or domain boundaries, further microscopic study, such as TEM and STM, are

necessary for atomic-scale understanding of the domain boundary in relation with the orientation of graphene hexagons.

3-8 Summary

We succeeded in observing the domain structure and boundaries of CVD-grown graphene on heteroepitaxial Cu(111) and Cu(100) films by combining LEEM and Raman measurements. The heteroepitaxial Cu films give large-area single-layer graphene film by ambient pressure CVD. The graphene grown on Cu(111) is found to have a single orientation in the large area with no detectable D-band except for at wrinkles. In contrast, the graphene on Cu(100) exhibits clear multi-domain structure with two preferential domain orientations, reflecting the mismatch of the lattice symmetry of graphene (six-fold symmetry) and the Cu lattice (four-fold). The graphene boundary is detected by the Raman mapping measurement. This is due to the 30º-rotated adjacent domains which cannot be atomically connected. Most of research works try to increase the graphene domain size through the optimization of CVD condition for Cu foils. In our method of CVD growth using heteroepitaxial single-crystalline Cu(111) film, the orientation of graphene nuclei is well controlled. Therefore, our work can present a new and alternative approach to grow “single crystalline” graphene.

References:

[1] H. Ago, Y. Ito, N. Mizuta, K. Yoshida, B. Hu, C. M. Orofeo, M. Tsuji, K. Ikeda, S. Mizuno, Epitaxial Chemical Vapor Deposition Growth of Single-Layer Graphene over Cobalt Film Crystallized on Sapphire. *ACS Nano* **4**, 7407 (2010).

[2] B. Hu, H. Ago, Y. Ito, K. Kawahara, M. Tsuji, E. Magome, K. Sumitani, N. Mizuta, K. Ikeda, S. Mizuno, Epitaxial Growth of Large-Area Single-Layer Graphene over Cu(111)/sapphire by Atmospheric Pressure CVD. *Carbon*, **50**, 57 (2012).

[3] J. M .Wofford, S. Nie, K. F. McCarty, N. C. Bartelt, O. D. Dubon, Graphene Islands on Cu Foils: The Interplay between Shape, Orientation, and Defects. *Nano Lett.* **10**, 4890 (2010).

[4] X. Li, C. W. Magnuson, A. Venugopal, J. An, J. W. Suk, B. Han, M. Borysiak, W. Cai, A. Velamakanni, Y. Zhu, L. Fu, E. M. Vogel, E. Voelkl, L. Colombo, R. S. Ruoff, Graphene Films with Large Domain Size by a Two-Step Chemical Vapor Deposition Process. *Nano Lett.*, **10**, 4328 (2010).

[5] L. Gao, J. R. Guest, N. P. Guisinger, Epitaxial Graphene on Cu (111). *Nano Lett.* **10**, 3512 (2010).

[6] C. V. Van, A. Kimouche, A. R. Plantey, O. Fruchart, P. B Guillemaud, N. Bendiab, J. Coraux, Epitaxial Graphene Prepared by Chemical Vapor Deposition on Single Crystal Thin Iridium Films on Sapphire. *Appl. Phys. Lett.* **98**, 181903 (2011).

[7] Y. Zhang, T. Gao, Y. Gao, S. Xie, Q. Ji, K. Yan, H. Peng, Z. Liu, Defect-like Structures of Graphene on Copper Foils for Strain Relief Investigated by High-Resolution Scanning Tunneling Microscopy. *ACS Nano* **5**, 4014 (2011).

[8] J. Cho, L. Gao, J. Tian, H. Cao, W. Wu, Q. Yu, E. N. Yitamben, B. Fisher, J. R. Guest, Y. P. Chen, N. P. Guisinger, Atomic-Scale Investigation of Graphene Grown on Cu Foil and the Effects of Thermal Annealing. *ACS Nano* **5**, 3607 (2011).

[9] L. Zhao, K.T. Rim, H. Zhou, R. He, T.F. Heinzm, A. Pinczuk, G.W. Flynn, A.N. Pasupathy, Influence of Copper Crystal Surface on the CVD Growth of Large Area Monolayer Graphene. *Solid State Commun.* **151**, 509 (2011).

[10] H. I. Rasool, E. B. Song, M. J. Allen, J. K. Wassei, R. B, Kaner, K. L. Wang, B. H. Weiller, J. K. Gimzewski, Continuity of Graphene on Polycrystalline Copper. *Nano Lett.* **11**, 251 (2011).

[11] H. Ago, I. Tanaka, M. Tsuji, K. Ikeda, Patterned Growth of Graphene over epitaxial Catalyst. *Small* **6**, 1226 (2010).

[12] C. V. Van, A. Kimouche, A. R Plantey, O. Fruchart, P. B. Guillemaud, N. Bendiab, J. Coraux, Epitaxial Graphene Prepared by Chemical Vapor Deposition on Single Crystal Thin Iridium Films on Sapphire. *Appl. Phys. Lett.* **98**, 181903 (2011).

[13] S. Gilje, S. Han, M. Wang, K. L. Wang, R. B. A. Kaner, Chemical Route to Graphene for Device Applications. *Nano Lett.* **7**, 3394 (2007).

[14] K. S. Kim, Y. Zhao, H. Jang, S. Y. Lee, J. M. Kim, K. S. Kim, J. H. Ahn, P. Kim, J. Choi, B. H. Hong, Large-scale pattern growth of Graphene Films for Stretchable Transparent Electrodes. *Nature* **457**, 706 (2009).

[15] A. Reina, S. Thiele, X. Jia, S. Bhaviripudi, M. S. Dresselhaus, J. A. Schaefer, L. Kong, Growth of Large-Area Single- and Bi-Layer Graphene by Controlled Carbon Precipitation on Polycrystalline Ni Surfaces. *Nano Res*. **2**, 509 (2009).

[16] H. Hibino, H. Kageshima, F. Maeda, M. Nagase, Y. Kobayashi, H. Yamaguchi, Microscopic Thickness Determination of Thin Graphite Films Formed on SiC from Quantized Oscillation in Reflectivity of Low-Energy Electrons. *Phys. Rev. B* **77**, 75413 (2008).

[17] Q. Yu, L. A. Jauregui, W. Wu, R. Colby, J. Tian, Z. Su, H. Cao, Z. Liu, D. Pandey, D. Wei, T. F. Chung, P. Peng, N. P. Guisinger, E. A. Stach, J. Bao, S.-S. Pei, Y. P. Chen. Control and Characterization of Individual Grains and Grain Boundaries in Graphene Grown by Chemical Vapor Deposition. *Nat. Mater.* **10**, 443 (2011).

[18] J. Lahiri, Y. Lin, P. Bozkurt, I. I. Oleynik, M. Batzill, An Extended Defect in Graphene as a Metallic Wire. *Nat. Nanotech.* 5, 326 (2010).

Chapter 4:

Transport properties and structure of the interface between CVD-grown graphene domains

Abstract:

In chemical vapor deposition (CVD) grown graphene, it is important to understand the interfacial structure of the merged domains, as well as their influence on the physical properties of graphene. Here, the structure and properties of the interfaces between the merged large hexagonal domains with controlled orientations were studied. Although the merged domains have various interfaces with/without wrinkles and/or increased defect-related Raman D-band intensity, the intra-domain transport showed higher carrier mobility reaching 20,000 cm^2/Vs on SiO_2 at 280 K (the mean value was 7,200 cm^2/Vs) than that measured for inter-domain areas, 6,400 cm^2/Vs (mean value 2,000 cm^2/Vs). The temperature dependence of the mobility suggested impurity scattering dominated at the interface even for the merged domains with the same orientation. This study highlights the importance of domain interfaces, especially on the carrier transport properties, in CVD-grown graphene.

4-5 Introduction

To achieve large-area growth of single-layer of graphene at a low cost, CVD on Cu catalyst is a very promising method. Although mechanical exfoliated graphene flakes demonstrate high carrier mobilities of 200,000 cm^2/Vs for suspended graphene[1] and ~10,000 cm^2/Vs for graphene on SiO_2 substrate,[2] CVD-grown single-layer of graphene transferred onto SiO_2 substrates generally exhibits low carrier mobilities, typically 1,000–5,000 cm^2/Vs. There are several possible reasons for the lower mobility of CVD-grown graphene, such as low crystallinity, transfer-induced defects and impurities, wrinkles formed during the CVD process and while transferring the films, and the presence of domain boundaries in polycrystalline CVD-grown graphene.

On conventional Cu foil, which is polycrystalline, the orientation of these hexagonal domains is not controlled. Thus, it is difficult to merge the domains seamlessly without defects at interfaces of graphene domains even though recent progresses have achieved large hexagonal graphene domains. However, epitaxial CVD growth using heteroepitaxial Cu films deposited on single-crystalline substrates, such as sapphire or MgO, can control the hexagonal domain orientation due to the crystal relationship between graphene and Cu. It is thus of interest to study how the growing hexagonal graphene domains merge together on heteroepitaxial Cu films, while keeping the same orientation.

In this chapter, the interfaces of the merged hexagonal graphene domains are investigated using atomic force microscopy (AFM), Raman spectroscopy, and charge transport measurements, highlighting the importance of interface engineering for high-performance devices.

4-6 Experiment

- Synthesis of hexagonal graphene domains

The heteroepitaxial Cu films on MgO (100) substrates were prepared using high temperature sputtering at ~300 °C. This experimental condition was same as that in Chapter 3-2. To grow the graphene films a Cu/MgO(100) substrate was placed in a quartz tube in an electric furnace and annealed at 1000 °C in the flow of H_2 (2.5% in Ar) gas for 40 min. After rising the furnace temperature to 1075 °C, the mixed gases, CH_4 (10 ppm) and H_2 (2.25%) in Ar, were flowed under ambient pressure.[3] After CVD for 20 min, the sample was rapidly cooled down to room temperature by taking the sample out of the furnace. The domain orientation was controlled using heteroepitaxial Cu(100) films.

- Transfer of graphene domains to SiO_2/Si substrate

As-grown hexagonal graphene was transferred onto SiO_2 (285 or 300 nm)/Si substrates using poly-methyl methacrylate (PMMA), thermal tape, and an etching solution of aqueous $FeCl_3$ and HCl.

- Characterization of hexagonal graphene domains

The as-grown graphene domains on Cu surface were observed by scanning electron microscopy (SEM). The transferred graphene films were analyzed with an optical microscope (NIKON Eclipse300), an AFM (Bruker, Nanoscope IIIa; Seiko Instruments Inc., SII SPA400), and a Raman spectroscope with a piezo stage (Tokyo Instruments, Nanofinder30). The excitation wavelength used for Raman spectroscopy was 532 nm.

- Fabrication and measurement of the graphene devices

Four terminal electrodes were patterned using electron beam lithography with PMMA, followed by vacuum evaporation of Ti and Au 5 nm and 30–50 nm thick, respectively. After annealing at 200 °C in a vacuum (~10^{-4} Pa) for a short time, electrical measurements were performed with the four-terminal system in a cryostat under a vacuum (~2×10^{-5} Pa), with a temperature ranging from 80 to 280 K.

4-7 Results and discussion

Large hexagonal graphene domains with lateral sizes of several tens of micrometers were formed on heteroepitaxial Cu(100) films by ambient pressure CVD at 1075 °C. Figure 4.1a–c shows SEM images of the hexagonal domains grown on Cu(100) films. A number of isolated hexagonal domains were observed together with some merged domains. Contrary to the polycrystalline Cu foils, the heteroepitaxial Cu(100) films limited the orientation of the graphene domains because of the epitaxial relationship, allowing the angle dependence of the merged domains to be studied.

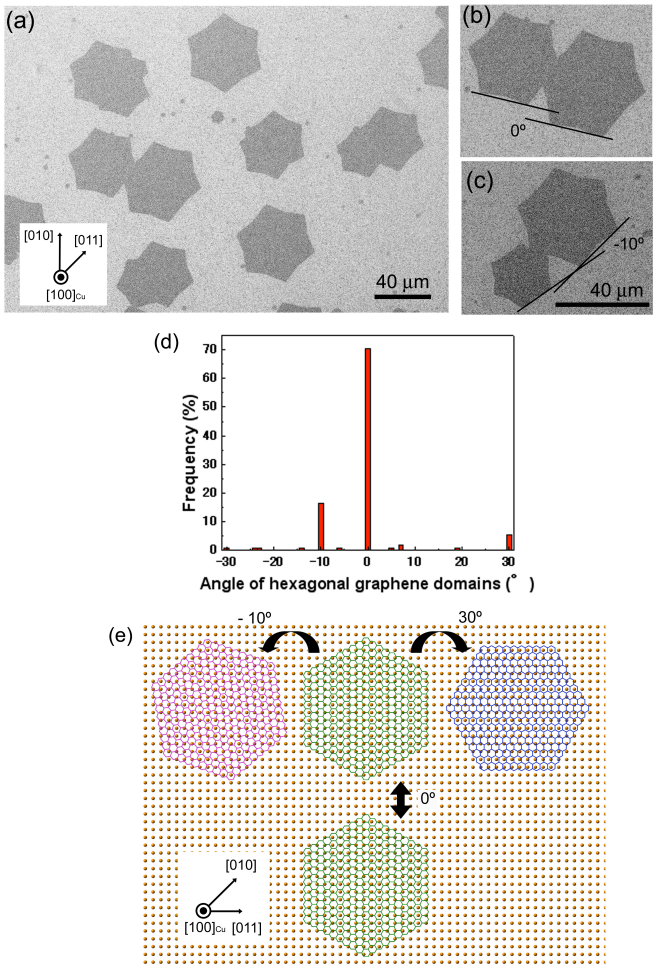

Figure 4.1 (a–c) SEM images of as-grown hexagonal graphene domains on a Cu(100) film. The heteroepitaxial Cu(100) film limited the orientation of the graphene domains, leading to the limited merged angles of 0° (b) and -10° (c). (d) Angle distributions of hexagonal graphene domains grown by CVD at 1075 ºC. The Cu [100] direction is defined as 0º. (e) Atomic models of graphene domains on the Cu(100) lattice.

Three main orientations, 0°, 30°, and -10°, were observed in the graphene domains, with respect to the underlying Cu lattice. Figure 4.1d,e indicates the angular distribution and atomic models, respectively. The rotation-free domains (0°) occupied about 70% of merged domains (Figure 4.1e). The 0° and 30° orientations are defined as $[10]_{graphene}//[011]_{Cu}$ and $[01]_{graphene}//[011]_{Cu}$, respectively. These two orientations were observed on the Cu(100) surfaces when they were grown at 1000 °C (Chapter 3). In both cases, one of the C-C bonds in the graphene film aligns parallel to a Cu-Cu bond. However, -10°-rotated graphene domains were also observed, likely because of the higher CVD temperature used (1075 °C). Accordingly, there were several types of merged domains with limited angles, as shown in Figure 4.1b and 4.1c. In this chapter, we mainly focus on the merged domains with the same angle (0° rotation).

The surface morphology and Raman spectra of the merged graphene domains transferred on SiO_2/Si substrates were studied. Figure 4.2 shows the optical microscope, AFM images, and the Raman data for the graphene domains that had the same orientation when they merged. The transferred graphene films showed a higher Raman 2D-band intensity than G-band intensity (I_{2D}/I_G ~1.5), a narrow 2D-band (30–40 cm^{-1} in width) and a substantially weak D-band. These results, together with the uniform optical contrast, confirm the growth of high-quality single-layer graphene domains.

At some of the interfaces of the merged domains, a clear line with height of 0.3–7 nm was observed along the interface in the AFM image, marked by an arrow in Figure 4.2b. Figure 4.4 illustrates the possible structures of the interfaces between the neighboring graphene domains grown on Cu surfaces. Because the observed height was greater than the thickness of one graphene layer (see Figure 4.2b), it is believed that this region corresponds to a graphene wrinkle, as illustrated in Figure 4.4b. However, in some cases, interfaces lower than 1 nm in height were observed, which may come from the overlap of graphene layers, as illustrated in Figure 4.4c. Among the 15 merged domains that were measured, seven

interfaces (46%) showed clear wrinkles or an overlap. The distribution is shown in Figure 4.3. Figure 4.2c,d is Raman mapping images of the I_{2D}/I_G and I_D/I_G intensity ratios, and Figure 4.2i shows the Raman spectra measured at numbered points. A weak but clear Raman D-band was observed along the wrinkles (spectrum 1 in Figure 4.2i), while the D-band intensity was negligible inside the graphene domains (spectrum 2). A weak D-band was observed for the other six merged domains that had wrinkles. Wrinkles are known to form during the CVD process and are caused by the different thermal expansion coefficients of graphene and Cu, as well as the wet-transfer process. The wrinkles observed at the interface likely originate from the collision of the developing graphene domains (Figure 4.4b). It is unlikely that the interface seen in Figure 4.2d is atomically connected.

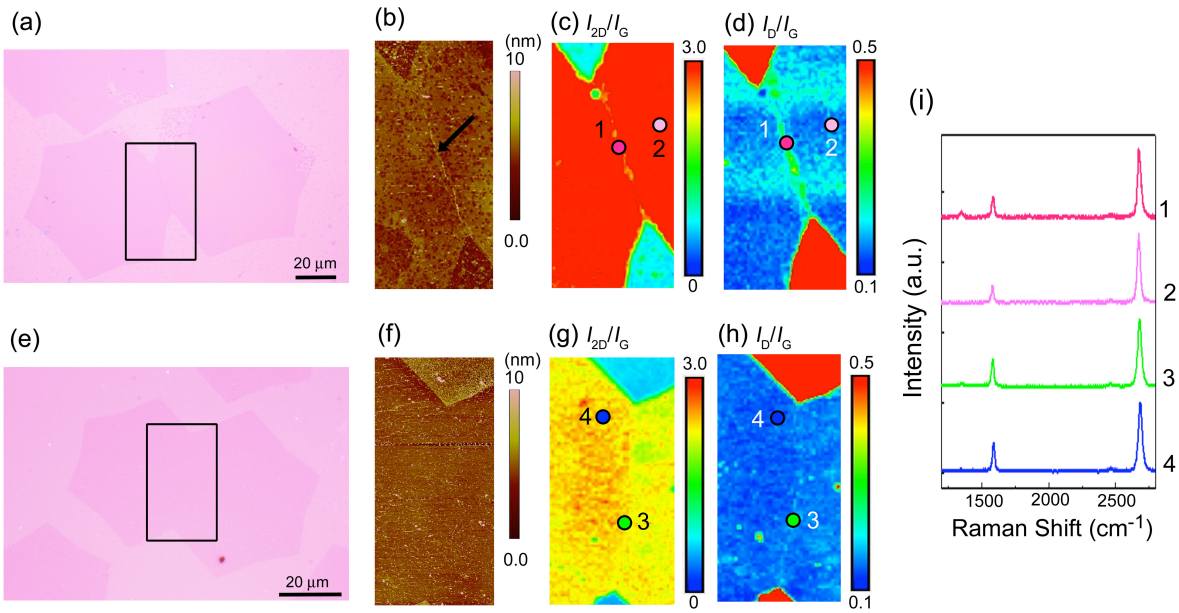

Figure 4.2 Optical micrograph (a), AFM image (b) and Raman mapping image of the I_{2D}/I_G (c) and I_D/I_G (d) ratios of the graphene domains with wrinkles along the interface. The wrinkle is indicated by the black arrow in (b). (e–h) shows the data without a clear wrinkle at the interface. These merged domains had the same angle (0° rotation). The AFM and Raman mapping areas are indicated by the black squares shown in (a) and (e). (i) Raman spectra measured at the points marked in (c), (d), (g), and (h).

Figure 4.2f shows that some of the merged domains possessed flat surfaces, even at their interfaces. In addition, about half of these wrinkle-free interfaces showed a negligible or very weak D-band (see Figure

4.2h and spectrum 3 in Figure 4.2i). The remaining half of the wrinkle-free interfaces showed a clear D-band (see Figure 4.3a). The wrinkled interfaces always had a Raman D-band. The distribution observed (Figure 4.3a) implied that there are variations in the wrinkle formation and the D-band intensity, even though only the domains merged with the same angle were studied.

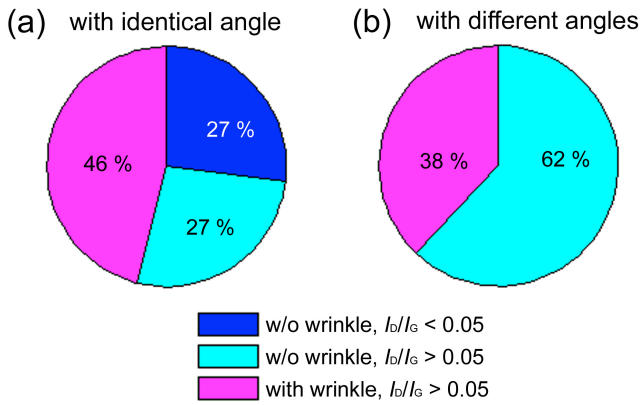

Figure 4.3 Distribution of interface properties in adjacent domains; merged with the same angle (a) and with different angles (b).

Figure 4.4d-f illustrates three possible interfaces that do not show an obvious height change: atomically smooth connection (Figure 4.4d), defective connection (Figure 4.4e), and terminated edges (Figure 4.4f). The atomically smooth, perfect interface should give no D-band as it will be a single-crystalline graphene domain. The latter two cases can potentially show a D-band because of the symmetry breaking, which basically originates in the defects or domain edges. The direct relationship between the interface structure and the Raman spectrum is unclear due to limitations in the spatial resolution (spot size ~600 nm) and sensitivity of the confocal Raman spectroscope used. Even though a negligible D-band was observed for some interfaces (Figure 4.2h), this does not prove a perfect connection. Further studies such as tip-enhanced resonance Raman spectroscopy (TERS) are necessary to better understand the structure of the interfaces. In spite of the spatial limits of both AFM and Raman, this work demonstrated that various types of interfaces could be formed, even for the merged domains with the same angle.

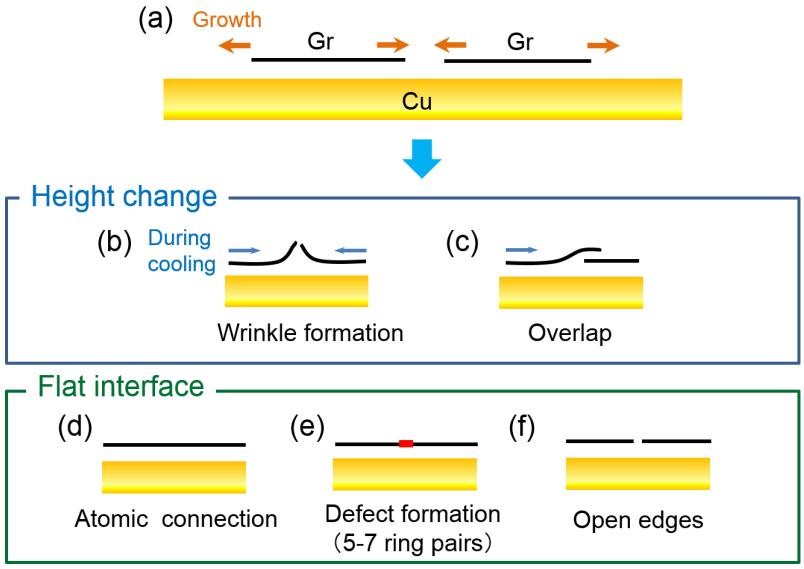

Figure 4.4 Schematic of the possible interfaces for the merged graphene domains. (a) Each graphene domain grew independently, but with the same hexagon orientation. After the CVD process, there were five possible interface structures; (b) wrinkle formation, (c) overlap, (d) perfect connection, (e) defect formation such as 5–7 membered rings and (f) open edges. (b) and (c) show the change in height, while (d) – (f) do not show a clear height change.

The merged domains were also measured with different angles. Figure 4.11 shows the result of the domains merged with a - 10° rotation. Among the 13 merged domains measured, seven of the merged domains showed wrinkles along the interface (Figure 4.4b). The result of the domains merged with a - 10° rotation are shown later in Figure 4.11. However, all the interfaces of the 13 merged domains showed a clear D-band. This signifies that it is difficult for rotated domains to connect seamlessly.

To further study the interfaces between adjacent domains, electrical measurements of the graphene devices were performed by attaching multiple Au/Ti electrodes, as shown in Figure 4.5. To avoid deterioration of the charge transport properties by multiple lithography-etching processes, the hexagonal graphene domains were not patterned. Instead, the carrier mobility was calculated by assuming a rectangular-shaped channel (Figure 4.5). L is a distance between two electrodes. The channel width, W, is calculated from the following formula:

$$W = \{W_1 + (W_2 \times 2) + W_3\}$$

The specific geometry of the merged domains and the exposed side edges may influence the calculated mobility, but these effects were not significant because of the large, micrometer-sized domains and interfaces, and the graphene's high carrier mobility. Structural defects, such as domain boundaries (shown in Figure 4.4b,c,e,f) and point defects generated by electron beam irradiation, are significant for the charge transport properties.[6] Therefore, the use of hexagonal domains instead of a rectangle compensated for this and the assumption is appropriate for comparing intra- (within a domain) and inter-domain (across domains) mobilities in one set of devices.

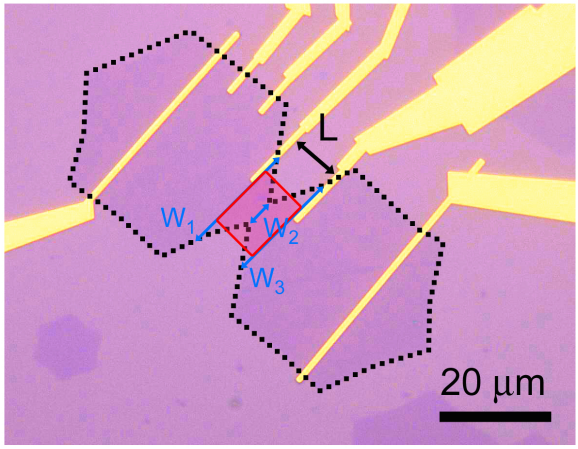

Figure 4.5 Optical microscope image of graphene FET. The channel area for an electrical transport measurement was approximated as shown by a red square.

Figure 4.6a shows an optical micrograph of a graphene device with identical orientation domains. In this device, a 7-nm-high wrinkle existed at the interface of the merged domains (Figure 4.6b). A number of parallel small lines observed in the AFM image can be originated in the transfer process, because the narrow lines run in almost one direction. Using Raman mapping, the linear feature of the D-band was observed along the interface (Figure 4.6c). For the four-terminal measurements, two outer electrodes were used as the source (S) and drain (D) electrodes (see Figure 4.6a). A gate voltage was applied to the

bottom of the Si substrates All of the measurements were performed in a vacuum (~5 × 10^{-5} Pa). The gate voltage dependence of the conductivity for both the intra- (electrodes 1–2) and inter-domain (electrodes 2–3) areas measured at 80 K is displayed in Figure 4.6d. The resistivity at the charge neutrality point (CNP, Dirac point) and the hole mobility measured for the intra-domain device (red curve) were 2,600 Ω·m and 10,000 cm^2/Vs, respectively. This mobility is very high, and almost comparable to that of exfoliated graphene on a SiO_2 substrate.[2] The inter-domain device (black curve) showed a resistivity and mobility of 21,000 Ω·m and 1,100 cm^2/Vs, respectively. The resistivity of the inter-domain area was eight times higher than that of the intra-domain area. Thus, the mobility was significantly suppressed when it was measured across a wrinkled interface.

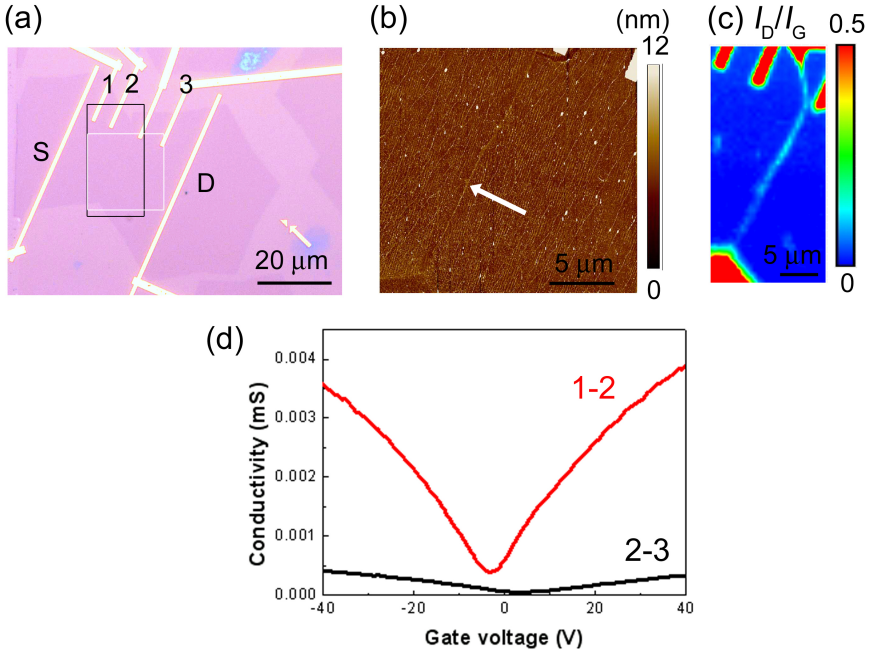

Figure 4.6 Optical micrograph (a), AFM image (b), I_D/I_G Raman mapping image (c) and the charge transport properties (d) of the hexagonal domains merged with a wrinkle along the interface. The wrinkle present at the interface is indicated by the white arrow in (b). AFM (b) and Raman mapping (c) were measured for the white and black areas shown in (a), respectively. The numbers in (d) indicate the electrode pairs used to measure the conductivity. Electrode pairs 1–2 and 2–3 correspond to the inter- and intra-domain, respectively.

Next, the merged hexagonal graphene domains without wrinkles at the interface were investigated, as

presented in Figure 4.7. The Raman mapping image (Figure 4.7c) indicated that the D-band was very weak for all of the graphene domains, even at the interface. Figure 5d shows the transfer characteristics for the areas with three different electrode pairs (electrode pairs 1–2, 2–3, and 3–4). The highest resistivity observed was 11,000 Ω·m at the CNP for electrode pair 2–3, which corresponds to the inter-domain area. The intra-domain devices showed resistivities of 6,400 Ω·m and 9,200 Ω·m for the 1–2 and 3–4 electrode pairs, respectively. The resistivity at the area between electrodes 3–4 was high, but still lower than that of electrodes 2–3. The carrier mobilities were determined to be 4,000, 2,500, and 2,600 cm^2/Vs for electrodes 1–2, 2–3, and 3–4, respectively. The inter-domain area (such as electrode pair 2–3) showed the lowest mobility. Therefore, the deterioration of the charge transport properties in graphene occurred even for the wrinkle-free interfaces. This suggested that there is an imperfect atomic connection between the neighboring domains.

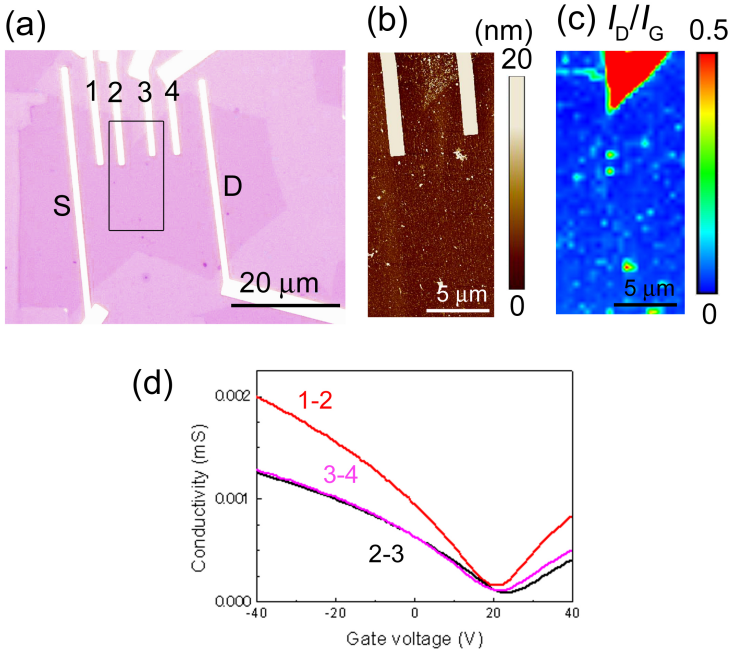

Figrure 4.7 Optical micrograph (a), AFM image (b), I_D/I_G Raman mapping image (c) and charge transport properties (d) of the hexagonal domains merged without wrinkles. No clear linear features were observed in both the AFM and Raman images. The Raman image was taken before attaching electrodes. Electrode pairs 1–2, 3–4 and 2–3 correspond to the inter- and intra-domains, respectively.

We note that the carrier transport property is very sensitive to the film transfer and device fabrication

processes. The Dirac point of the merged device shown in Figure 4.7 shifted to a positive voltage of ~20 V. It is speculated that this shift originated in a residual contaminant encapsulated between graphene and the SiO_2 surface.[10] This unintentional doping effect and/or impurity contamination reduced the charge carrier mobility. However, the general tendency within the single merged domains was consistent for all of the nine devices tested (Figure 4.8).

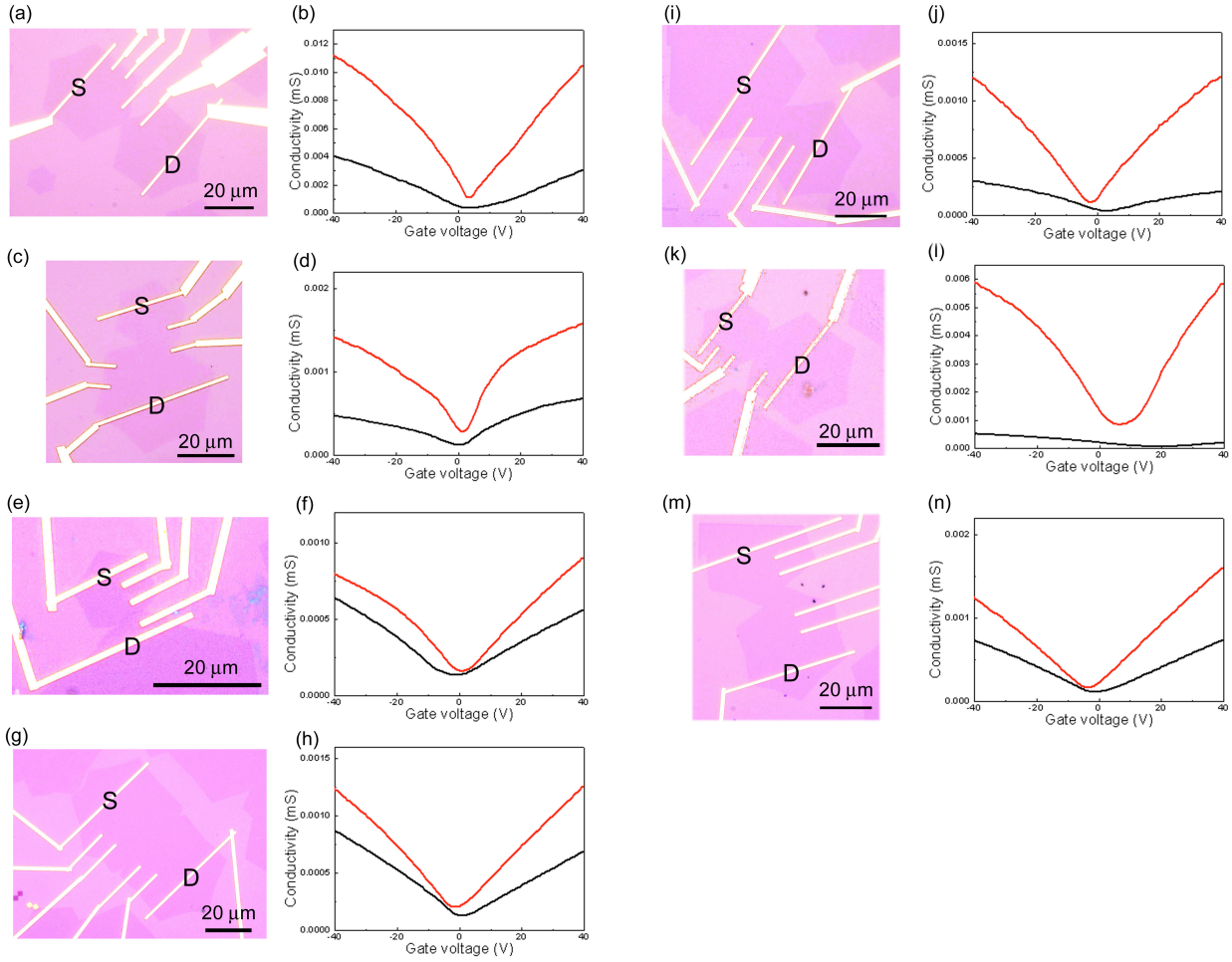

Figure 4.8 Optical micrograph (a,c,e,g,i,k,m) and charge transport properties (b,d,f,h,j,l,n) of the merged hexagonal graphene domains.

Figures 4.9a and b summarize the resistivity at the CNP and the carrier mobility for nine devices (in Figure 4.8) with 0° rotation, measured at 80 K. This data contains all of the devices measured, irrespective of the presence of wrinkles and the appearance of a Raman D-band at their interfaces. The inter-domain devices showed a higher resistivity and a lower mobility than the intra-domain devices. The mean resistivity at the intra-domain area was 4,400 Ω·m, and that at the inter-domain area was 13,000 Ω·m, which is three times larger than the intra-domain area. In addition, the distribution of the resistivity was scattered at the inter-domain across the two domains. The mean mobility at the inter-domain area was 2,700 cm^2/Vs at 80 K (2,100 cm^2/Vs at 280 K), which is less than half of that in the intra-domain area that had a mobility of 9,900 cm^2/Vs (7,200 cm^2/Vs at 280 K) (see Figure 4.9b). These results strongly suggest that electrical scattering sites are present at the interfaces of adjacent graphene domains.

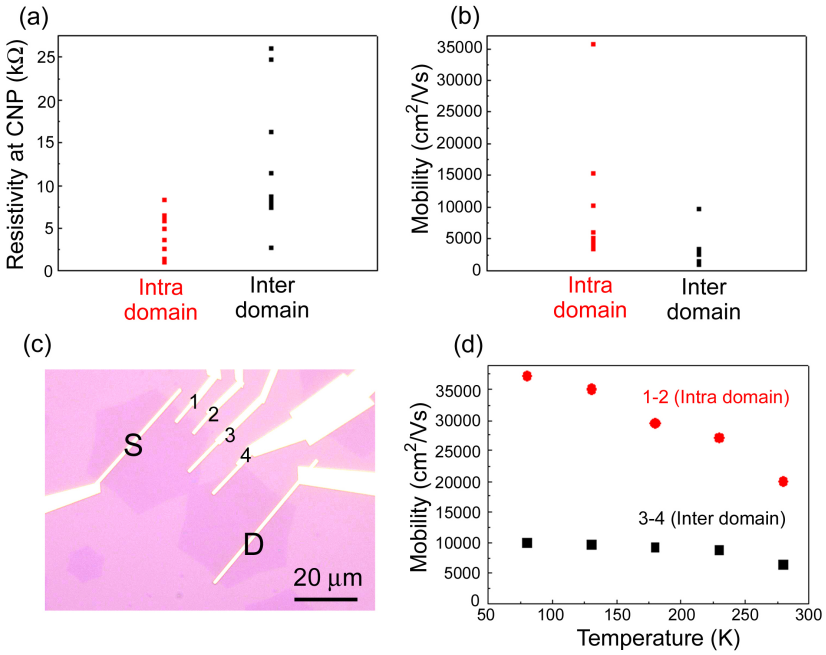

Figure 4.9 Comparison of the resistivity (a) and mobility (b) of the adjacent domains, merged with the same angle (0° rotation). Nine isolated merged domains were measured. (c) Merged domains used to measure the temperature dependence of the hole mobility shown in (d). Red and black data show the mobilities of the intra-domain inter-domain areas, respectively.

The temperature dependence of the carrier transport was measured for the devices, shown in Figure 4.9c

and d. Different temperature dependences were observed for the intra- and inter-domain devices. The mobility of the intra-domain device decreased with increasing temperature, which is consistent with the devices made with exfoliated graphene.[7] This temperature dependence indicates that the thermally activated phonon scattering of the charge carriers is enhanced at higher temperatures, implying the absence of severe defects within the hexagonal domains. The carrier mobility was very high at 20,000 cm^2/Vs for the intra-domain devices at 280 K, which is higher than that for typical exfoliated graphene devices. Thus, our single-crystalline graphene domain is extremely high quality.

The mobility of the inter-domain device was almost constant in the measured temperature range. This temperature dependence showed that impurity scattering influences the transport properties. The inter-domain device showed the highest mobility of 9,600 cm^2/Vs at 80 K (6,400 cm^2/Vs at 280 K). This interface-induced charge carrier scattering was observed in all of the nine graphene devices, even for the interfaces without wrinkles and a Raman D-band. Therefore, it is likely that the interface between the domains, even those merged with the same angle, contained structural defects, as illustrated in Figure 4.4e and f. These linear defects acted as carrier scattering sites, thus lowering the mobility. As discussed earlier, the spatial resolution of the AFM and Raman measurements was not sufficient to detect such atomic defects. Although the hexagonal graphene domains had the same angle, nucleation occurred randomly, making it difficult to seamlessly connect a series of hexagonal rings. The connection of the growing front of the graphene domains, with limited exposure to the Cu surface, is a dynamic and complicated phenomenon. It is speculated that a much higher temperature, near the melting temperature of carbon, might be necessary to ensure atomic-level connection between adjacent graphene domains, as illustrated in Figure 4.4d.[7-9] It is considered that this is related to the domain size of graphene, as large domains require high energies to reconstruct the atomic lattice of the graphene hexagon network. However, smaller domains do not need high energy to entirely reconstruct the graphene lattice. Therefore,

further optimization of the growth conditions could enhance the atomic connection of the merged graphene interfaces, realizing large-area single crystal graphene sheets. Alternatively, current-induced heating may be also able to heal the interface defects of merged graphene domains.

The charge transport properties varied depending on the nature of the merged domains. Some devices showed different temperature dependences from the result shown in Figure 4.9d. Figure 4.10 shows some of the devices that had the highest mobility as well as the largest CNP shift at ~200 K. Since the wet-transfer process was carried out using an etching solution (HCl, $FeCl_3$) and H_2O (see Experimental Section), impurities may be trapped between the graphene and SiO_2 surface. A recent report on the fabrication of artificial stacks in two-dimensional sheets suggested that impurities, such as hydrocarbons, are present between the transferred graphene and SiO_2/Si substrate.[10] Before the measurements were performed, the graphene devices were annealed in a vacuum at 200 °C to remove any impurities, and it was confirmed using AFM measurements that there were no significant impurities on the surfaces of the transferred graphene sheets. However, it was difficult to completely remove any trapped impurities underneath the transferred graphene sheets, because graphene can deform elastically and is impermeable.[11-13] To use CVD-grown graphene in high-performance electrical devices, reduction of the impurities should be considered.

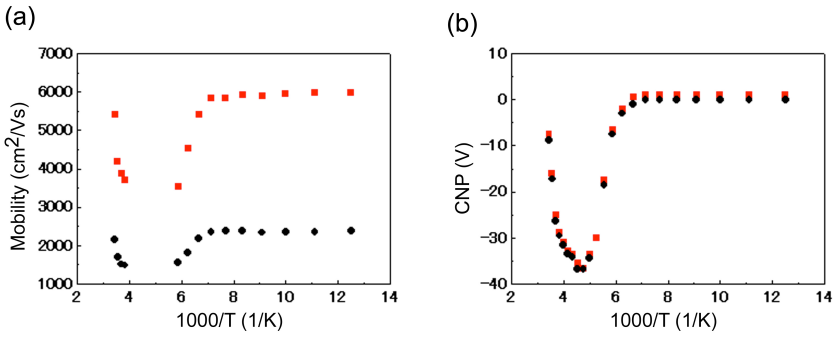

Figure 4.10 Temperature dependence of mobility (a) and CNP (b) of inter-domain (red) and intra-domain (black) devices.

Here, I would like to discuss graphene domains merged with different orientations. The angle between

two graphene domains was -10 º and measurement areas of both AFM and Raman mapping are displayed in an optical image (Figure 4.11a). Some lines were observed between graphene domains by AFM, as seen in Figure 4.11c. Optical micrograph (Figure 4.11a) and Raman mapping images of I_{2D}/I_G and I_G/I_D rations (Figure 4.11d) indicated that graphene was single-layer included parts of few layer regions and linear D-band. Thus, these lines in AFM can be assigned wrinkles and overlapped area in graphene. Graphene device in four terminal systems were fabricated as shown in Figure 4.11a. The resistivity were 5900 and 7300Ω・m at the intra-domain (between electrodes 1 and 2) and the inter-domain (between electrodes 2 and 3) in Figure 4.11a, and the hall-mobility 2200 cm^2/Vs at the intra-domain F and 1400 cm^2/Vs at the inter-domain G were estimated based on conductivity in Figure 4.11b. Again, at the inter-domain region, carrier scattering is suggested to be predominant.

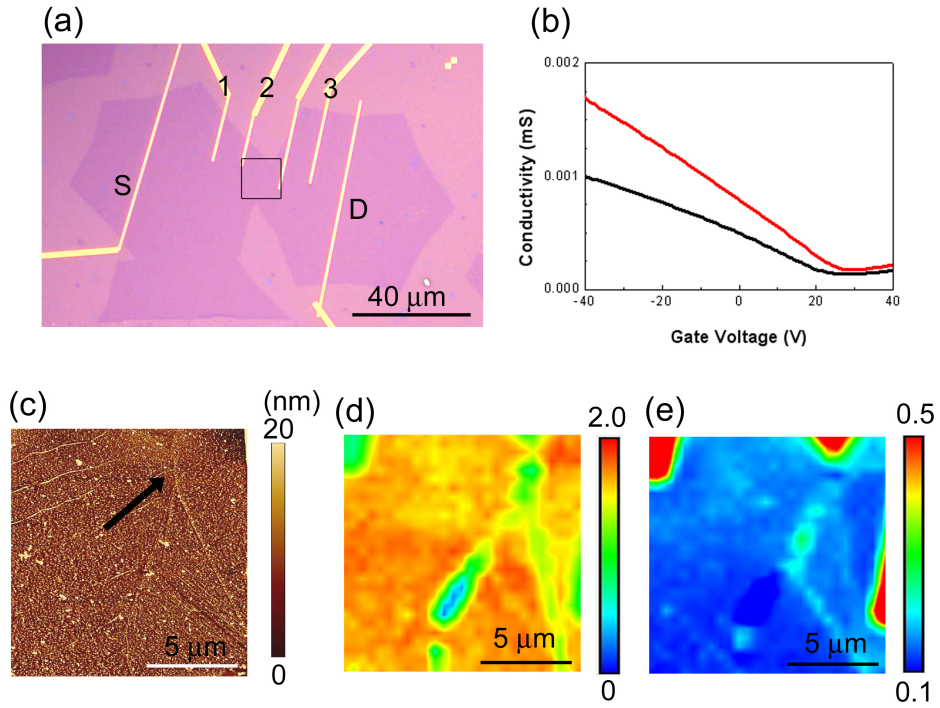

Figure 4.11 Optical micrograph (a), AFM image (c), and Raman mapping image I_{2D}/I_G (d) and I_D/I_G (e) (c) of hexagonal domains merged with a different angle (-10 º). Clear wrinkle and D-band are observed at this interface. (b) Transport properties of graphene device shown in (a).

Recently, some experimental works on the charge transport properties of CVD-grown graphene across

two graphene domains have been reported.[14-17] Investigations using scanning tunneling microscopy (STM) and spectroscopy (STS) suggest that the domain boundaries in CVD-grown graphene induce disorder scattering and result in a high potential barrier.[14,15] It has also been reported that domain boundaries increase the electrical resistance of graphene, compared with single domain areas.[16,17] This study focused on merged domains that all had the same angle, and from temperature dependence measurements we revealed that thermally activated phonon scattering is dominant at the intra-domains, while impurity scattering occurs at the inter-domains.

4-8 Summary

The charge carrier scattering sites and mechanisms were investigated in CVD-grow graphene using charge transport measurements across the interfaces of two large hexagonal domains that were grown on heteroepitaxial Cu films. Approximately half of the merged domains showed clear wrinkles along the interfaces, indicating that thermal stress induced the wrinkle formation at the boundaries. Some of the interfaces of the merged domains showed no wrinkles and a negligible D-band. The carrier transport was reduced, even at these interfaces. In addition, the temperature dependence of the mobility showed different tendencies for the intra-domain and inter-domain devices. The latter suffered from impurity scattering, caused by imperfect interfaces. This work indicates that the domain interface has a strong influence on the charge carrier transport properties and could be useful in the development of high-performance graphene-based electronics.

References:

[1] K. I. Bolotin, K. J. Sikes, Z. Jiang, M. Klima, G. Fudenberg, J. Hone, P. Kim, H.L. Stormer, Ultrahigh Electron Mobility in Suspended Graphene. *Solid State Commun.* **146**, 351 (2008).

[2] K. S. Novoselov, A. K. Geim, S. V. Morozov, D. Jiang, Y. Zhang, S. V. Dubonos, I. V. Grigorieva, A. A. Firsov, Electric Field Effect in Atomically Thin Carbon Films. *Science* **306**, 666 (2004).

[3] H. Ago, K. Kawahara, Y. Ogawa, S. Tanoue, M. A. Bissett, M. Tsuji, H. Sakaguchi, R. J. Koch, F. Fromm, T. Seyller, K. Komatsu, K. Tsukagoshi, Epitaxial Growth and Electronic Properties of Large Hexagonal Graphene Domains on Cu(111) Thin Film. *Appl. Phys. Express* **6***,* 075101 (2013).

[4] Y. Ban, E. Y. Sherman, Shape-dependent charge and spin transport through an electron waveguide. *J. Appl. Phys*, **113**, 043716 (2013).

[5] S. Ihnatsenka, G. Kirczenow, Effect of edge reconstruction and electron-electron interactions on quantum transport in graphene nanoribbons. *Phys. Rev. B* **88**, 125430 (2013).

[6] H. S. Song, S. L. Li, H. Miyazaki, S. Sato, K. Hayashi, A. Yamada, N. Yokoyama, K. Tsukagoshi, Origin of the relatively low transport mobility of graphene grown through chemical vapor deposition. *Sci. Rep.* **2**, 337 (2012).

[7] Y. Wang, A. J. Page, Y. Nishimoto, H.-J. Qian, K. Morokuma, S. Irle, Template Effect in the Competition between Haeckelite and Graphene Growth on Ni(111): Quantum Chemical Molecular Dynamics Simulations. *J. Am. Chem. Soc.* **133**, 18837 (2011).

[8] A. Barreiro, F. Börrnert, S. M. Avdoshenko, B. Rellinghaus, G. Cuniberti, M. H. Rümmeli, L. M. K. Vandersypen, Understanding the Catalyst-Free Transformation of Amorphous Carbon into Graphene by Current-Induced Annealing. *Sci. Rep.* **3**, 1115 (2013).

[9] B. Westenfelder, J. C. Meyer, J. Biskupek, S. Kurasch, F. Scholz, C. E. Krill, U. Kaiser, Transformations of Carbon Adsorbates on Graphene Substrates under Extreme Heat. *Nano Lett.* **11**, 5123 (2011).

[10] S. J. haigh, A. Gholinia, R. jalil, S. Romani, L. Britnell, D. C. Elias, K. S. Novoselov, L. A. Ponomarenko, A. K. Gime, R. Gorbachev, Cross-Sectional Imaging of Individual Layers and Buried Interfaces of Graphene-Based Heterostructures and Superlattices. *Nat. Mater.* **2012**, *11*, 764.

[11] T. Georgiou, L. Britnell, P. Blake, R. V. Gorbachev, A. Gholinia, A. K. Geim, Graphene Bubbles with Controllable Curvature. *Appl. Phys. Lett.* **99**, 093103 (2011).

[12] J. Zabel, R. R. Nair, A. Ott, T. Georgiou, A. K. Geim, K. S. Novoselov, A. Casiraghi, Raman Spectroscopy of Graphene and Bilayer under Biaxial Strain: Bubbles and Balloons. *Nano Lett.* **12**, 617 (2012).

[13] E. Strolyarova, D. Stolyarov, K. Bolotin, S. Ryu, L. Liu, K. T. Rim, M. Klima, M. Hybertsen, I. Pogorelsky, I. Pavlishin, K. Kusche, J. Hone, P. Kim, H. L. Stormer, V.Yakimenko, G. Flynn, Observation of Graphene Bubbles and Effective Mass Transport under Graphene Films. *Nano Lett*. **9**, 332 (2009).

[14] J. C. Koepke, J. D. Wood, D. Estrada, Z. Y. Ong, K. T. He, E. Pop, J. W. Lyding, Atomic-Scale Evidence for Potential Barriers and Strong Carrier Scattering at Graphene Grain Boundaries: A Scanning Tunneling Microscopy Study. *ACS Nano* **7**, 75 (2013).

[15] K. W. Clark, X.-G. Zhang, I. V. Vlassiouk, G. He, R. M. Feenstra, A.-P. Li, Spatially Resolved Mapping of Electrical Conductivity across Individual Domain (Grain) Boundaries in Graphene. *ACS Nano* **7**, 7956 (2013).

[16] L. A. Jauregui, H. Cao, W. Wu, Q. Yu, Y. P. Chen, Electronic properties of grains and grain boundaries in graphene grown by chemical vapor deposition. *Solid State Commun.* **151***,* 1100 (2011).

[17] A. W. Tsen, L. Brown, M. P. Levendorf, F. Ghahari, P. Y. Huang, R. W. Havener, C. S. Ruiz-Vargas, D. A. Muller, P. Kim, J. Park, Tailoring Electrical Transport across Grain Boundaries in Polycrystalline Graphene. *Science* 336, 1143 (2012).

Chapter 5:

Self-assembly of polar phthalocyanine molecules on CVD-grown graphene

Abstract:

Integration of functional organic molecules with graphene is expected to promote the development of graphene-based flexible electronics with novel properties. Here, the self-assembled structure of dipole phthalocyanine molecules, chloro-aluminum phthalocyanine (ClAlPc), on single-layer graphene grown by chemical vapor deposition (CVD) over a Cu film was characterized by low-temperature scanning tunneling microscopy (LT-STM). The phthalocyanine molecules show highly ordered assembled structures on the CVD-grown graphene, and these molecular layers extend continuously over the steps of the Cu film. I also observed specific boundaries in the self-assembled molecule arrays, which can be explained by the presence of domain boundaries in the graphene. The STM results suggest that CVD-grown graphene is a good molecular assembly template for surface functionalization and these molecular arrays facilitate the study of the domain structures in CVD-grown graphene.

5-5 Introduction

Graphene's unique properties promise applications in many fields, in particular in flexible electronics. Graphene is also a good candidate for tuning the surface properties after transfer to a target substrate, such as changing the substrate's surface energy, hydrophilicity/hydrophobicity, chemical reactivity, and charge injection efficiency.[1-5] Self-assembly of functional molecules on graphene is a promising method for the realization of graphene-based flexible electronics without degrading the sp^2 network of graphene, because the π-π interaction is a non-covalent interaction between the π orbitals of the graphene and adsorbed molecules, thus maintaining the original sp^2-network of graphene. The understanding and control of assembled structures of adsorbed molecules on graphene is important in terms of potential applications in nanoscale fabrication as well as functionalization of graphene devices.

In the previous reports of phthalocyanine molecules deposited on graphene grown on metal surface, molecular self-assembled structures are correlated with the surface structure, such as the moiré corrugation of graphene and underlying metal substrate which acts as trapping sites of molecules.[6-10] So far, these studies were limited to highly-oriented pyrolytic graphite (HOPG)[11-13] substrates and single-layer graphene grown on Ru(0001),[6-8] Rh(111),[9] Ir(111),[10] and SiC[14] inside an ultra-high vacuum (UHV) chamber equipped with a scanning tunneling microscope (STM). Considering the current advances in chemical vapor deposition (CVD) growth and transfer of graphene, it is interesting to study graphene grown on Cu catalyst as a template for the self-assembled phthalocyanine.[14,15] Although CVD growth on Cu can provide a uniform and large-area single-layer graphene film, the as-grown graphene usually has a multi-domain structures with domain boundaries which may degrade the physical properties of graphene. Therefore, it is also interesting to investigate the effects of domain structure and boundaries in CVD-grown graphene on the assembled structures of adsorbed molecules.

In this chapter, a low-temperature STM (LT-STM) study of self-assembled structures of polar

phthalocyanine molecules, chloro-aluminum phthalocyanine (ClAlPc), on multi-domain single-layer CVD-grown graphene grown over a Cu(100) film is presented. It is found that the ClAlPc molecules form highly ordered 2D superstructures continuously on the graphene surface. The orientation and the grain boundaries of the self-assembled 2D molecular arrays depend on the domain boundaries of CVD-grown graphene, indicating that the geometry of CVD-grown graphene has a pronounced influence on the assembled structure of the organic molecules.

5-6 Experiment

- *Graphene growth by CVD and its characterizations*

A heteroepitaxial Cu(100) film with a 500 nm thickness was deposited on a single-crystalline MgO (100) substrate at high temperature by radio-frequency (RF) magnetron sputtering (Shibaura Mechatoronics Corp., CFS-4ES). Single-layer graphene was grown over this Cu(100) film by ambient pressure CVD at 1000 °C with flowing CH_4, H_2 , and Ar gases for 10 minutes. This experimental condition was same as that in Chapter 3-2. As-grown graphene were investigated by scanning electron microscopy (SEM), atomic force microscopy (AFM), Raman spectroscopy, and LT-STM.

- *Thermal deposition of ClAlPc molecules*

The as-grown graphene was exposed to air before loading into a UHV chamber. The graphene/Cu(100)/MgO(100) was placed inside the UHV chamber connected to a LT-STM measuring chamber, followed by annealing at 200 °C to clean the graphene surface. After cleaning the graphene surface, a ClAlPc molecular source was heated at 285 °C to evaporate onto the graphene surface which was kept at near room temperature without heating the substrate. This deposition process was done under a base pressure lower than ~10^{-7} Pa, and the amount of surface adsorbed molecules was controlled by the evaporation time.

- *LT-STM observation*

LT-STM was carried out at ~ -196 °C (77 K) and under ~10^{-8} Pa with a constant current mode to characterize the atomic structure of the as-grown graphene and the packing geometry of ClAlPc molecules on it.[17] All the STM images shown in this chapter reflect height profiles.

- *Thermal annealing process of ClAlPc molecular array*

Effect of thermal annealing on the molecular packing structure was also investigated by heating ClAlPc arrays on the graphene substrate at 100-265 °C in vacuum without supplying additional ClAlPc molecules.

5-7 Results and discussion

Figure 5.1 shows results about as-grown graphene on a Cu(100) film. These wrinkles were seen by SEM (Figure 5.1c). We also observed wrinkles in graphene (marked by arrows in Figure 5.1b), which are ascribed to different thermal expansion coefficients of graphene and Cu metal. The surface roughness is estimated to be less than 0.5 nm RMS in a 10 μm square area based on the AFM image shown in Figure SI-1a. The growth of single-layer graphene on the heteroepitaxial Cu(100) film was confirmed by Raman spectroscopy in Figure 5.1b. The narrow full-width half maximum (FWHM) of the 2D band (<30 cm^{-1}), high intensity ratio of the 2D to G bands (2D/G ratio ~ 1.8), and negligible D band intensity indicate that high-quality single-layer graphene is grown on the Cu surface (Figure 5.1c).

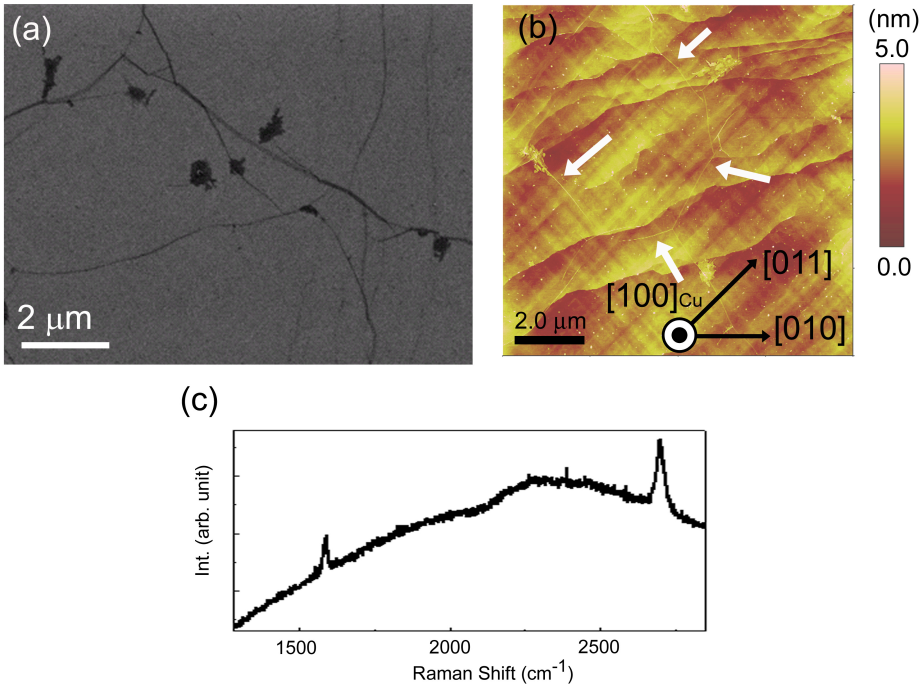

Figure 5.1 SEM image (a), AFM image (b), and Raman spectrum (c) of as-CVD graphene grown on a heteroepitaxial Cu(100) film. White arrows in (b) indicate wrinkles in CVD-grown graphene.

The use of a heteroepitaxial Cu(100) film allows us to control the structure of the resulting graphene domains, as discussed in Chapter 3. Figure 5.2 shows the surface morphology and atomic structure of as-grown CVD-grown graphene on the Cu(100) measured by STM. STM as well as AFM images indicate that there are two types of surface steps; periodic steps running along the <001> and <011> direction and other steps with random orientation (Figures 5.1b, 5.2a,c). Typical step height was around 0.2-0.4 nm, as seen in Figure 5.2d. I found that graphene grows continuously across steps on the Cu film (Figures 5.2e,f).

Note that our graphene/Cu(100) surface shows no moiré patterns in the STM images (Figures 5.2). This suggests that the graphene is decoupled from the Cu film.[18-20] In our experiment, graphene was grown by CVD under the ambient pressure and exposed in the air to be transferred into the UHV chamber, followed by thermal annealing in vacuum for the STM measurement. This air exposure can cause the

oxidation of the Cu film and may also intercalate gases between the graphene and Cu, leading to the decoupling of CVD-grown graphene from the Cu surface.[21,22]

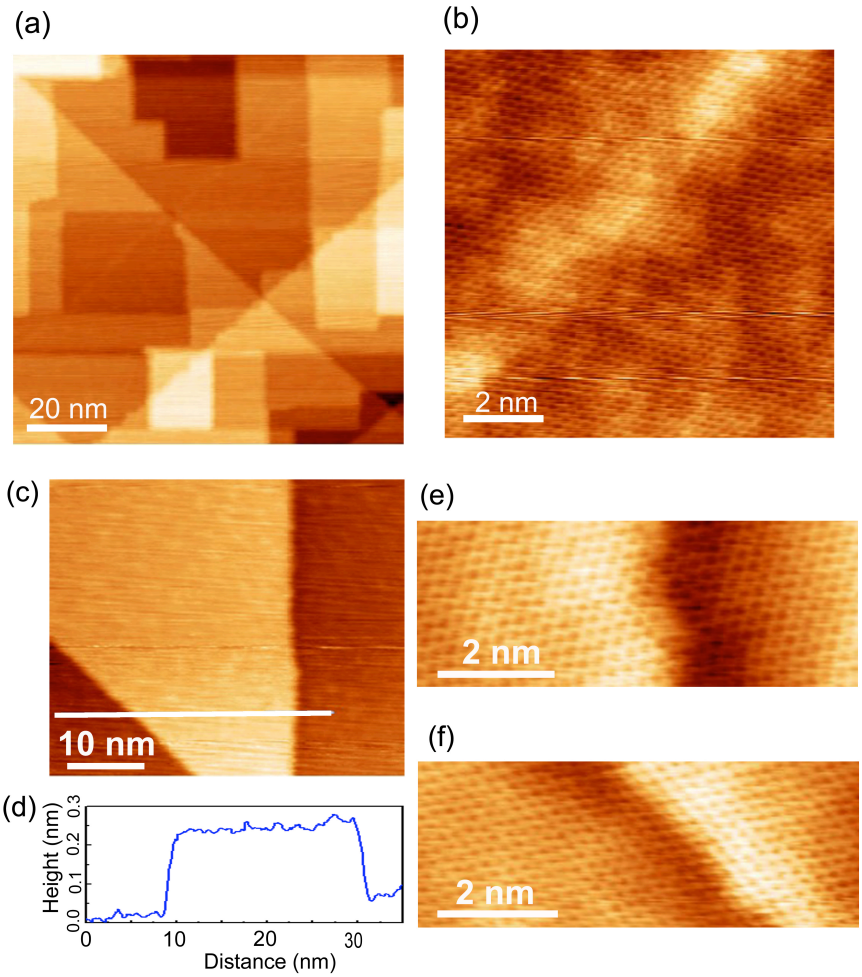

Figure 5.2 (a-c,e,f) STM images of CVD-grown graphene on the Cu film measured for different scan areas, 100×100 nm (a) and 10×10 nm (b) and (b) height profile measured along the white line in (c). CVD-grown graphene continuously grew across Cu steps. The high-resolution images along the right and left steps in (c) shown in (e) and (f), respectively. Scanning parameters:(a) V_{tip} = 2.0 V, I = 80 pA; (b, c,e,f) V_{tip} = 1.0 V, I = 80 pA.

Although moiré patterns were not observed, the honeycomb lattice of graphene was clearly observed by our LT-STM measurement, as shown in Figure 5.3. I observed two major orientations in the graphene lattice at several arbitrary points, $[10]_{graphene}//[011]_{Cu(100)}$ and $[01]_{graphene}//[011]_{Cu(100)}$. These two relative

orientations are depicted in the insets of Figures 5.3. These two main orientations reflect the difference of the lattice symmetry of graphene (six-fold symmetry) and the Cu lattice (four-fold symmetry), being consistent with our previous LEED and LEEM results.[39] Thus, the graphene on the Cu(100) has a multi-domain structure with well-defined domain orientations, which offers a good platform to analyze a self-assembled molecular structure in relation to graphene's domain structure. Because of the limited scan area of the STM, we could not find domain boundaries in the single-layer graphene.

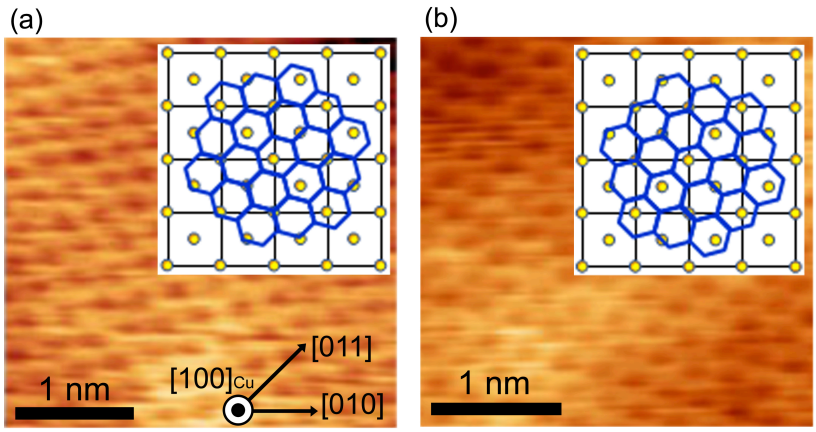

Figure 5.3 The high resolution STM images of as-grown graphene on Cu(100). The insets show a crystallographic relationship between graphene and Cu(100) lattice. Blue and yellow atoms represent carbon and Cu atoms, respectively. Scanning parameters: V_{tip} = 1.0 V, I = 100 pA.

Next I deposited ClAlPc molecules onto the graphene/Cu(100) by thermal evaporation. Figures 5.4a,b represent atomic models of a ClAlPc molecule viewed from the top and side, respectively. This phthalocyanine molecule is selected as a model system mainly due to the presence of rigid π-conjugated network which is supposed to interact with graphene through π–π interaction. In addition, this ClAlPc molecule has a permanent dipole moment perpendicular to the π-plane, which can be used to obtain a large dipole moment in graphene. This molecule is also useful in organic solar cells, because it acts as an electron donor through the control of their molecular configuration.[23,24] Figure 5.4c is an STM image of

the phthalocyanine molecules adsorbed on the graphene surface. The adsorbed ClAlPc molecules produced a highly ordered structure on the CVD-grown graphene due to the π–π interaction and protruding Cl atoms. The molecular arrays have a uniform and continuous structure. In this case, graphene was almost fully covered with the first ClAlPc layer and partially with a second layer. The height difference of the first and second layers was 0.3 nm, corresponding to the thickness of a single phthalocyanine molecule. High-magnification STM images measured for the first and second layers are shown in Figures 5.4d and e, respectively. Different atomic images were observed in the first and second layers. The π-planes of ClAlPc molecules lay down in parallel with the graphene surface, and there are two orientations with respect to Cl position; Cl atom pointing to vacuum (Cl-up) and Cl atom pointing to graphene (Cl-down). The four-lobe feature with a bright central protrusion observed in the first layer (Figure 5.4d) was assigned to the Cl-up configuration. Here, the bright spots in Figure 5.4d correspond to Cl atoms. On the other hand, the Cl-down configuration was observed for the second layer, displaying a square-shaped π-network of the phthalocyanine molecules (Figure 5.4e). Both the first and second layers have a square unit cell of ClAlPc molecules, with lattice constants of $a=b=1.58$ nm and $\gamma=90°$. The schematic model of a unit cell of ClAlPc molecules deposited on graphene is depicted in Figure 5.4f. The Cl-up configuration observed for the first ClAlPc layer is a consequence of the effective π–π interaction between the graphene and phthalocyanine, avoiding the unstable Cl-down configuration due to steric hindrance of the protruding Cl atom. In the case of the second layer, ClAlPc molecules are likely to be located at the hollow sites in the first layer with the Cl-down configuration in order to make a closed packed structure and the electrostatic interaction energetically stable. The second layer has the same orientation with the first layer, but the relative position is offset by $a/2$ against to the first layer. The observed self-assembled structure of ClAlPc molecules are similar to that observed on a HOPG surface.[27-29] Thus, it is considered that the underlying Cu film does not strongly influence the

orientation of the phthalocyanine molecules. This suggests that the molecular array has the same structure even on a graphene sheet transferred onto any substrates. Owing to the well-defined graphene lattice on the Cu(100), we can determine the relative orientation of ClAlPc molecules in the first layer respect to the graphene lattice, $<11>_{graphene}$ // $<11>_{ClAlPc}$, as displayed in Figure 5.4f. It is also observed that the atomic steps of the Cu film with a height around 0.2-0.5 nm do not affect the packing geometry and the orientation of the ClAlPc molecules. Figure 5.4 d,e show STM images of ClAlPc molecules assembled across the atomic steps of the underlying Cu surface. This indicates that ClAlPc layers can continuously extend over Cu steps.

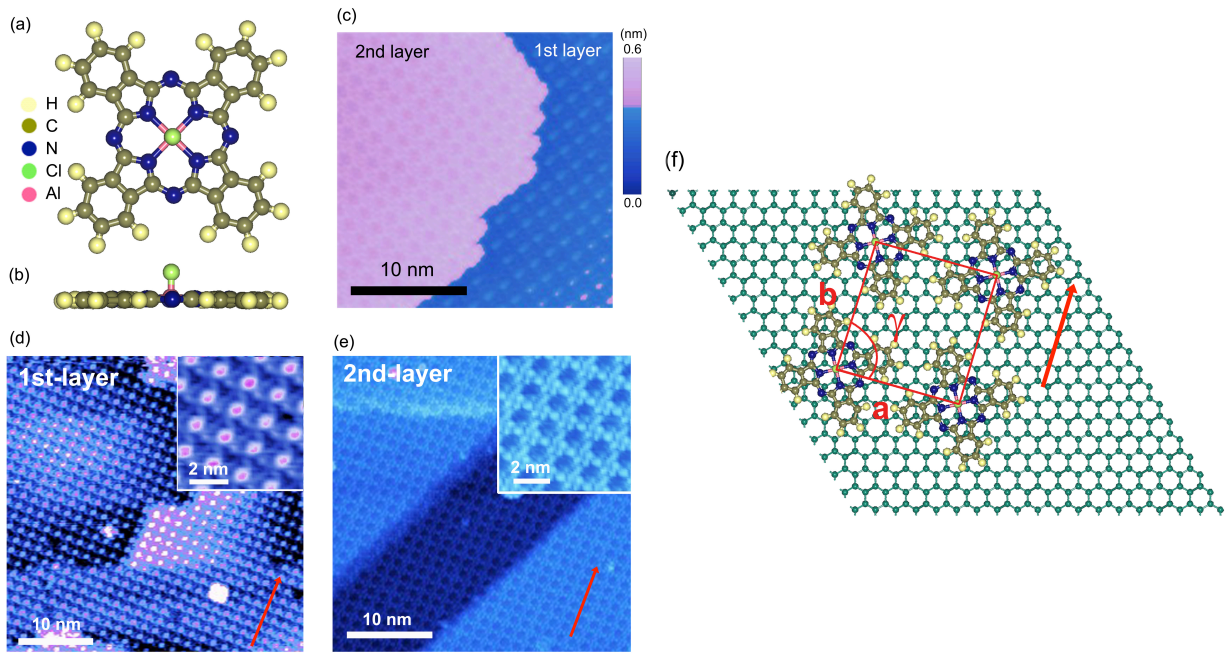

Figure 5.4 (a,b) Structure of a ClAlPc molecule viewing from top and side. (c-e) STM image of the assembled film of ClAlPc molecules of the first (d) and second layers (e) on graphene/Cu(100). The ClAlPc arrays show continuous films across the Cu steps. Insets in (d,e)show the magnified images. (e) Schematic model of a unit cell of ClAlPc molecules with respect to graphene lattice. Red arrows represent the direction parallel to b axis in the unit cell of ClAlPc molecules. Scanning parameters: (c) V_{tip} = 2.5 V, I =75 pA; (a) V_{tip} = 2.0 V, I = 75 pA; (b) V_{tip} = 2.5 V, I = 65 pA.

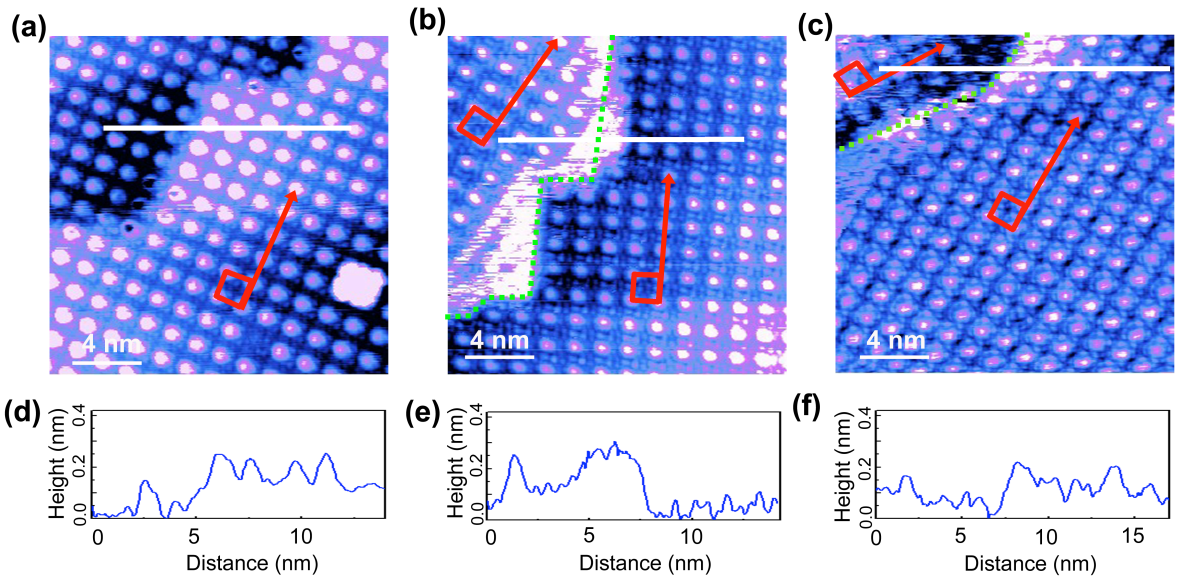

Figure 5.5 (a) STM images of self-assembled ClAlPc molecular arrays (first layer) formed at the steps of the Cu film. The adsorbed molecules form a continuous film crossing the steps. (b,c) Grain boundaries of self-assembled ClAlPc molecules. The red squares and arrows in panels a–c represent the unit cell of ClAlPc and the direction parallel to b axis of the unit cell, respectively. The green broken lines show the grain boundaries of molecular arrays. (d–f) Height profiles measured along the white lines in (a–c). Scanning parameters: (a, c) V_{tip} = 2.0 V, I = 80 pA; (b) V_{tip} = 2.8 V, I = 60 pA.

However, in some areas, we found clear grain boundaries in the self-assembled ClAlPc molecule array, as shown in Figures 5.5b,c. The orientation of the molecular unit cell was rotated by ~ 30° at these grain boundaries (from here, we use "grain" and "domain" for molecules and graphene, respectively). Here, we discuss the origin of changing the orientation of the molecular unit cell. Since the angle of grain rotation (~30º) is consistent with that of the rotation of two neighboring graphene domains shown in Figure 5.3, it is likely that the domain boundaries of graphene induce the observed grain boundary formation in the self-assembled films. There are other possibilities of the origin of the grain rotation observed in the self-assemble film; (i) atomic steps of Cu film, (ii) grain boundaries within a single graphene domain, and (iii) wrinkles in the CVD-grown graphene. The change of the packing direction at the Cu atomic steps (i) is considered unlikely, because we observed the continuity of the ClAlPc film across the Cu atomic steps (see Figures 5.4d,e and 5.5a). Secondaly, the grain boundaries inside a

graphene domain (ii) can be excluded, because the grain boundaries of the self-assembled film are generally accompanied with the disordered atomic packing along the boundary.[25,26] Also, imaging of the wrinkles in CVD-grown graphene (iii) is not possible by our STM observations, because a steep height change due to wrinkle cannot be followed by a STM tip.[27,28] Therefore, we can conclude that the domain boundaries of CVD-grown graphene make an impact on changing the orientation of the molecular unit cell.

In the previous literature, liquid crystalline molecules with a long alkyl chain were used to visualize the graphene domains.[29] LEEM was also used to analyze structures of graphene formed on a metal surface and SiC substrate, but the lateral resolution of LEEM is not sufficient for the observation of domain boundaries and/or atomic defects. In our case, our LT-STM of phthalocyanine molecules gives more precise atomic scale information on the graphene grain boundaries. We should note that it is difficult to directly observe graphene domain boundaries by our LT-STM without the phthalocyanine molecules, as the domain size of our CVD-grown graphene is much larger than the standard STM observation areas. Low magnification STM measurement is not applicable to the atomic scale observation of graphene, but the self-assembled molecules on graphene enabled us to distinguish the domain boundaries even by low magnification imaging.

Finally, we studied effects of thermal annealing on the self-assembled film of the ClAlPc molecules deposited on CVD-grown graphene in order to understand the structural stability of the molecular layers. Firstly, the entire graphene surface was covered with the co-existed bilayer and monolayer ClAlPc molecules with some molecular vacancies (Figure 5.6a). As already mentioned, these molecular arrays form continuously across the Cu steps. The graphene covered with ClAlPc layers was annealed in vacuum to partially desorb the assembled molecules. The annealing at ~114 °C was found to remove the second ClAlPc molecular layer randomly (Figure 5.6b). After further increase of the substrate

temperature up to 230 ºC, the second layer completely evaporated, leaving the uniform first layer (Figure 5.6c). The packing geometry as well as the orientation of the phthalocyanine molecules did not change by this thermal annealing; while subsequent annealing over 240 °C removed most of the adsorbed molecules of the first layer. The surface coverage of the second and first layer ClAlPc at different annealing temperature is shown in Figure 5.6d.

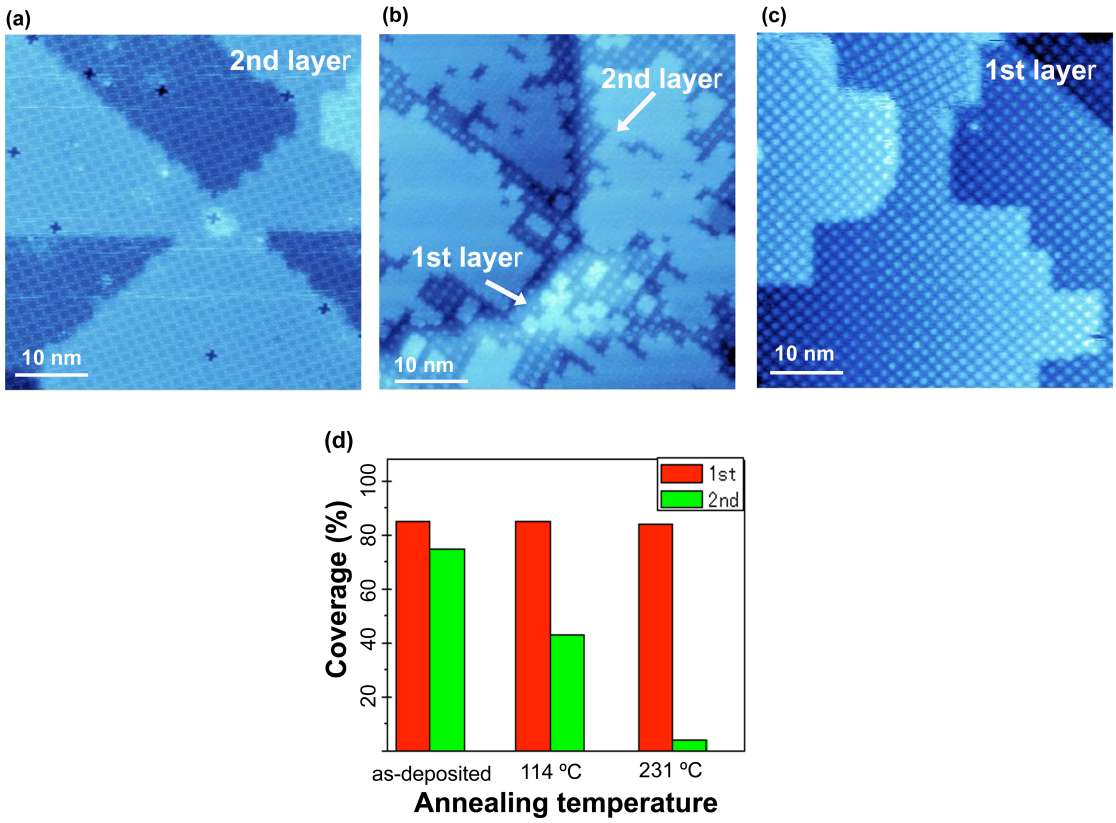

Figure 5.6 Annealing temperature dependence of the ClAlPc assembled films on graphene. (a) Graphene is mostly covered with the first ClAlPc layer and partial second layer. (b) After annealing at 114 °C, the second layer molecules are desorbed partially. (c) After annealing at 231 °C, most of the second layer molecules are desorbed. (d) Surface coverage of first and second layers measured after heat treatment at different temperatures. Scanning parameters: (a) V_{tip} = 2.0 V, I = 90 pA; (b) V_{tip} = 2.0 V, I = 60 pA ; (c) V_{tip} = 2.5 V, I = 80 pA.

Our result clearly indicates that interaction between ClAlPc molecules and graphene surface is stronger than that between the first and second layers of the molecules. Therefore, graphene is an ideal substrate

to accommodate functional organic molecules to form a uniform and stable single layer molecular film. The CVD-grown transferrable graphene offers a promising approach to modify the target substrate surface not only by the transferred graphene itself but also by the overlaying self-assembled molecules with different properties, such as a dipole moment like ClAlPc. Therefore, our findings open a new way to modify the substrate surface by self-assembly on graphene as well as to visualize domain boundaries of graphene.

5-8 Summary

The assembled structures of polar phthalocyanine molecules, ClAlPc, on single-layer CVD-grown graphene with a controlled multi-domain structure are studied by using LT-STM. The CVD-grown graphene on Cu(100) film are decoupled, showing no obvious moiré pattern, and the ClAlPc molecules can form a highly ordered 2D molecular dipole arrays on the graphene surface. Grain boundaries of self-assembled ClAlPc layers with ~30º rotation are observed, which are related to the domain boundary of underlying graphene. These results demonstrate that the CVD-grown graphene is a good template for self-assembly of π−conjugated molecules and that the molecular assembled structure can be used as a molecular probe to visualize the graphene's domain boundaries. The annealing experiment verifies that the molecule-graphene interaction is stronger than van der Waals interaction between the interlayer ClAlPc molecules. Our studies highlight a possible route to functionalize large-area CVD-grown graphene by molecular assembly for future flexible electronic applications of graphene. This molecular assembly approach also offers a new method of molecular-level visualization of graphene's domain boundaries

References:

[1] J. Rafiee, X. Mi, H. Gullapalli, A. V. Thomas, F. Yavari, Y. Shi, P. M. Ajayan, N. A. Koratkar, Wetting Transparency of Graphene. *Nature* **11**, 217 (2012).

[2] C. J. Shih, Q. H. Wang, S. Lin, K.-C. Park, Z. Jin, Breakdown in the Wetting Transparency of Graphene. *Phys. Rev. Lett.* **109**, 176101 (2012).

[3] H. Y. Mao, R. Wang, Y. Wang, T. C. Niu, J. Q. Zhong, M. Y. Huang, D. C. Qi, K. P. Loh, A. T. S. Wee, W. Chen, Chemical Vapor Deposition Graphene as Structural Template to Control Interfacial Molecular Orientation of Chloroaluminium Phthalocyanine. *Appl. Phys. Lett.* **99**, 093301 (2011).

[4] Q.-H. Wu, G. Hong, T. W. Ng, S. T. Lee, Substrate Effect on the Electronic Structures of CuPc/Graphene Interfaces. *Appl. Phys. Lett.* **100**, 161603 (2012).

[5] W. H. Lee, J. Park, S. H. Sim, S. B. Jo, K. S. Kim, B. H. Hong, K. Cho, Transparent Flexible Organic Transistors Based on Monolayer Graphene Electrodes on Plastic. *Adv. Mater.* **23**, 1752 (2011).

[6] J. Mao, H. Zhang, Y. Jiang, Y. Pan, M. Gao, W. Xiao, H.-J. Gao, Tunability of Supramolecular Kagome Lattices of Magnetic Phthalocyanines Using Graphene-Based Moiré Patterns as Templates. *J. Am. Chem. Soc.* **131**, 14136 (2009).

[7] H. G. Zhang, J. T. Sun, T. Low, L. Z. Zhang, Y. Pan, Q. Liu, J. H. Mao, H. T. Zhou, H. M. Guo, S. X. Du, F. Guinea, H.-J. Gao, Assembly of Iron Phthalocyanine and Pentacene Molecules on a Graphene Monolayer Grown on Ru(0001). *Phys. Rev. B* **84**, 245436 (2011).

[8] Brugger, T.; Günther, S. G.; Wang, B.; Dil, J. H.; Bocquet, M.-L.; Osterwalder, J.; Wintterlin, J.; Greber, T. Comparison of Electronic Structure and Template Function of Single-Layer Graphene and a Hexagonal Boron Nitride Nanomesh on Ru(0001). *Phys. Rev. B*, **79**, 045407 (2011).

[9] A. J. Pollard, E. W. Perkins, N. A. Smith, A. Saywell, G. Goretzki, A. G. Phillips, S. P. Argent, H. Sachdev, F. Müller, S. Hüfner, S. Gsell, M. Fischer, M. Schreck, J. Osterwalder, T. Greber, S. Berner, N. Champness, P. Beton, Supramolecular Assemblies Formed on an Epitaxial Graphene Superstructure. *Angew. Chem., Int. Ed.* **49**, 1794 (2010).

[10] S. K. Hämäläinen, M. Stepanova, R. Drost, P. Liljeroth, J. Lahtinen, J. Sainio, Self-Assembly of Cobalt-Phthalocyanine Molecules on Epitaxial Graphene on Ir(111). *J. Phys. Chem. C* **116**, 20433 (2012).

[11] S. Kera, H. Yamane, H. Honda, H. Fukagawa, K. K. Okudaira, N. Ueno, Photoelectron Fine Structures of Uppermost Valence Band for Well-Characterized ClAl-Phthalocyanine Ultrathin Film UPS and MAES Study. *Surf. Sci.* 571 (2004).

[12] Y. L. Hang, R. Wang, T. C. Niu, S. Kera, N. Ueno, J. Pflaum, A. T. S. Wee, W. Chen, One Dimensional Molecular Dipole Chain Arrays on Graphite via Nanoscale Phase Separation. *Chem. Comm*. **46**, 9040 (2010).

[13] T. C. Niu, Y. L. Huang, J. T. Sun, S. Kera, N. Ueno, A. T. S. Wee, W. Chen, Tunable Two-Dimensional Molecular Dipole Dot Arrays on Graphite. *Appl. Phys. Lett*. **99**, 143114 (2011).

[14] H. Huang, S. Chen, X. Gao, W. Chen, A. T. S. Wee, Structural and Electronic Properties of PTCDA Thin Films on Epitaxial Graphene. *ACS Nano* **2009**, *3*, 3431-3436 (2009).

[15] K. Xiao, W. Deng, J. K. Keum, M. Yoon, I. V. Vlassiouk, K. W. Clark, A.-P. Li, I. I. Kravchenko, G. Gu, E. A. Payzant, B. G. Sumpter, S. C. Smith, J. F. Browning, D. B. Geohegan, Surface-Induced Orientation Control of CuPc Molecules for the Epitaxial Growth of Highly Ordered Organic Crystals on Graphene. *J. Am. Chem. Soc.* **135**, 3680 (2013).

[16] P. Järvinen, S. K. Hämäläinen, K. Banerjee, P. Häkkinen, M. Ijäs, A. Harju, P. Liljeroth, Molecular Self-Assembly on Graphene on SiO_2 and h−BN Substrates. *Nano Lett*, **13**, 3199 (2013).

[17] H. L. Zhang, W. Chen, L. Chen, H. Huang, X. S. Wang, J. Yuhara, A. T. S. Wee, C_{60} Molecular Chains on α−Sexithiophene Nanostripes. *Small* **3**, 2015 (2003).

[18] I. Jeon, H. Yang, S.-H. Lee, J. Heo, D. H. Seo, J. Shin, U.-I Chung, Z. G. Kim, H.-J. Chung, S. Seo, Passivation of Metal Surface States: Microscopic Origin for Uniform Monolayer Graphene by Low Temperature Chemical Vapor Deposition. *ACS Nano* **5**, 1915 (2011).

[19] J. Cho, L. Gao, J. Tian, H. Cao, W. Wu, Q. Yu, E. N. Yitamben, B. Fisher, J. R. Guest, Y. P. Chen, N. P. Guisinger、 Atomic-Scale Investigation of Graphene Grown on Cu Foil and the Effects of Thermal Annealing. *ACS Nano* **5**, 3607 (2011).

[20] H. I. Rasool, E. B. Song, M. Mecklenburg, B. C. Regan, K. L. Wang, B. H. Weiller, J. K. Gimzewski, Atomic-Scale Characterization of Graphene Grown on Copper (100) Single Crystals. *J. Am. Chem. Soc.* **133**, 12536 (2011).

[21] K. T. He, J. D. Wood, G. P. Doidge, E. Pop, J. W. Lyding, Scanning Tunneling Microscopy Study and Nanomanipulation of Graphene-Coated Water on Mica. *Nano Lett*. **2012**, *12*, 2665−2672.

[22] X. Feng, S. Maier, M. Salmeron, Water Splits Epitaxial Graphene and Intercalates. *J. Am. Chem. Soc.* **134**, 5662 (2012).

[23] R. F. Bailey-Salzman, B. P. Rand, S. R. Forrest, Near-Infrared Sensitive Small Molecule Organic Photovoltaic Cells Based on Chloroaluminum Phthalocyanine. *Appl. Phys. Lett.* **91**, 013508 (2007).

[24] B. Verreet, R. Müller, B. P. Rand, K. Vasseur, P. Heremans, Structural Templating of Chloro-Aluminum Phthalocyanine Layers for Planar and Bulk Heterojunction Organic Solar Cells. *Org. Electronics* **12**, 2131 (2011).

[25] Y. Wakayama, Assembly Process and Epitaxy of the F_{16}CuPc Monolayer on Cu(111). *J. Phys. Chem. C*, **111**, 2675 (2007)

[26] Y. L. Huang, Y. Lu, T. C. Niu, H. Huang, S. Kera, N. Ueno, A. T. S. Wee, W. Chen, Reversible Single-Molecule Switching in an Ordered Monolayer Molecular Dipole Array. *Small*, **28**, 1423 (2012) .

[27] Y. Zhang, T. Gao, Y. Gao, S. Xie, Q. Ji, K. Yan, H. Peng, Z. Liu, Defect-like Structures of Graphene on Copper Foils for Strain Relief Investigated by High-Resolution Scanning Tunneling Microscopy. *ACS Nano* **5**, 4014 (2011).

[28] M. Lanza, Y. Wang, A. Bayerl, T. Gao, M. Porti, M. Nafria, H. Liang, G. Jing, Z. Liu, Y. Zhang, Y. Tong, H. Duan, Tuning Graphene Morphology by Substrate Towards Wrinkle-Free Devices: Experiment and Simulation. *J. Appl. Phys.* **113**, 104301 (2013).

[29] D. W. Kim, Y. H. Kim, H. S. Jeong, H.-T. Jung, Direct Visualization of Large-Area Graphene Domains and Boundaries by Optical Birefringency. *Nat. Nanotechnol*. **7**, 29 (2011).

Chapter 6:

Conclusions and Outlook

6.1 Conclusions

In this thesis, the domain structure of graphene synthesized by chemical vapor deposition (CVD) and its influence on electrical properties and molecular assembly are discussed. Orientation control of graphene domains has been achieved by epitaxial CVD growth using Cu(111) and Cu(100) films. The key point is the crystallographic symmetry matching of graphene and Cu catalyst film. The combination of LEEM and Raman measurements allowed the observation of the domain structure and boundaries in CVD-grown graphene, combined with the corresponding distribution of the Raman D-band intensity. This epitaxial CVD approach leads to the formation of large hexagonal graphene domains with controlled orientations and enables the evaluation of the electrical charge transport at the interfaces across two graphene domains. Charge transport measurements evinced the significant carrier scatting at the interface of domains. It is suggested that further understanding of the growth mechanism should improve the structural control of graphene, improving its physical properties. At the same time, however, graphene devices within the hexagonal domains show high quality with few defects. The carrier mobility of around 20,000 cm^2/Vs at 280 K was remarkably higher than that of typical exfoliated graphene devices. It clearly shows that our

single-crystalline graphene domains are extremely high quality. Therefore, my achievements are believed to contribute to the development of large-scale graphene synthesized by CVD for its integration in graphene based electronics applications.

The molecular self-assembly on CVD-grown graphene with a controlled multi-domain structure also haa been studied. The dipole phthalocyanine molecules, chloro-aluminum phthalocyanine (ClAlPc), can form a highly ordered 2D molecular dipole arrays with respect to the graphene lattice as well as domain structure. To determine configurations of ClAlPc molecules, the π–π interaction between graphene and these molecules is important. These studies highlight that CVD-grown graphene acts as a good molecular assembly template for surface functionalization and these molecular arrays have the possibility to visualize the domain structures in CVD-grown graphene.

6.2 Future Outlook

The discussion in this thesis has been almost entirely limited to single-layer graphene. However, CVD growth can produce multi-layered graphene as well.[1,2] For double-layer graphene, especially, the graphene's band structure is determined by these stacking angles, allowing subsequent control over electrical and optical properties.[3-5] And also, it is possible to open band gap with 0.2−0.3 eV by applying a vertical electric field.[6] This approach requires further studies about selective growth of AB-stacked double-layer graphene. The optimization and investigation of the stacking structure at the interface between these two vertical layers are also interesting issues.

Moreover, very recently, various kinds of layered two-dimensional (2D) materials have become an interesting research topic because the exfoliation of graphene from bulk graphite has opened up the possibility of isolating and exploring the fascinating properties of atomic layers of other 2D layered materials. Upon reduction to single/few atomic layers these new materials will offer functional flexibility,

new properties, and novel applications. For example, a hexagonal boron nitride (h-BN) thin sheet has been reported as a good candidate for graphene devices in order to enhance mobility, reduced carrier inhomogeneity and intrinsic doping.[7] Transition metal dichalcogenides (TMDCs) thin films have potential applications in flexible photovoltaic device due to their tunable band structure and light adsorption across a wide range.[8,9] The combinations of various two-dimensional (2D) materials in vertical stacks, so called heterostructures, are a promising approach to explore novel materials because of predicted excellent properties. [10] However, some reports have demonstrated that artificial heterostructures prepared by a multi-transfer process suffer from residual impurities, causing undesirable scattering in electrical transport measurements.[11] Thus, it is important and necessary for the design of novel materials to realize the direct growth of these heterostructures combining different layered materials.[12,13] The studies on suitable combinations and functionalized methods to obtain the intended beneficial properties should be rapidly progressing.

Graphene and other nanocarbon materials have great potential to provide a breakthrough for new nanoelectronics. The integration with other 2D materials are expected to progress the novel science and applications as well.

References:

[1] K. Yan, L. Fu, H. Peng, Z. Liu, Designed CVD Growth of Graphene via Process Engineering. *Acc. Chem. Res.* **46**, 2263 (2013).

[2] L. Liu, H. Zhou, R. Cheng, W. J. Yu, Y. Liu, Y. Chen, J. Shaw, X. Zhong, Y. Huang, X. Duan, High-Yield Chemical Vapor Deposition Growth of High-Quality Large-Area AB-Stacked Bilayer Graphene. *ACS Nano* **6**, 8241 (2012).

[3] J. M. B. Lopes dos Santos, N. M. R. Peres, A. H. Castro, Graphene Bilayer with a Twist: Electronic Structure. *Phys. Rev. Lett.* **99**, 256802 (2007).

[4] R. W. Havener, H. Zhuang, L. Brown, R. G. Hennig, J. Park, Angle-Resolved Raman Imaging of Interlayer Rotations and Interactions in Twisted Bilayer Graphene. *Nano Lett*. **12**, 3162 (2012).

[5] K. Kim, S. Coh, L. Tan, W. Regan, J. Yuk, E. Chatterjee, M. Crommie, M. Cohen, S. Louie, A. Zettl, Raman Spectroscopy Study of Rotated Double-Layer Graphene: Misorientation- Angle Dependence of Electronic Structure. *Phys*. *Rev*. *Lett*. **108**, 246103 (2012).

[6] J. B. Oostinga, H. B. Heersche, X. Liu, A. F. Morpurgo, L. M. K. Vandersypen, Gate-Induced Insulating State in Bilayer Graphene Devices. *Nat*. *Mater*. **7**, 151 (2008).

[7] C. R. Dean, A. F. Young, I. Meric, C. Lee, L. Wang, S. Sorgenfrei, K. Watanabe, T. Taniguchi, P. Kim, K.L. Shepard, J. Hone, Boron Nitride Substrates for High-Quality Graphene Electronics. *Nat. Nanotechnol*. **5**, 722 (2010).

[8] L. Britnell, R. M. Ribeiro, A. Eckmann, R. Jalil, B. D. Belle, A. Mishchenko, Y.-J. Kim, R. V. Gorbachev, T. Georgiou, S. V. Morozov, A. N. Grigorenko, A. K. Geim, C. Casiraghi, A. H. Castro Neto, K. S. Novoselov, Strong Light-Matter Interactions in Heterostructures of Atomically Thin Films. *Science* **340**, 1311 (2013).

[9] S. Mouri, Y. Miyauchi, K. Matsuda, Tunable Photoluminescence of Monolayer MoS_2 via Chemical Doping. *Nano Lett.* **13**, 5944 (2013).

[10] A. Geim, I. V. Grigorieva, Van der Waals Hterostructures. *Nature* **499**, 419 (2013).

[11] Y.-F. Lin, W. Li, S.-L. Li, Y. Xu, A. Aparecido-Ferreira, K. Komatsu, H. Sun, S. Nakaharaia K. Tsukagoshi. Barrier inhomogeneities at vertically stacked graphene-based heterostructures. Nanoscale, **6**, 795 (2014).

[12] S. M. Kim, A. Hsu, P. T. Araujo, Y.-H. Lee, T. Palacios, M. Dresselhaus, J.-C. Idrobo, K. K. Kim, J. Kong, Synthesis of Patched or Stacked Graphene and hBN Flakes: A Route to Hybrid Structure Discovery. *Nano Lett*. **13**, 933 (2013).

[13] W. Ge, K. Kawahara, M. Tsuji, H. Ago, Large-Scale Synthesis of NbS_2 Nanosheets with Controlled Orientation on Graphene by Ambient Pressure CVD. *Nanoscale* **5**, 5773 (2013).

Acknowledgements

I appreciate everything, everyone connected to my life.

My first thanks are to my supervisor Associate Professor Hiroki Ago. He always created better conditions, not only of the experimental equipment but also the human environment, for us all to do research. I learned many things from him about how to think properly and logically in regards to science. Professor M. Tsuji and Assistant Professor T. Tsuji also kindly supported me, thank you very much. I am grateful to the other laboratory members for sharing wonderful and fruitful times. Especially regarding English, Dr. M. A. Bissett and Dr. C. M. Orofeo took care of me so often. I would also like to thank to my schoolmates in the Ph.D. course. We grew through friendly competition and encouraged each other.

During my Ph.D, I received many opportunities for research collaborations and internships. These experiences provided me great benefit and made positive impact on my research life. Professor S. Mizuno and Assistant Professor K. Ikeda in Kyushu University helped us to characterize graphene related to Cu crystalline. Professor Mizuno is also my Ph.D reviewer. For LEEM analysis, we discussed together with Dr. H. Hibino of NTT Basic Research Laboratories. I spent two months in National University of Singapore, Singapore, supervised by Assistant Professor W. Chen and Professor A. T. S. Wee. I also visited Dr. Tsukagoshi's laboratory in National Institute for Materials Science (NIMS) in Tsukuba, Japan, and studied the investigation of nano-scale electronic device. Thanks a lot for many discussions. I also owe a great deal to Dr. K. Komatsu in NIMS, and Tianchao and Swee Liang in NUS for supporting my experiments and appreciate my Ph.D reviewer Professor M. Nishida in Kyushu University and my Master degree supervisor Professor J. Yamaki in Kyoto University for their kind helps.

I acknowledge financial support from a Grant-in-Aid for JSPS Fellows, the Global Center of Excellence (GCOE) of Novel Carbon Resource Sciences and Graduation School of Engineering Sciences at Kyushu University, and the International Collaboration Fund (ICF) at NUS.

Finally, I sincerely thank my dear mother and family for their understanding and support during my study in graduate school.

List of publications

Chapter 3

Y. Ogawa, B. Hu, C. M. Orofeo, M. Tsuji, K. Ikeda, S. Mizuno, H. Hibino, H. Ago

"Domain Structure and Boundary in Single-Layer Graphene Grown on Cu (111) and Cu (100) films"

J. Phys. Chem. Lett., 3(2), 219-226 (2012).

Chapter 4

Y. Ogawa, K. Komatsu, K. Kawahara, M. Tsuji, K. Tsukagoshi, H. Ago

"Structure and Transport Properties of the Interfaces Between CVD-grown Graphene Domains"

Nanoscale submitted (2013).

Chapter 5

Y. Ogawa, T. Niu, S. L .Wong, M. Tsuji, A. T. S. Wee, W. Chen, H. Ago

"Self-assembly of polar phthalocyanine molecules on graphene grown by chemical vapor deposition"

J. Phys. Chem. C, 117(42), 21849–21855 (2013).

Publications not included in this thesis

[1] H. Ago, I. Tanaka, Y. Ogawa, R. M. Yunus, M. Tsuji, H. Hibino

"Lattice-Oriented Catalytic Growth of Graphene Nanoribbons on Heteroepitaxial Nickel Films"

ACS Nano, 7(12), 10825-10833 (2013).

[2] P. Solis Fernandz, K. Yoshida, Y. Ogawa, M. Tsuji, H. Ago

"Dense Arrays of Highly Aligned Graphene Nanoribbons Produced by Substrate-Controlled Metal-Assisted Etching of Graphene"

Adv. Mater., 25(45), 6562–6568 (2013).

[3] H. Ago, K. Kawahara, Y. Ogawa, S. Tanoue, M. A. Bissett, M. Tsuji, H. Sakaguchi, R. J. Koch, F. Fromm, T. Seyller, K. Komatsu, K. Tsukagoshi

"Epitaxial Growth and Electronic Properties of Large Hexagonal Graphene Domains on Cu(111) Thin Film"
Appl. Phys. Express, 6(7), 075101-1-4 (2013).

[4] H. Ago, Y. Ogawa, M. Tsuji, S. Mizuno, H. Hibino
"Catalytic Growth of Graphene: Towards Large-Area Single-Crystalline Graphene"
J. Phys. Chem. Lett., 3(16), 2228-2236 (2012).

[5] C. M. Orofeo, H. Hibino, K. Kawahara, Y. Ogawa, M. Tsuji, K. Ikeda, S. Mizuno, H. Ago "Influence of Cu Metal on the Domain Structure and Carrier Mobility in Single-Layer Graphene"
Carbon, 50(6), 2189-2196 (2012).

[6] B. Hu, H. Ago, C. M. Orofeo, Y. Ogawa, M. Tsuji
"On the Nucleation of Graphene in Chemical Vapor Deposition"
New J. Chem., 36(1), 73-76 (2012).

[7] H. Ago, T. Ayagaki, Y. Ogawa, M. Tsuji
"Ultra-High Vacuum-Assisted Control of Metal Nanoparticles for Horizontally-Aligned Single-Walled Carbon Nanotubes with Extraordinary Uniform Diameters"
J. Phys. Chem. C, 115(27), 13247-13253 (2011).

[8] H. Ago, Y. Nakamura, Y. Ogawa, M. Tsuji
"Combinatorial Catalyst Approach for High-density Growth of Horizontally Aligned Single-Walled Carbon Nanotubes on Sapphire"
Carbon, 49(1), 176-186 (2011).

[9] Y. Ogawa, H. Ago, M. Tsuji
"Epitaxial Growth of Faceted Co Nanoparticles on Sapphire Surfaces"
Chem. Lett., 39(9), 964-965 (2010).